An Adjustable-Ratio Flow Dividing Hydraulic Valve

A Thesis Submitted to the
College of Graduate Studies and Research
in Partial Fulfillment of the Requirements
for the Degree of Master of Science
in the Department of Mechanical Engineering,
University of Saskatchewan, Saskatoon
Canada

By
Travis Kent Wiens
August 2004

©Travis Wiens, August 2004. All rights reserved.

Permission to Use

In presenting this thesis in partial fulfillment of the requirements for a postgraduate degree from the University of Saskatchewan, I agree that the Libraries of this University may make it freely available for inspection. I further agree that the permission for copying this thesis in any manner, in whole or in part for scholarly purposes, may be granted by the professors who supervised my work or, in their absence, by the Head of the Department or Dean of the College in which my thesis work was conducted. It is understood that any copying or publication or use of this thesis or parts thereof for financial gain shall not be allowed without my written permission. It is also understood that due recognition shall be given to me and to the University of Saskatchewan in any scholarly use which may be made of any material in my thesis.

Requests for permission to copy or to make other use of material in this thesis, in whole or part, should be addressed to:

Head, Department of Mechanical Engineering
University of Saskatchewan
College of Engineering
57 Campus Drive
Saskatoon, Saskatchewan, S7N 5A9
Canada

Acknowledgements

I would like to acknowledge and thank my supervisors, Professors R.T. Burton and G. Schoenau for their support, in all things technical and financial. My thanks also go to Professor J. Ruan of the Zhejiang University of Technology for hosting my visit and for assistance in designing and producing the prototype. I would also like to thank Mr. D. Bitner, Mr. D. Crone, and Engineering Shops for technical help. Finally, I'd like to acknowledge the long-lasting support of my parents.

Abstract

This thesis proposes a new type of hydraulic valve: an adjustable-ratio flow divider. This valve attempts to split one input flow into two output flows in a predetermined ratio, independent of load pressure or total flow. The valve uses a “two dimensional” structure to form a two-stage valve with only one moving part; the pilot stage uses the spool’s rotary position, and the main stage uses its linear position. This arrangement allows for a cheaper, simpler valve with smaller volumes (translating into faster response). The ratio of outlet flows can be set “on the fly” by the angular position of the spool, driven by a stepper motor or other low-power input.

In order to evaluate the initial feasibility of the concept, steady state and dynamic models were developed and the effects of the physical parameters were studied. Two non-linear non-derivative multiobjective optimization strategies were used to determine the optimum parameters for a prototype. Finally, the prototype’s performance was experimentally examined and appears to work as expected.

Contents

Permission to Use i

Acknowledgements ii

Abstract iii

Nomenclature xi

1 Introduction 1

1.1 Background 1

1.1.1 Operation of a Typical Flow Divider Valve 2

1.2 Literature Review 3

1.3 Objectives 4

1.4 Thesis Overview 5

2 Analysis of the Adjustable Ratio Flow Divider 6

2.1 General Structure and Operation 6

2.2 Ideal Steady State Analysis 9

2.3 Dynamic Model 13

3 Parameter Selection and Evaluation 20

3.1 Performance Evaluation Method 20

3.2 Relationships Between Parameters 24

3.3 ODE Solution Method 26

3.4 Sensitivity 27

3.5 Optimization of Parameters 48
  3.5.1 Complex Method 49
  3.5.2 Genetic Algorithm 49
  3.5.3 Aggregation of Objectives 50

4 Experimental Verification 52

4.1 Introduction 52
4.2 Tests 54
4.3 Initial Tests 54
4.4 Test for Repeatability 55
4.5 Effect of Pressure Drop 58
4.6 Effect of Load Pressure Difference 59
4.7 Effect of Spool Rotation 59
4.8 Summary 59

5 Conclusions and Recommendations 61

5.1 Conclusions 61
5.2 Recommendations for Further Work 62

A Derivation of Equations Governing Pilot Stage Flow 66

B Physical Parameters 72

B.1 dividerparams.m 72
B.2 optimizedparams.m 73

C Matlab/Octave and C Code 75

C.1 calcparams.m 75
C.2 changeall.m 76
C.3 divloadcc.cc 81
C.4 gadiv.m 86
C.5 divfitag.m 87
C.6 complexdiv.m 90
C.7 complex.m 91

D Prototype Machining Drawings **93**

E Experimental Procedures **100**

E.1 Instrumentation 100

E.2 Calibration of Instruments 100

E.3 Experimental Procedure 101

E.4 Experimental Error 104

E.4.1 Flow Measurement Uncertainty 105

E.4.2 Pressure Measurement Uncertainty 107

F Combiner and Divider/Combiner Valve Concept **108**

List of Figures

1.1 A typical flow divider valve. 3

2.1 Circuit diagrams of a typical flow divider and the adjustable ratio valve. . . 7
2.2 Cutaway view of the proposed valve. 8
2.3 Exploded view of the valve. 8
2.4 Schematic view of the same valve 9
2.5 Hydraulic bridges 10
2.6 Ideal flow ratio graph 13
2.7 Leakage paths 14
2.8 Flow forces can be reduced by using a rimmed orifice. 14
2.9 Nomenclature used for pilot flows. 17

3.1 Sample simulated step response 22
3.2 Cumulative steady state and dynamic error 23
3.3 Effect of radius 28
3.4 Effect of radius 29
3.5 Effect of radius 29
3.6 Effect of radius 30
3.7 Effect of groove thickness 31
3.8 Effect of groove thickness 32
3.9 Effect of groove thickness 32
3.10 Effect of radial clearance 33
3.11 Effect of radial clearance 34

3.12 Effect of pressure drop 35

3.13 Effect of pressure drop 36

3.14 Effect of pressure drop 36

3.15 Effect of pressure drop ratio 37

3.16 Effect of pressure drop ratio 38

3.17 Effect of pressure drop ratio 38

3.18 Effect of fractional orifice opening 39

3.19 Effect of fractional orifice opening 40

3.20 Effect of fractional orifice opening 40

3.21 Effect of fractional orifice opening 41

3.22 Effect of rim thickness 42

3.23 Effect of rim thickness 43

3.24 Effect of Coulomb Friction 44

3.25 Effect of Coulomb Friction 45

3.26 Effect of viscosity 46

3.27 Effect of viscosity 47

3.28 Effect of viscosity 47

3.29 The complex method 50

4.1 Photos of the valve prototype, showing holding plate (1), stepper motor and mounting plate (2), valve block (3), seal gland (4), spool (5), and gear (6). . 53

4.2 The circuit diagram of the system used to test the valve prototype. The valve body contains the pilot stages and the variable orifices. 54

4.3 Photo of the test circuit, showing pump (1), fixed orifices (2), valve block (3), counterbalance valves (4), and three-way bypass valve (5). 55

4.4 Experimental flow step response 56

4.5 Experimental pressure response 56

4.6 Repeatability of flow measurements 57

4.7 Standard deviation of flow measurements 57

4.8 Experimental flow response to spool rotation 60

A.1 Leakage paths 66

A.2 Leakage paths 67

A.3 Nomenclature used for pilot flows. 70

E.1 Calibration curves for the absolute pressure transducers. 101

E.2 Calibration curves for the differential pressure transducers. 102

E.3 Calibration curves for the flow transducers. 102

E.4 The circuit diagram of the system used to test the valve prototype. The valve body contains the pilot stages and the variable orifices. 103

E.5 Photo of the test circuit, showing pump (1), fixed orifices (2), valve block (3), counterbalance valves (4), and three-way bypass valve (5). 103

E.6 Comparison of how the flow calibration curves have drifted over time. The solid curves show the calibration used to collect the data, while the dashed curves show the result of a recalibration after the data was collected. 106

F.1 Difference between a divider and combiner valve 109

F.2 Proposed divider/combiner valve 110

List of Tables

3.1 House of Quality 48
3.2 House of Quality 51
3.3 Optimized Parameters 51

4.1 Steady state and dynamic error 58
4.2 Load pressure's effect on error 59

E.1 Pressure calibration coefficients 101
E.2 Estimated Pressure Uncertainty (90%) 107

Nomenclature

Unless otherwise stated, subscripts 1 and 2 refer to the two outlet branches.

$\%E_{ss}$	Steady state error [%]
β	Bulk modulus [Pa]
δ	Radial clearance between spool and casing [m]
ΔP_L	Load pressure difference [Pa]
ΔP_o	Desired pressure drop across fixed orifice [Pa]
ΔP_t	Desired total pressure drop [Pa]
ΔP_{fixed}	Measured pressure drop across fixed orifice [Pa]
λ	Aggregation matrix
μ	Viscosity [Ns/m^2]
ν	Kinematic viscosity [mm^2/s]
ϕ	Angular position of the spool [rad]
ϕ_0	Maximum angular position of spool [rad]
ρ	Density [kg/m^3]
ρ_{steel}	Density of steel [kg/m^3]
A	Area of spool end [m^2]
A_L	Area of load orifice [m^2]
A_v	Area of variable orifices [m^2]
A_o	Area of fixed orifices [m^2]
A_{rim}	Area of rim [m^2]
b	Width of pilot groove [m]
B_f	Viscous damping coefficient [Ns/m]
c	Pilot stage constant
C_a	Pilot stage constant [Pa]
C_b	Pilot stage constant [Pa]
C_c	Pilot stage constant [Pa]
C_d	Pilot stage constant [Pa]
C_{do}	Discharge coefficient for the fixed orifices
C_{dv}	Discharge coefficients for variable orifices

C_d	Discharge coefficient for load orifice
d_o	Initial opening of variable orifices [m]
E_{CUDY}	Cumulative dynamic error [m^3]
E_{CUSS}	Cumulative steady state errror [m^3]
E_{CU}	Cumulative error [m^3]
F_c	Coulomb friction force [N]
F_i	The i^{th} objective [various units]
F_i^*	Goal for the i^{th} objective [units match F_i]
FO	Fractional variable orifice opening at $x = 0$
h	Length of pilot stage leakage path [m]
K	Flow coefficient [m$^{7/2}$/kg$^{1/2}$]
L_a	Length between lands [m]
L_L	Sum of the land lengths [m]
L_t	Spool length [m]
L_v	Clearance between spool end and chamber end at $x = x_{max}$ [m]
m	Spool mass [kg]
MR	Mass ratio of the machined spool to that of a solid spool with the same dimensions
P_b	Pressure acting on spool ends [Pa]
P_s	Source pressure [Pa]
P_a	Pressure between fixed and variable orifices [Pa]
P_L	Load pressure [Pa]
P_{tan}	Constant used to modify pressures for use in tanh [Pa]
Q_b	Flow into spool end chamber [m^3/s]
Q_L	Flow to load from valve [m^3/s]
Q_s	Total source flow [m^3/s]
Q_{axi}	Flow from sensing groove to pilot stage [m^3/s]
Q_{axo}	Flow from pilot stage to P_a [m^3/s]
Q_{cxi}	Flow into the pilot stage from the source pressure [m^3/s]
Q_{cxo}	Pilot flow entering sensing groove [m^3/s]
Q_{la}	Leakage flow to P_a [m^3/s]
Q_{lb}	Leakage flow from spool end chamber [m^3/s]
Q_{Lo}	Flow through load orifice [m^3/s]
Q_{Lxd}	Desired load flow (ideal) [m^3/s]
Q_{Lxss}	Steady state load flow [m^3/s]
Q_L	Load flow [m^3/s]
Q_{so}	Desired source flow at pressure drop ΔP_o [m^3/s]
Q_s	Flow through the fixed orifice [m^3/s]
r	Spool radius [m]

r_v	Radius of variable orifice [m]
t	Time [s]
t_s	Settling time [s]
t_{cum}	Time used when calculating cumulative error [s]
V_a	Intermediate flow chamber volumes [m^3]
V_b	Volume of spool end chamber [m^3]
V_s	Source volume [m^3]
V_{bxo}	Volume of spool end chamber when $x = 0$ [m^3]
V_L	Volume of load line [m^3]
w_i	Weight for the i^{th} objective
x	Linear position of spool [m]
x_{max}	Maximum linear spool displacement [m]
x_{tan}	Modifier for use of tanh [m]

Chapter 1

Introduction

1.1 Background

A common problem in hydraulic applications is the synchronization of two loads, such as two cylinders that must match each other's position. A typical solution to this problem is to use a flow divider valve, defined as a valve which attempts to split the flow to two circuits in some prescribed ratio, independent of load pressure or source flow.

There are many applications where flow divider valves are used to achieve synchronization of linear actuators. An example of this is in the theater where the stage may be raised and lowered using two or more hydraulic actuators, while maintaining a horizontal orientation, even if the stage is not evenly loaded (Hogan and Burrows, 1994). A similar application is where two rotary actuators must maintain a constant speed, such as a differential lock for mobile equipment with a hydraulic transmission (Stroempl, 1990). To ensure that there is no loss of traction, one or more flow dividers are used to supply equal flow to the motors driving the individual wheels.

A similar problem is the synchronization of two processes that do not necessarily require equal flows, but require a certain ratio of flows (which can change in time). An example is a thread-cutting process, where the workpiece rotational speed and the tool feed rate are much less important than the ratio between them. A second example is an auger-fed feed or fertilizer blending operation. Two or more hydraulically driven augers are run at a set ratio to blend two materials in a set, but easily adjustable ratio (for easy adjustment of protein level in feed or nitrogen/phosphate ratio in fertilizer, for instance).

Another common use for flow-divider valves is to ensure equal distribution of lubricating oil to different parts of a machine. This ensures that a particular location is not starved for oil if the local back-pressure increases.

A different, but related problem is one where two flows must be combined in a certain ratio. This appears in hydraulic meter-out circuits, as well as chemical processes where two liquids must be mixed in a controlled ratio. A “domestic” example of flow combination is a valve that can combine hot and cold water in a shower such that the mixture (and therefore the temperature) remains constant when the supply pressures change, such as when a toilet is flushed, preventing scalding.

There are currently three major problems with flow-divider/combiner valves. The first problem is that their steady state flow dividing accuracy can be low. This problem has been studied by a number of researchers, including Kwan (1978) and Chan (1980), and a number of solutions have been presented. The second problem is that the time response of the divider valve to changes in load may be slow, allowing a large position error to build up before the valve can respond (Guo, 1987). The third problem is that the ratio of flows is typically fixed; that is, a valve is manufactured to supply a 50:50 flow division ratio that can not be changed. Very little, if any, research has been applied to this third problem and is therefore the focus of this thesis.

1.1.1 Operation of a Typical Flow Divider Valve

A typical spool flow divider valve, shown in Figure 1.1, includes two main parts: a pair of fixed orifices and a pair of hydrostatic orifices mounted on one spool. The pressures downstream of the fixed orifices, P_{a1} and P_{a2}, act on the spool ends to adjust the hydrostatic orifices to maintain equilibrium. In the ideal case, neglecting flow forces and friction, at equilibrium $P_{a1} = P_{a2}$. From the orifice equation for the fixed orifice, the two inlet flows, Q_{s1} and Q_{s2}, are

$$Q_{s1} = K_1\sqrt{(P_s - P_{a1})} \tag{1.1}$$

and

$$Q_{s2} = K_2\sqrt{(P_s - P_{a2})} \tag{1.2}$$

where P_s is the inlet pressure and K_1 and K_2 are approximately constant for large Reynolds number flows. If $P_{a1} = P_{a2}$ at equilibrium, and identical orifices are used ($K_1 = K_2$), then the flows are equal. If the load changes, the pressure change will force the spool to a new equilibrium position. For example, considering Figure 1.1, if the flow through branch 1 momentarily increases, (1) P_{a1} will decrease (as P_s is initially unchanged), (2) the pressure imbalance between P_{a1} and P_{a2} will force the spool to the left, (3) thereby closing the left orifice and opening the right one, (4) which increases P_{a1} and decreasing P_{a2} until force equilibrium is regained, at which point the ratio of outlet flows has been restored. It should be noted that the right orifice opens as the left orifice closes, increasing its flow such that, although the magnitudes of the flows may have changed, the *ratio* has not.

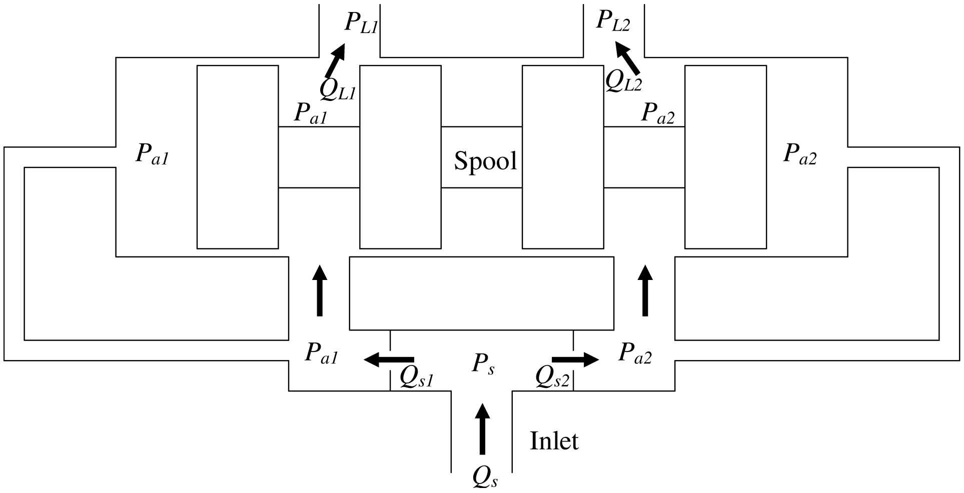

Figure 1.1: A typical flow divider valve.

In the ideal case, the ratio of outlet flows is equal to the ratio of K_1 to K_2, which is generally equal to the ratio of the areas of the fixed orifices.[1] Unfortunately, unless a second spool is used to adjust the relative areas of the "fixed" orifices, the divider can only be used to divide the flow at a fixed ratio. Also, if there is any external force on the spool, the end pressures will not be equal at equilibrium and therefore the flows will not be divided in the desired ratio. This flow division error can be caused by flow forces or leakage (and will be further described in subsequent chapters).

1.2 Literature Review

As noted in the introduction, there is a significant and useful body of work studying the form, function and performance of typical flow divider valves. The most recent major project was performed by Fedoroff (1990) whose thesis dissertation provides a very good review of the previous literature. A summary of this literature is included in this section, but the reader should refer to his work for details.

One of the first theoretical models describing the accuracy of a flow divider valve was developed in 1979 by Kwan and also presented in Kwan et al. (1979). He showed that the flow division error is equal to the external forces on the spool (due to friction, flow forces, etc) divided by the spool end area and the pressure drop across the fixed orifice. He also developed a second stage spool that used a lever to increase the effective area of the spool, and hence, reduce division error.

---

[1] This assumes equal discharge coefficient and fluid density.

Chan (1980) and Chan et al. (1981) concentrated on reducing flow forces and discovered that if a thin rim was machined into the orifice, the flow forces could be greatly reduced. His valve was able to reduce flow division error greatly and this orifice design has been implemented in most commercial flow divider valves that use configurations similar to his.

Due to the nonlinearities involved in most hydraulic valves, both Kwan and Chan had restricted their research to steady state performance (while they did develop linear dynamic models, these results were not practically applied). By 1987 digital computers had developed to the point where numerical solutions to the non-linear dynamic equations could be found and Guo (1987) and Guo et al. (1988) developed a good dynamic model of a typical flow divider valve. He was also the first to point out the importance of the dynamic error: the position error accumulated in the time that it takes for the valve to respond to a load disturbance.

The previous researchers had established that the steady state and dynamic performance of a typical flow divider valve was strongly dependent on the pressure drop across the fixed orifice. The performance could be improved for low flow rates by using small orifices, but this meant very large pressure losses at large flows. Zhang et al. (1988), Zhang et al. (1993), Fedoroff (1990) and Fedoroff et al. (1992) presented an “auto-regulator”, a pressure-controlled pair of orifices that replaced the fixed orifices, thereby maintaining a reasonable pressure drop over a wide range of flows. Zhang also introduced a hardware modification that allows a valve to operate as either a flow divider or combiner, depending on the direction of flow. The result of these two innovations was a flow divider/combiner valve with high precision (low division error, <5%) that could operate over a large range of flows.

As the typical flow divider valve is quite a mature technology, little academic research has been performed on the valves since Zhang and Fedoroff’s work in the early 1990s, instead, research and publications have concentrated on applications. For an example, Stroempl (1990) presented a differential lock for hydrostatic transmissions based on flow divider valves. However, none of these applications featured an adjustable ratio of output flows. That is, if a valve was manufactured to provide a 50-50 division of flows, it was very difficult to achieve a different ratio at a later time.

1.3 Objectives

The general objective of this project was to establish the feasibility of a new design of a flow divider valve that can split a flow with an adjustable flow ratio. The valve should be able to accurately divide flows in a controllable ratio, over a wide range of flows and load pressures. Further, it should be possible to set the desired ratio of flows with a low power electronic input. The valve should demonstrate a fast response to disturbances in load pressure and should have low pressure losses. Furthermore, the valve should not be unduly expensive, complex, or fragile.

This primary objective can be split into a number of smaller secondary objectives. The first objective was to conceive and develop a conceptual design for the valve. The second was to develop the differential equations of a dynamic model which would facilitate a theoretical feasibility study. The third objective was to use the dynamic model to optimize parameters for a prototype design and the last objective was to evaluate the steady state and dynamic performance of the prototype valve.

1.4 Thesis Overview

This section includes an overview of this dissertation. Chapter 1, this chapter, includes an introduction, literature review and objectives. Chapter 2 introduces the proposed valve and includes development of steady state and dynamic models. Chapter 3 presents a sensitivity study and optimization strategy, as well as the optimized prototype design. In Chapter 4, the performance of the valve is experimentally determined and Chapter 5 will present conclusions and comment on possible future work such as converting the divider to a divider/combiner configuration.

Chapter 2

Analysis of the Adjustable Ratio Flow Divider

This chapter presents the development of a mathematical model of the proposed adjustable-ratio flow divider valve. First, the structure and basic operation of the valve are presented, followed by the models used for dynamic and steady-state simulation. These models will be used to demonstrate both the steady state and dynamic performance of the valve in subsequent chapters.

2.1 General Structure and Operation

The adjustable-ratio flow divider valve proposed in this study works on a similar principle to that of a typical flow divider (as discussed in Section 1.1.1). However, the controlling pressures acting on the spool ends are modified by the pilot stage, as shown in Figure 2.1. In a typical flow divider spool, the pressures acting on the spool are ported from directly downstream of the fixed orifices. In the new valve proposed in this thesis, two hydraulic bridges[1] are connected in parallel with the fixed orifices to modify these driving pressures (see Figure 2.1). The two bridges are physically connected such that when one pressure tap moves toward P_s, the other moves further away (toward P_{a2}.)

The basic physical construction of the valve is shown in Figures 2.2 and 2.3 and its schematic in Figure 2.4; the concept takes advantage of the "2-D" concept introduced by Ruan et al. (2001) and Cui (1991) to allow both the pilot stage and main stage to exist on the same spool. The spool has motion in two dimensions: linear (sliding along

---

[1] A hydraulic bridge is the fluid equivalent of the electrical rheostat. Whereas the output of a rheostat is an electrical potential that is linearly dependent on the voltage tap's position, a hydraulic bridge produces a pressure that is linearly dependent on the pressure tap's position.

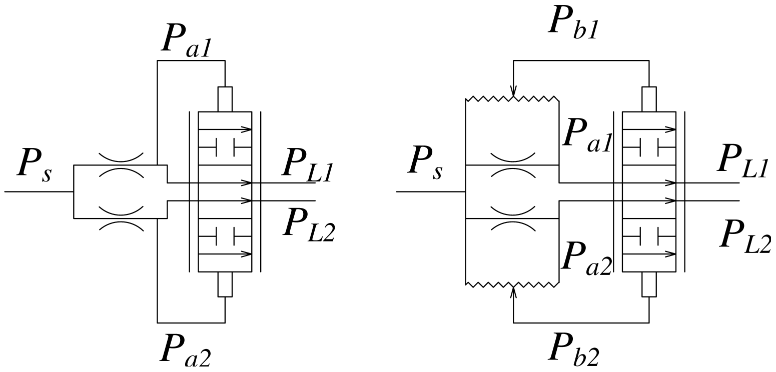

Figure 2.1: Circuit diagrams of a typical fixed-ratio flow divider (left) and the variable ratio flow divider (right). Each consists of two fixed orifices and two variable orifices. The difference between the two is the pilot stage, composed of two hydraulic bridges, which allows the ratio of outlet flows to be changed.

the sleeve axis) and rotary (the complete spool rotates), hence the label "2-D". The linear motion provides the flow dividing function (as in a traditional valve). Control pressures act on the spool's outermost lands to move the spool linearly and change the area of the variable orifices to compensate for load changes. The rotary motion is used to set the position of the hydraulic bridges of the pilot stage.

On each of the outer lands, there is a circumferential groove, labeled 6 in Figures 2.2 and 2.4, the ends of which are connected to the source pressure (P_s) and the intermediate pressure for each branch (P_{a1} or P_{a2}). Partway along the length of this circumferential groove is a perpendicular groove (the sensing channel, 7 in Figures 2.2 and 2.4) in the valve casing which intersects the first groove and taps the output pressure. This output is connected to the spool end chamber at pressure P_{b1} or P_{b2}. The position of the circumferential groove relative to the sensing channel is determined by the angular position of the spool.

Consider Figure 2.5. At the extreme positive angle, $P_{b1} = P_{a1}$ and $P_{b2} = P_s$. At the zero position $P_{b1} = P_s$ and $P_{b2} = P_{a2}$, while intermediate positions give pressures that vary approximately linearly between P_s and the P_b values. Thus, by rotating the spool, the spool end pressures (P_{b1} and P_{b2}) can be adjusted, which, in turn, can be used to set the dividing ratio.

To illustrate the operation of the valve, consider how the valve reacts to a change in load. Consider Figure 2.4. Under ideal[2] steady state conditions, P_{b1} is equal to P_{b2}. However, P_{a1} may not be equal to P_{a2} if the spool is rotated away from the centre position (for unequal flow division). From a steady state position, if the load changes so as to decrease the line pressure such that the flow in branch 1 (the left branch in Figure 2.4) increases, the intermediate pressure, P_{a1}, will decrease. Since one of the ends of the hydraulic bridge

---

[2] No friction or flow forces

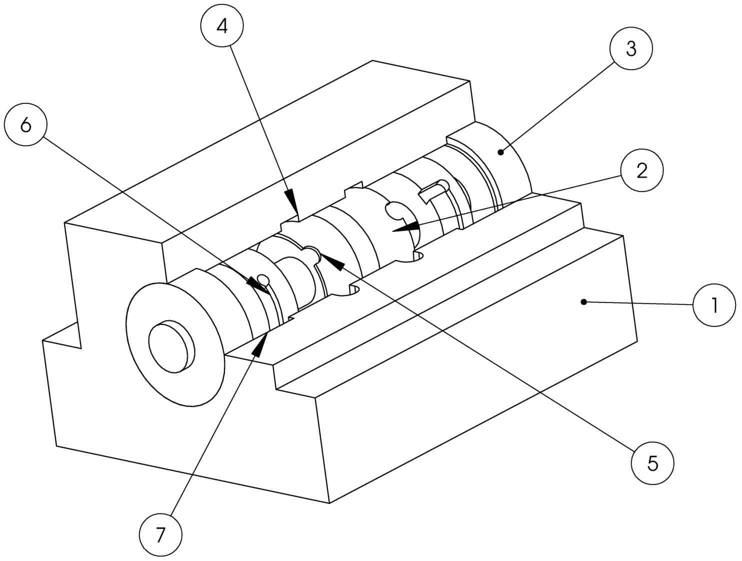

Figure 2.2: Cutaway view of the proposed flow divider valve, showing casing (1), spool (2), and seal glands (3). The main stage orifices consist of grooves in the casing (4) and semicircular notches on the spool (5), while the pilot stages consist of circumferential grooves in the spool (6) and axial grooves (sensing channels) in the casing (7).

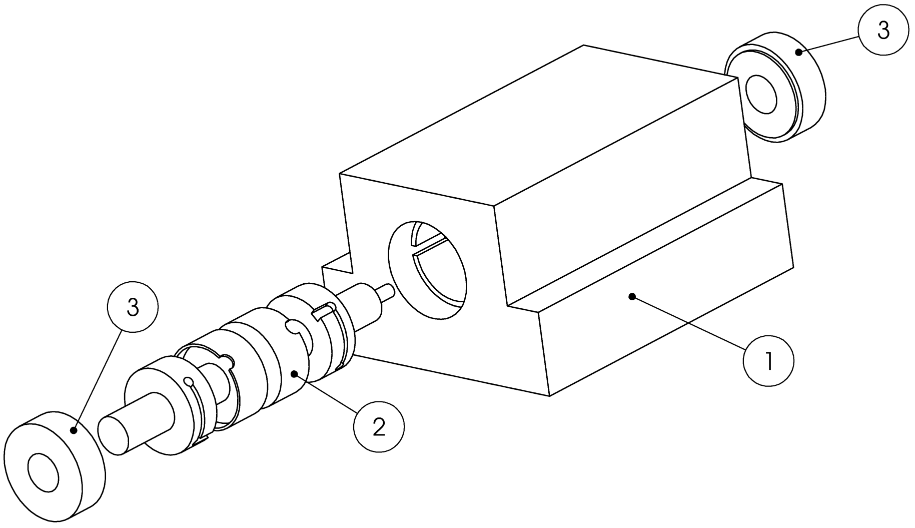

Figure 2.3: Exploded view of the valve, showing casing (1), spool (2) and seal glands (3).

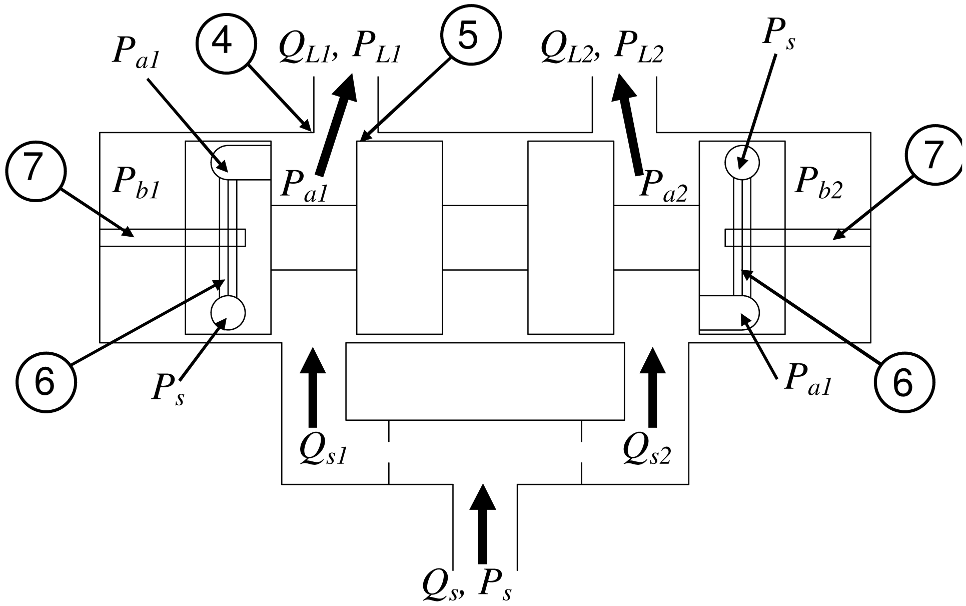

Figure 2.4: Schematic view of the same valve, with pressure and flow nomenclature. The flow enters at the bottom and splits into the left branch or right branch where it passes through the fixed and variable orifices before going on the load. The left branch is denoted by a subscript 1 in the nomenclature and the right branch by a 2. The pilot flows are connected by internal passages in the spool.

is connected to P_{a1}, P_{b1} will also decrease (although not to the same extent as P_{a1} since the other end of the hydraulic bridge is connected to the source pressure). As there is now a force imbalance on the spool (P_{b1} is less than P_{b2}), the spool will move to the left, closing the orifice in branch 1 and opening that in branch 2. This tends to reduce the flow in branch 1 (increasing P_{a1} and hence P_{b1}) and to increase the flow in branch 2 (decreasing P_{a2} and P_{b2}). P_{a1} increases and P_{a2} decreases until force equilibrium is again achieved when P_{b1} equals P_{b2} and the flows are in the original ratio. This ratio is determined by how much a change in P_{a1} effects P_{b1} which, in turn, is determined by the position of the hydraulic bridges (or the spool's rotary position). A more detailed relationship between the spool's angular position and the dividing ratio is developed in the following section.

2.2 Ideal Steady State Analysis

The objective of the following analysis is to develop an equation for the ratio of steady state load flows in analytical form. This will show that under ideal conditions, the source flow can be divided to two circuits with a constant ratio independent of the load.

Consider the following "ideal" case for this valve, which requires a number of simplifying assumptions:

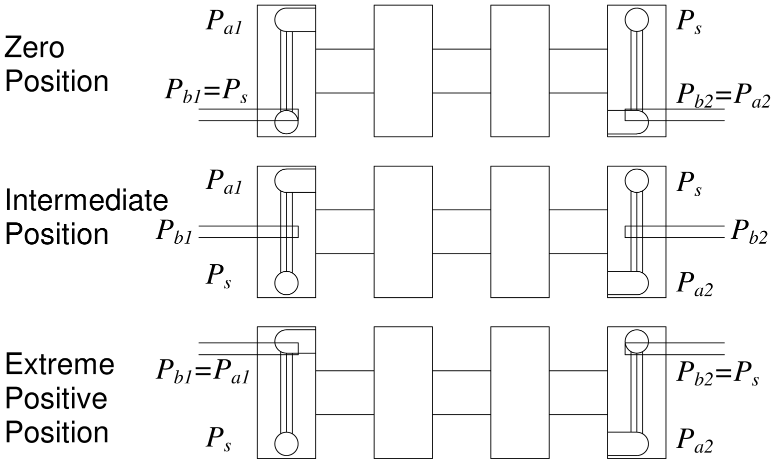

Figure 2.5: The hydraulic bridges used to set the dividing ratio. The top figures, labeled "Zero Position" show the relative positions of the grooves when the angular position of the spool, ϕ, is at zero relative to the casing. "Extreme Positive Position" shows the maximum angle ($\phi = \phi_0$), and the middle shapes show an intermediate position. The pressures in the sensing channels, P_{b1} and P_{b2}, vary linearly between P_s and P_{a1} or P_{a2}.

- no leakage,
- no flow forces,
- no Coulomb or static friction,
- constant discharge coefficients (i.e. turbulent flows through the orifices),
- laminar flow and no entrance or exit effects in the hydraulic bridges, and
- equal spool end areas.

Although some of these assumptions are rather restrictive, this analysis is only intended to show how the valve's rotary position affects the ratio of the load flows and that load pressure fluctuations are compensated for.

A basic schematic of the proposed 2-D adjustable flow divider valve was shown in Figure 2.4. Source flow enters the valve at the bottom and is split into two main flows, which pass through the two fixed orifices. If the inlet pressure is at P_s, the orifice equation (Merritt, 1967) can be used to calculate the flows Q_{s1} and Q_{s2} in each branch:

$$Q_{s1} = C_{do1} A_{o1} \sqrt{\frac{2}{\rho}\,(P_s - P_{a1})}; \tag{2.1}$$

$$Q_{s2} = C_{do2} A_{o2} \sqrt{\frac{2}{\rho}\,(P_s - P_{a2})}. \tag{2.2}$$

In the absence of leakage and for small pilot flows, at steady state these flows are equal to the outlet load flows, Q_{L1} and Q_{L2}.

The major difference between a typical flow divider and the new valve proposed in this thesis is the rotary pilot stage, consisting of two hydraulic bridges, each of which contains a circumferential groove on the spool, intersected by a perpendicular sensing channel in the casing. On the left hand side of the spool, the top end of the bridge is connected to P_{a1} and the bottom is connected to P_s, as shown in Figure 2.5. The pressure along this groove varies approximately linearly between P_{a1} and P_s (Ruan et al., 2001). There is a perpendicular groove in the valve body (the sensing channel), which taps the pressure from the groove in the land, and connects it to the spool end, supplying a pressure P_{b1}. In the simplest case, with no entrance effects or leakage, the steady state pressure is given by

$$P_{b1} = P_s - \left(\frac{\phi}{\phi_o}\right)(P_s - P_{a1}) \tag{2.3}$$

where ϕ is the angular position of the spool and ϕ_o is the maximum angle, at which the sensing channel reaches the end of the groove.

A similar structure exists on the right-hand side of the spool, although the pressures are switched; P_s is connected to the top end of the groove and P_{a2} is connected to the bottom. The symmetrical equation is then:

$$P_{b2} = P_{a2} - \left(\frac{\phi}{\phi_o}\right)(P_{a2} - P_s). \tag{2.4}$$

In the absence of flow forces and friction and if the spool end areas are equal, the spool moves to an equilibrium position such that

$$P_{b1} = P_{b2}. \tag{2.5}$$

By solving the system equations 2.1, 2.2, 2.3, 2.4, and 2.5, the ratio of steady state load flows, $\frac{Q_{L1}}{Q_{L2}}$, is given by

$$\frac{Q_{L1}}{Q_{L2}} = \frac{C_{d1}A_{o1}}{C_{d2}A_{o2}}\sqrt{\frac{\phi_o}{\phi} - 1} \tag{2.6}$$

where
C_d = orifice discharge coefficients,
A_o = fixed orifice areas,
ϕ = spool angular position, and
ϕ_o = maximum angle, which is also equal to the angular length of the groove.

This equation demonstrates that ideally, the flow ratio can be changed by adjusting the spool's angular position with respect to the angular length of the groove. Usually, A_{o1} and

C_{d1} are equal to A_{o2} and C_{d2} respectively; however, A_{o1} and A_{o2} can be made dissimilar to obtain unequal flow division. This requires a change in the orifice area each time the ratio is to be changed, which could be achieved through another spool valve, but this needlessly adds cost and complexity.

One other important fact to notice is that no knowledge of the load pressure or total source flow are needed to derive this equation. As long as the valve can reach an equilibrium position such that $P_{b1} = P_{b2}$, the desired flow ratio will be achieved, demonstrating insensitivity to load pressure variations (under these ideal assumptions).

By applying the fact that the sum of the load flows is equal to the source flow, an equation for the load flow as a fraction of the source flow can be developed as:

$$\frac{Q_{L1}}{Q_s} = \frac{\frac{Q_{L1}}{Q_{L2}}}{\frac{Q_{L1}}{Q_{L2}} + 1} \tag{2.7}$$

This fraction is plotted in Figure 2.6. This figure illustrates how the ratio of load flows can be adjusted by changing the rotary position of the spool. While this function is non-linear, a large near-linear portion exists near the central position, which is the range that the valve is most likely to be operated in. This linearity can be an advantage in that it simplifies analysis and can improve performance if the valve is to included in a more complex control circuit. Notice also that in equation 2.6 the flow division ratio at this central position is not necessarily 50-50, as other base ratios can be achieved by using non-equal fixed orifice areas. Several different fixed orifice ratios are shown in the figure.

It is important to remember that this is an “ideal” result. It will be shown in a later section that there can be significant errors between the ideal and actual flows if more realistic assumptions are used. For example, flow forces exert a particularly strong influence on this error, as they invalidate the equilibrium condition of $P_{b1} = P_{b2}$.

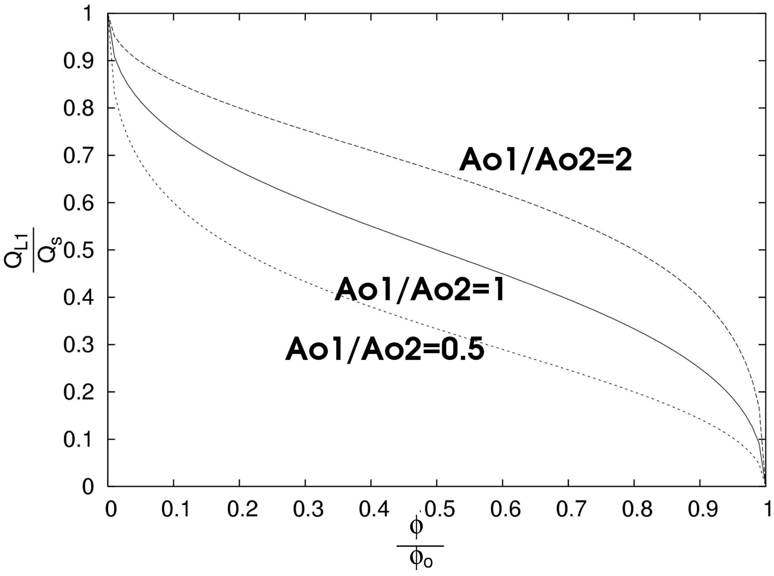

Figure 2.6: The non-dimensional ideal flow for identical fixed orifices, as well as 2:1 and 1:2 fixed orifice ratios. Notice the approximately linear region between $\frac{\phi}{\phi_o} = 0.25$ and 0.75.

2.3 Dynamic Model

Due to the complexity of the proposed valve, attention must be paid to the valve dynamics in order to ensure stability and a reasonable time response. Guo (1987) noted that an important measure of flow divider performance was the cumulative error; that is, the position error accumulated by the load in the time it takes the valve to respond to a disturbance. The objective of this section is to present the describing equations that may be used to predict the dynamic performance of the flow divider valve in response to inputs of changes in source flow, spool rotary position, and load pressures.

This analysis is much more general than that presented in the steady state analysis. The major assumptions made are:

1. The leakage flows from the pilot stage groove follow a path perpendicular to the groove, as shown in Figure 2.7. That is, it is assumed that the ends of the groove and the sensing channel do not affect the leakage flow. This assumption permits the use of a greatly simplified leakage model and the loss of accuracy should be small since leakage is believe to have a small effect on the dynamic response.
2. The only flow forces are due to the area of the orifice face (i.e. the jet angle is forced near to 90° by the machined rim). This assumption is based on Chan's [1980] analysis of a high precision flow divider valve. He hypothesized that if a thin rim

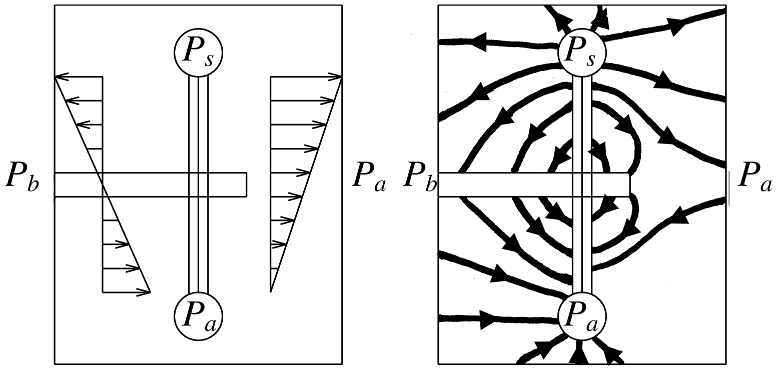

Figure 2.7: This figure shows the difference between the simplified leakage paths used for the analysis (left) and flow lines for a more realistic leakage path (right). All the leakage is assumed to flow in the axial direction between the spool pilot groove and either edge of the land. Since the pressure changes approximately linearly between ends of the groove, the flow also varies linearly. In reality there is likely some leakage between the pilot groove and the sensing groove, and also in the circumferential direction between the ends of the two grooves.

was machined into the orifice face (as in Figure 2.8), the fluid jet could be directed radially with respect to the spool, thereby reducing the classical Bernoulli flow forces to the point that they are insignificant. However, Chan believed that when these flow forces were eliminated another flow force became significant. This flow force is due to the pressure profile on the rim's face as the fluid pressure drops across the orifice. Current research at the University of Saskatchewan is expected to determine the reason for this force reduction.

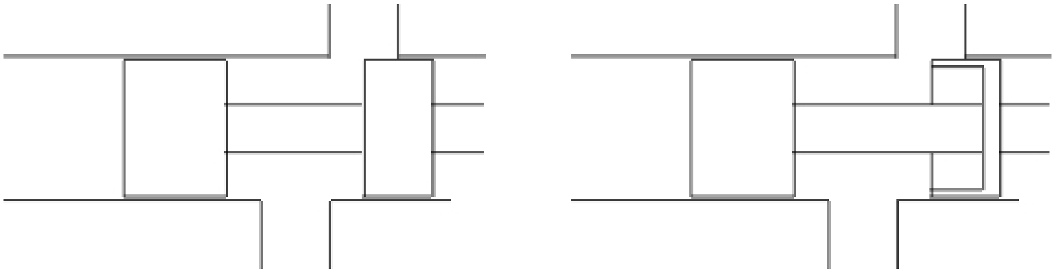

Figure 2.8: The geometry of the orifice is believed to have a large effect on the resultant flow forces. The left figure shows a typical orifice which can cause large flow forces, while if a rim is machined into the orifice face (as shown at right) the flow forces are reduced.

3. Constant discharge coefficients (i.e. turbulent flows through the orifices). The assumption of constant discharge coefficients is based on the fact that there will not be large variations in the Reynold's number, as the purpose of the valve is to maintain constant flows from a flow source of considerable magnitude. The main reason that

this assumption is not valid in the analysis of other valves is they operate with a "nearly-closed" orifice, a condition that a flow divider should only experience under extreme transient conditions such as start-up or shut-down.

4. Constant fluid properties.

5. Laminar flow in the hydraulic bridges. Also, no entrance or exit effects.

6. Equal spool end areas.

The system of non-linear dynamic equations used to simulate valve performance is given in equations 2.8 through 2.45. Nomenclature for the parameters and states is listed on page xi. A more complete development of these equations can be found in Appendix A.

Because the flow to the divider is modelled as coming from a fixed displacement pump (essentially a flow source), the pressure upstream is usually not constant (and if it is restricted by a relief valve or pressure compensated pump, the pressure control is a byproduct of changing the flow). If the system does operate under a flow source condition, the upstream pressure is obtained from:

$$P_s = \frac{\beta}{V_s} \int \left[Q_s - Q_{s1} - Q_{s2} - 2Q_{c1i} - 2Q_{c2i}\right] dt \tag{2.8}$$

It should be noted that all differential equations have initial conditions, but as they are all equal to zero in this analysis, all initial conditions are neglected for simplicity.

The flow through the fixed orifices (see Figure 2.4) is given by equations 2.9 and 2.10.

$$Q_{s1} = \tanh\left(\frac{P_s - P_{a1}}{P_{tan}}\right) C_{do1} A_{o1} \sqrt{\frac{2}{\rho}\left|P_s - P_{a1}\right|} \tag{2.9}$$

$$Q_{s2} = \tanh\left(\frac{P_s - P_{a2}}{P_{tan}}\right) C_{do2} A_{o2} \sqrt{\frac{2}{\rho}\left|P_s - P_{a2}\right|} \tag{2.10}$$

It should be noted that in a typical flow divider valve, if a 50-50 flow division ratio is desired, then these two orifices are usually precision machined to be identical. In the case of the proposed adjustable-ratio flow divider, the relative areas of these orifices determine the ratio of output flows when the rotary position is centred, but adjustment in the rotary position of the spool allows for compensation for manufacturing inaccuracies.

The "tanh" term in these equations allows for reversing flow. While the flow should not reverse under any but the most extreme transient conditions, this term is included for completeness. It would be more accurate to use a "sign" operator instead, but this introduces a discontinuity in the equation which many numerical ODE solvers have difficulty with. As long as a large value for P_{tan} is used, tanh is a good (and continuous) approximation.

The intermediate pressures (between the fixed and variable orifices) are given by equations 2.11 and 2.12. In a typical flow divider, these pressures are channeled directly to the spool ends. However, in this valve, these pressures are modified by the "bridge" circuit in the rotary pilot stage before acting on the spool.

$$P_{a1} = \frac{\beta}{V_{a1}} \int \left[Q_{s1} - Q_{L1} + 2Q_{a1o} + Q_{la1}\right] dt \tag{2.11}$$

$$P_{a2} = \frac{\beta}{V_{a2}} \int \left[Q_{s2} - Q_{L2} + 2Q_{a2o} + Q_{la2}\right] dt \tag{2.12}$$

The flows through the variable orifices are described by equations 2.13 and 2.14. These are also the load flows that are used when calculating the dividing ratio.

$$Q_{L1} = \tanh\left(\frac{P_{a1} - P_{L1}}{P_{tan}}\right) C_{dv1} A_{v1} \sqrt{\frac{2}{\rho} \left|P_{a1} - P_{L1}\right|} \tag{2.13}$$

$$Q_{L2} = \tanh\left(\frac{P_{a2} - P_{L2}}{P_{tan}}\right) C_{dv2} A_{v2} \sqrt{\frac{2}{\rho} \left|P_{a2} - P_{L2}\right|} \tag{2.14}$$

In the above equations, the orifice areas are a function of the spool's linear position. Although any orifice shape could have been selected, a circular orifice was chosen since it is a simple (and therefore less costly) shape to machine. Preliminary analysis does not indicate that the shape has a large effect on performance. The areas of the partially open circular orifices are given by:

$$A_{v1} = r_v^2 \arccos\left(\frac{(d_o - x)}{r_v}\right) - (d_o - x)\sqrt{r_v^2 - (d_o - x)^2} \tag{2.15}$$

$$A_{v2} = r_v^2 \arccos\left(\frac{(d_o + x)}{r_v}\right) - (d_o + x)\sqrt{r_v^2 - (d_o + x)^2} \tag{2.16}$$

The force balance equation for the spool's linear motion is given by equation 2.17. This includes forces due to the end pressures, flow forces and viscous and Coulomb friction. The flow force is not due to the classical form of Bernoulli forces, but is due to the pressure profile acting on the area of the rim face (see Chan (1980)). Again, notice the use of "tanh" to avoid a discontinuity in the friction force.

$$\dot{x} = \frac{1}{m} \int \left[(P_{b1} - P_{b2}) A + \frac{A_{rim1}}{2}(P_{L1} - P_{a1}) - \frac{A_{rim2}}{2}(P_{L2} - P_{a2}) - B_f \dot{x} - F_c \tanh\left(\frac{\dot{x}}{\dot{x}_{tan}}\right)\right] dt \tag{2.17}$$

where

$$A_{rim1} = 2t_{rim}\sqrt{r_v^2 - (d_o - x)^2} \tag{2.18}$$

$$A_{rim2} = 2t_{rim}\sqrt{r_v^2 - (d_o + x)^2} \tag{2.19}$$

The equations describing the flows in the pilot stage grooves are given below. This follows the analysis introduced in Ruan et al. (2001) and details are found in Appendix A. The analysis takes into account the fact that the flow varies along the length of the groove due to leakage. Refer to Figure 2.9 for nomenclature.

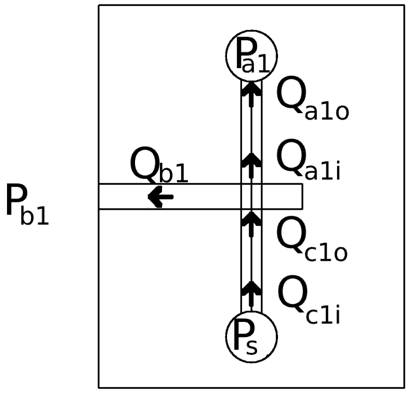

Figure 2.9: Nomenclature used for pilot flows. The flow entering the pilot groove (e.g. Q_{c1i}) is different than that leaving (Q_{c1o}) because of leakage. Similar nomenclature is used for branch 2.

$$Q_{a1i} = \frac{b^4}{185\mu r\sqrt{c}}\left(-C_{a1}\sin\frac{\phi_0-\phi}{\sqrt{c}} + C_{b1}\cos\frac{\phi_0-\phi}{\sqrt{c}}\right) \tag{2.20}$$

where

$$c = \frac{6b^4h}{185r^2\delta^3}, \tag{2.21}$$

$$C_{a1} = -\frac{P_{b1}-P_{a1}}{2} \tag{2.22}$$

$$C_{b1} = \frac{P_{b1}-P_{a1}}{2}\frac{\left(1+\cos\frac{\phi_0-\phi}{\sqrt{c}}\right)}{\sin\frac{\phi_0-\phi}{\sqrt{c}}} \tag{2.23}$$

$$Q_{c1o} = \frac{b^4}{185\mu r\sqrt{c}}\left(C_{c1}\sin\frac{\phi}{\sqrt{c}} - C_{d1}\cos\frac{\phi}{\sqrt{c}}\right) \tag{2.24}$$

where

$$C_{c1} = P_s - \frac{P_{b1}+P_{a1}}{2} \tag{2.25}$$

$$C_{d1} = \frac{\frac{P_{b1}-P_{a1}}{2} - \left(P_s - \frac{P_{b1}+P_{a1}}{2}\right)\cos\left(\frac{\phi}{\sqrt{c}}\right)}{\sin\left(\frac{\phi}{\sqrt{c}}\right)}. \tag{2.26}$$

$$Q_{b1} = Q_{c1o} - Q_{a1i}. \tag{2.27}$$

$$Q_{c2o} = \frac{b^4}{185\mu r\sqrt{c}}\left(C_{a2}\sin\frac{\phi_0-\phi}{\sqrt{c}} - C_{b2}\cos\frac{\phi_0-\phi}{\sqrt{c}}\right) \tag{2.28}$$

$$Q_{a2i} = \frac{b^4}{185\mu r\sqrt{c}}\left(-C_{c2}\sin\frac{\phi}{\sqrt{c}} + C_{d2}\cos\frac{\phi}{\sqrt{c}}\right) \tag{2.29}$$

where

$$C_{a2} = P_s - \frac{P_{b2}+P_{a2}}{2} \tag{2.30}$$

$$C_{b2} = \frac{\frac{P_{b2}-P_{a2}}{2} - \left(P_s - \frac{P_{b2}+P_{a2}}{2}\right)\cos\left(\frac{\phi_0-\phi}{\sqrt{c}}\right)}{\sin\left(\frac{\phi_0-\phi}{\sqrt{c}}\right)} \tag{2.31}$$

$$C_{c2} = -\frac{P_{b2}-P_{a2}}{2} \tag{2.32}$$

$$C_{d2} = \frac{P_{b2}-P_{a2}}{2}\frac{\left(1+\cos\frac{\phi}{\sqrt{c}}\right)}{\sin\frac{\phi}{\sqrt{c}}} \tag{2.33}$$

$$Q_{a1o} = C_{b1}\frac{b^2}{\mu}\sqrt{\frac{\delta^3}{185h}} \tag{2.34}$$

$$Q_{c1i} = -C_{d1}\frac{b^2}{\mu}\sqrt{\frac{\delta^3}{185h}} \tag{2.35}$$

$$Q_{a2o} = C_{d2}\frac{b^2}{\mu}\sqrt{\frac{\delta^3}{185h}} \tag{2.36}$$

$$Q_{c2i} = C_{b2}\frac{b^2}{\mu}\sqrt{\frac{\delta^3}{185h}} \tag{2.37}$$

The major difference between the proposed valve and a typical fixed-ratio flow divider is that the pressures acting on the ends of the spool lands are modified by the pilot stage. These pressures are given by equations 2.38 and 2.40. Notice that the chamber volume changes as the spool moves linearly, which can have an effect on the dynamic performance.

$$P_{b1} = \frac{\beta}{V_{b1}}\int\left[2Q_{b1} - \dot{x}A - Q_{lb1}\right]dt \tag{2.38}$$

where

$$V_{b1} = V_{b1o} + xA \tag{2.39}$$

$$P_{b2} = \frac{\beta}{V_{b2}}\int\left[2Q_{b2} + \dot{x}A - Q_{lb2}\right]dt \tag{2.40}$$

where

$$V_{b2} = V_{b2o} - xA. \tag{2.41}$$

The equations for the valve's internal leakage are found in equations 2.42 through 2.45 (derived in Appendix A). While these equations are complicated, as long as the clearance between the spool and casing is small, they have a small effect. However, as there appear to be complex interactions between leakage and other parameters, these equations should not be neglected until these interactions are better understood.

$$\begin{aligned}
Q_{lb1} &= \frac{2r\delta^3}{12\mu h}\left(\frac{P_{b1}-P_{a1}}{2}\phi_0 + \sqrt{c}\left[-C_{c1}\sin\frac{\phi}{\sqrt{c}} + C_{d1}\left(\cos\frac{\phi}{\sqrt{c}}-1\right) - \ldots\right.\right. \\
&\qquad \left.\left. C_{a1}\sin\frac{\phi_0-\phi}{\sqrt{c}} + C_{b1}\left(\cos\frac{\phi_0-\phi}{\sqrt{c}}-1\right)\right]\right) && (2.42) \\
Q_{la1} &= \frac{2r\delta^3}{12\mu h}\left(\frac{P_{b1}-P_{a1}}{2}\phi_0 - \sqrt{c}\left[-C_{c1}\sin\frac{\phi}{\sqrt{c}} + C_{d1}\left(\cos\frac{\phi}{\sqrt{c}}-1\right) - \ldots\right.\right. \\
&\qquad \left.\left. C_{a1}\sin\frac{\phi_0-\phi}{\sqrt{c}} + C_{b1}\left(\cos\frac{\phi_0-\phi}{\sqrt{c}}-1\right)\right]\right) && (2.43) \\
Q_{lb2} &= \frac{2r\delta^3}{12\mu h}\left(\frac{P_{b2}-P_{a2}}{2}\phi_0 + \sqrt{c}\left[-C_{c2}\sin\frac{\phi}{\sqrt{c}} + C_{d2}\left(\cos\frac{\phi}{\sqrt{c}}-1\right) - \ldots\right.\right. \\
&\qquad \left.\left. C_{a2}\sin\frac{\phi_0-\phi}{\sqrt{c}} + C_{b2}\left(\cos\frac{\phi_0-\phi}{\sqrt{c}}-1\right)\right]\right) && (2.44) \\
Q_{la2} &= \frac{2r\delta^3}{12\mu h}\left(\frac{P_{b2}-P_{a2}}{2}\phi_0 - \sqrt{c}\left[-C_{c2}\sin\frac{\phi}{\sqrt{c}} + C_{d2}\left(\cos\frac{\phi}{\sqrt{c}}-1\right) - \ldots\right.\right. \\
&\qquad \left.\left. C_{a2}\sin\frac{\phi_0-\phi}{\sqrt{c}} + C_{b2}\left(\cos\frac{\phi_0-\phi}{\sqrt{c}}-1\right)\right]\right). && (2.45)
\end{aligned}$$

The above equations constitute a model of the valve, given inputs of source flow, Q_s, spool rotary position, ϕ, and load pressures, P_{L1} and P_{L2}. These equations are used in the next chapter to simulate the valve's performance. This simulation is used to study the effect of parameters on the performance of the system (steady state and dynamic), evaluate the valve's performance and, finally, to optimize the physical parameters.

Chapter 3

Parameter Selection and Evaluation

One of the most important uses for numerical simulation in a design capacity is to reduce prototyping time and cost by using simulation to select appropriate physical parameters before any manufacturing begins. It can also be used to assess the performance of the design, in order to ensure that it exhibits adequate performance to warrant production. Finally, it can be used to help the engineer to infer unobservable inner workings of the design when trouble-shooting problems. This chapter details the criteria used to evaluate valve performance, the computational tools used to simulate the operation of the valve, a study of the sensitivity to the various parameters and the methodology used to arrive at the optimized parameters used for the first prototype.

3.1 Performance Evaluation Method

Before selecting parameters for a design, it is necessary to have a quantitative method of evaluating the result. The design proposed in this study must have a number of qualities:

1. The flow division error should be low. This error has both dynamic and steady state components, as defined later in this section.
2. The pressure losses across the valve should be low.
3. There should be no signs of instability.
4. The design should be inexpensive and easy to manufacture.

In order to test the dynamic response of the valve, it is necessary to have a standard test and load. The simplest test to simulate is to apply a step in one of the load pressures. However, in practice a step in pressure can be very difficult to achieve, in order to experimentally verify the simulation. Therefore, a practical load must be added to the model. The simplest load is an orifice. If a turbulent, sharp-edged orifice and small line volume are added to each branch of the model, four additional equations are introduced to describe the pressure and flow to the loads:

$$P_{L1} = \frac{\beta}{V_{L1}} \int (Q_{L1} - Q_{Lo1})\, dt \tag{3.1}$$

$$P_{21} = \frac{\beta}{V_{L2}} \int (Q_{L2} - Q_{Lo2})\, dt \tag{3.2}$$

$$Q_{Lo1} = C_{dL1} A_{L1} \sqrt{\frac{2}{\rho} P_{L1}} \tag{3.3}$$

$$Q_{Lo2} = C_{dL2} A_{L2} \sqrt{\frac{2}{\rho} P_{L2}} \tag{3.4}$$

The model now has inputs of Q_s, ϕ, A_{L1}, and A_{L2} (the load orifice areas). As a standard test, the rotary position of the spool is centred ($\phi = \phi_0/2$) and a flow of $Q_s = 1 \times 10^{-3}\ m^3/s$ is applied. The orifice areas are initially set so that the steady state load pressures are 10 MPa. The simulation is allowed to reach steady state; then the orifice area of branch 1 is decreased such that the steady state load pressure rises to 15 MPa (while the other area is held constant). In an industrial setting, these values of flow and pressure would typically be matched to the desired application. However, as this is a research valve, the values were arbitrarily selected to be compatible with the equipment and instrumentation available in the university laboratory. Figure 3.1 show the flows resulting when the simulation is run using the arbitrary non-optimum parameters found in Appendix B.

For this standard test it is necessary to develop a method of evaluating the response, based on the criteria outlined earlier. The first quality is relatively straight-forward: error. The most common measure of error is steady state error, defined for a typical flow divider as

$$\%E_{ss} = \frac{Q_{L1} - Q_{L2}}{Q_s} \times 100\% \tag{3.5}$$

evaluated at steady state. However, this assumes that the ratio of output flows is 50-50. As the novel feature of the proposed valve is the ability to change the flow division ratio, a new definition of steady state error is required. The following definition is proposed which allows for changing division ratios:

$$\%E_{ss} = \frac{|Q_{L1} - Q_{L1d}| + |Q_{L2} - Q_{L2d}|}{Q_s} \times 100\% \tag{3.6}$$

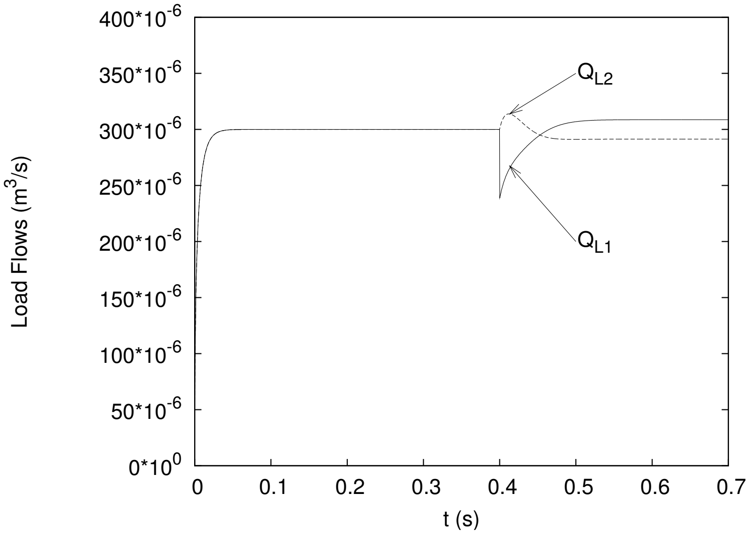

Figure 3.1: A sample step response of the simulated valve. This shows the two outlet flows responding to a step change in one of the load pressures. This simulation was calculated using the non-optimum parameters found in Appendix B.

where the subscript "d" signifies the desired flow, calculated using equation 2.6 from the ideal steady state analysis.

Guo (1987) noticed that when a flow divider is used to synchronize two hydraulic actuators, there can be a significant positional error accumulated before the system reaches steady state. This is due to the large temporary flow dividing error that occurs before the valve can compensate. Guo defined this cumulative error for a 50:50 divider ratio as

$$E_{CU} = \int_0^{t_{cum}} (Q_{L2} - Q_{L1})\,\mathrm{d}t. \tag{3.7}$$

where t_{cum} is the test time. In this study, a modified version is proposed which takes into account the possibility of a changing divider ratio:

$$E_{CU} = \int_0^{t_{cum}} [(Q_{L1} - Q_{L1d}) - (Q_{L2} - Q_{L2d})]\,\mathrm{d}t. \tag{3.8}$$

It can be informative to separate the total cumulative error into dynamic and steady state portions, as shown in Figure 3.2. The cumulative steady state error is

$$E_{CUSS} = [(Q_{L1ss} - Q_{L1d}) - (Q_{L2ss} - Q_{L2d})]\,t_{cum} \tag{3.9}$$

where Q_{Lss} is the steady state flow. The cumulative dynamic error is then

$$E_{CUDY} = \int_0^{t_s} [(Q_{L1} - Q_{L1ss}) - (Q_{L2} - Q_{L2ss})]\,\mathrm{d}t \tag{3.10}$$

where t_s is the settling time, defined as the time at which the flows settle to within 2% of their final value.

These can also be written as a percentage of the cumulative source flow, Q_s,

$$\%E_{CUSS} = \frac{[(Q_{L1ss} - Q_{L1d}) - (Q_{L2ss} - Q_{L2d})]\, t_{cum}}{Q_s\, t_{cum}} \times 100\% \tag{3.11}$$

$$\%E_{CUDY} = \frac{\int_0^{t_s} [(Q_{L1} - Q_{L1ss}) - (Q_{L2} - Q_{L2ss})]\, \mathrm{d}t}{Q_s\, t_{cum}} \times 100\% \tag{3.12}$$

Note that the t_{cum} terms in 3.11 cancel, so this equation is identical to equation 3.6, with the exception of the absolute value operator.

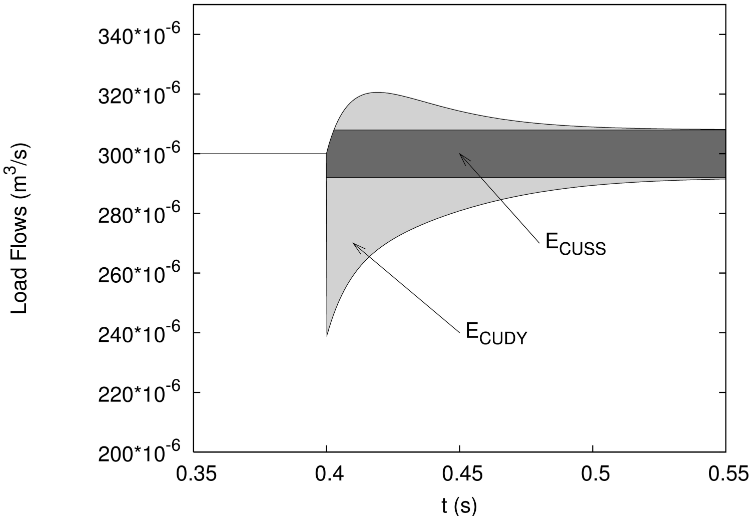

Figure 3.2: A sample flow result showing the cumulative steady state error, E_{CUSS}, and the cumulative dynamic error, E_{CUDY}, for the case of equal flow division. The total cumulative error, E_{CU}, is the sum of the two.

Thought must be put into the selection of the test length, t_{cum}, when comparing cumulative errors as this determines the weighting of the dynamic and steady state contributions to the total cumulative error. For example, if a test time close to the settling time is chosen, the steady state portion is less important than the dynamic part. However, as the test time increases, the contribution of the steady state error grows, but the dynamic portion stays constant, decreasing its relative importance. The intended application of the valve should be used to determine t_{cum}; for example, if the valve was to be used to drive conveyors, a very large time would be chosen, as the load pressure is likely constant over periods of minutes or hours. Conversely, if the valve was to be used to control fuel flow to an engine, the load pressure changes occur on the order of milliseconds. Again, as this is a research valve, the test time was selected somewhat arbitrarily as $0.2s$, which should be suitable for mobile industrial equipment.

The first two qualities required of the valve, steady state and dynamic accuracy, have been considered. The third quality, pressure loss, needs a few words of explanation. The purpose of the flow divider valve is to maintain a set ratio of flows by controlling the pressure drop across the adjustable orifices to compensate for the difference in load pressure. Therefore, it is impossible to reduce the pressure drop across one branch of the valve beyond this load pressure difference. However, the pressure drop in the other branch can theoretically go to zero, and should be reduced as much as possible. The valve with the best efficiency (and heat production traits) is one that causes the lowest pressure drop *in the branch with the greater load pressure.* For the rest of this report, when the pressure drop across the valve is discussed, this is the intended meaning.

The fourth quality, instability, could be determined by linearizing the model equations and applying the Routh-Hurwitz criterion (Phillips and Harbor, 2000). For a complex non-linear system, it can be difficult to ensure stability, as the calculation must be repeated for all possible operating points. Since a numerical simulation is available, the results of the Matlab/Octave simulation can be used to determine possible regions of instability.

The final criteria, ease and cost of manufacturing, is perhaps too complex to leave to a computational algorithm to determine an accurate value, as finding a single function that can estimate manufacturing time and cost requires years of experience and expertise beyond that of the author. However, it is possible to qualitatively evaluate certain aspects of the design. For example, it is more difficult and expensive to manufacture a valve with very small clearances (requiring tight tolerances) than one with larger clearances and looser tolerances. Since no way of automatically calculating a quantitative value for this item was available, it will only appear in the analysis in a qualitative form.

3.2 Relationships Between Parameters

While the parameters used in the model equations have physical meaning, they may often not have an obvious effect on the performance of the valve; indeed, two parameters may work in combination in terms of performance effects. For example, if the spool cross-sectional area increases, so should the mass. This section outlines these relationships between parameters.

The first relation involves the spool radius, r and the spool end area:

$$A = \pi r^2 \tag{3.13}$$

The spool mass is given by

$$m = MR\ A\ L_t \rho_{steel} \tag{3.14}$$

where

MR = mass ratio of the machined spool to that of a solid spool of the same diameter and length with no material removed,

L_t = spool total length, and

ρ_{steel} = density of steel.

The ratio of the spool's total length to the sum of the length of lands is used to find the land length

$$L_L = L_L \frac{L_t}{L_L} \tag{3.15}$$

which is needed to calculate the viscous damping of the spool. Assuming that the radius of the spool is large relative to the clearance, Couette flow analysis can be used to determine the viscous friction factor, B_f:

$$B_f = \frac{2\pi r L_L \mu}{\delta}. \tag{3.16}$$

For a typical divider valve, the steady state error is inversely proportional to the pressure drop across the fixed orifice (Kwan, 1978). Although the proposed valve has a different configuration, there is a similar relationship. Therefore, rather than specifying an orifice diameter for the fixed orifice, it is more useful to specify a desired pressure drop, ΔP_o, at a given flow, Q_{so}, using

$$A_o = \frac{Q_{so}}{C_{do}\sqrt{\frac{2}{\rho}\Delta P_o}} \tag{3.17}$$

for each branch.

Similarly, the adjustable orifices can be sized using a desired pressure drop and flow when the orifice is fully open. For a circular ports the radius, r_v is given by

$$r_v = \sqrt{\frac{Q_{so}}{C_{dv}\pi\sqrt{\frac{2}{\rho}(\Delta P_t - \Delta P_o)}}} \tag{3.18}$$

where ΔP_t is the desired total pressure drop across the valve. It is also useful to specify the valve opening when the spool is centred by a fraction rather than by length, so

$$d_o = r_v(1 - 2FO) \tag{3.19}$$

where FO stands for fraction open.

The spool end volumes should increase to accommodate a larger spool or longer maximum stroke, x_{max}, so

$$V_{1o} = (L_{v1} + x_{max})\, A \tag{3.20}$$

and

$$V_{2o} = (L_{v2} + x_{max})\,A \tag{3.21}$$

where L_v is the clearance between the spool and the cap of the valve chamber at the end of its stroke.

The flow chamber volumes can be calculated geometrically. If one assumes that half of the radius is machined away between lands for a length of L_a, the volume in each chamber is

$$V_a = \pi\left(r^2 - \left(\frac{r}{2}\right)^2\right) L_a. \tag{3.22}$$

The above equations, together with the model developed in Section 2.3, were used to evaluate the effects of various parameters. The results of this analysis are presented in Section 3.4.

3.3 ODE Solution Method

The system of equations developed in Chapter 2 can be classified as a system of stiff, nonlinear ordinary differential equations (ODEs). For some simple ODEs, it is possible to obtain a closed-form analytical equation for the states with respect to time. However, hydraulic systems are notoriously nonlinear so this method is not typically practical (nor even possible). The system of more than 30 equations used to simulate this valve, many of which are non-linear, is much too complex to attempt an analytical solution. In this case, an approximate solution must be computed numerically. There are many ODE solution algorithms and software packages available, each with strengths and weaknesses. Two similar software packages, Matlab and Octave, were chosen to perform the calculations required to carry out the "`ode15s`" and "`LSODE`" ODE solution algorithms, respectively. Matlab and Octave were selected because they both provide comprehensive mathematic and plotting frameworks and include the programming ability required to automate "batch runs" of simulations. The `ode15s` and `LSODE` solvers are based on the NDF (Numerical Differentiation Formulas) and BDF (Backward Differentiation Formulas), respectively, designed for stiff ODEs and provided the fastest solution times for test equations.

3.4 Sensitivity

In this section, the sensitivity of the valve's performance to the various parameters is evaluated. This evaluation is performed by systematically varying the parameters one at a time and examining the effects when simulating the tests developed in Section 3.1.

The first parameter to be examined is the spool radius. This has effects on the spool end area, pilot groove lengths, leakage path areas, and spool mass. The spool radius was varied over a range of 8 to 20 mm. The resultant load flows are shown in Figure 3.3, and Figures 3.4 and 3.5 show the radius's effects on the cumulative errors, and settling time, respectively (there is little effect on the valve's pressure losses). It should be noted that while these curves appear continuous, they were created from a large number of discrete points. As noted by Kwan (1978), the spool's radius has a pronounced effect on the spool's steady state accuracy, reducing an error of over 4% (8 mm) to zero. However, as the steady state error improves, the dynamic performance degrades, with an increase in dynamic error (in the negative direction). One should notice in Figure 3.4 that while the steady state error is positive (before the absolute value is calculated), the dynamic error is negative, tending to cancel each other out. Therefore, for this loading condition, the total cumulative error goes to zero when the radius is approximately 10 mm. Of course, this depends on the time used to calculate the cummulative error (in this case 0.2 s).

One aspect to notice is what happens when the radius is further reduced to 3 mm. In this case, it appears that control of the valve is lost, as show in Figure 3.6, with the two flows diverging to an extreme dividing error.

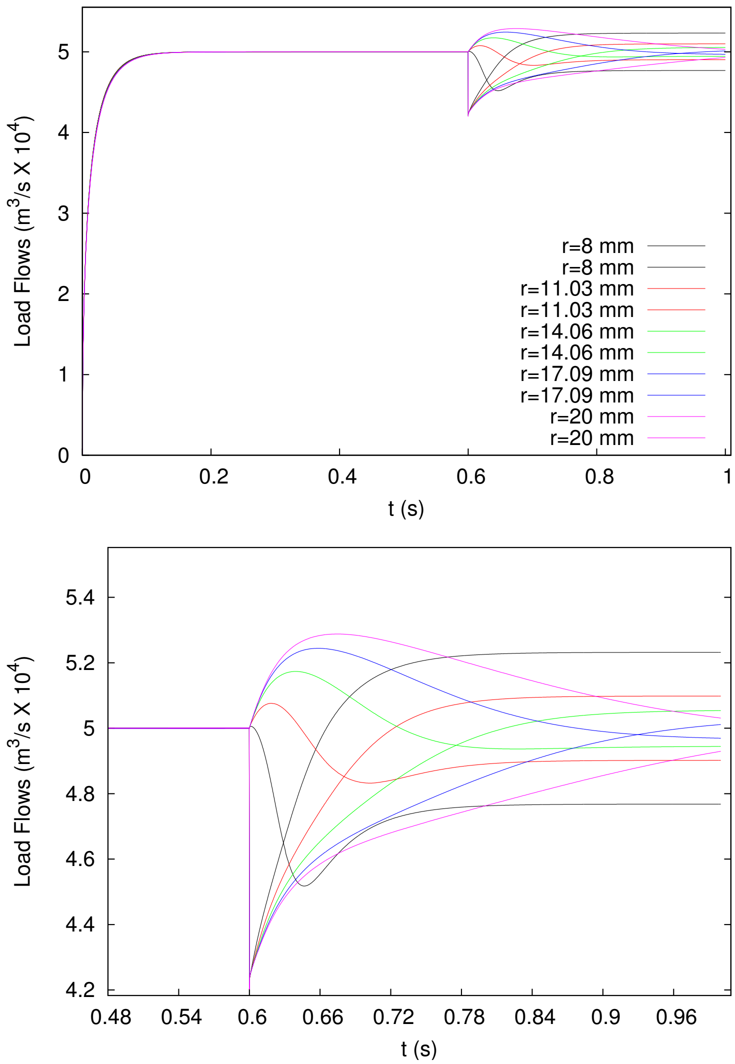

Figure 3.3: Load flow response to a step in load orifice area, showing effect of changing spool radius, r. Lower image is an enlarged view of the step response (with the same color key).

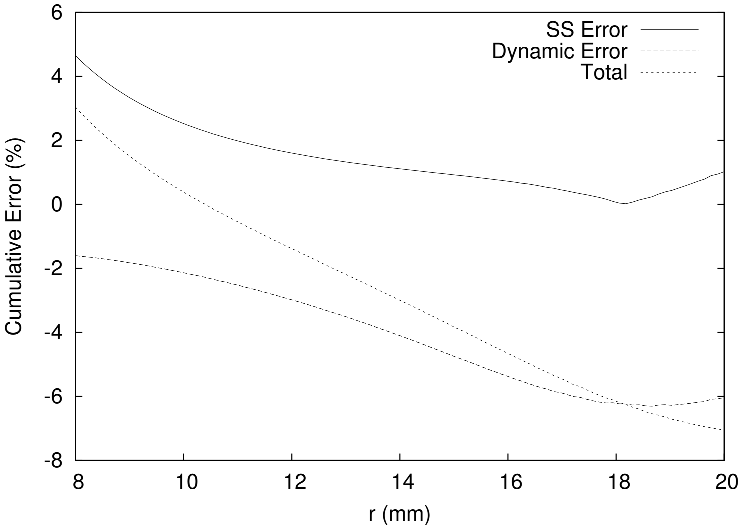

Figure 3.4: Effect of radius on the steady state and accumulated error after 0.2 s

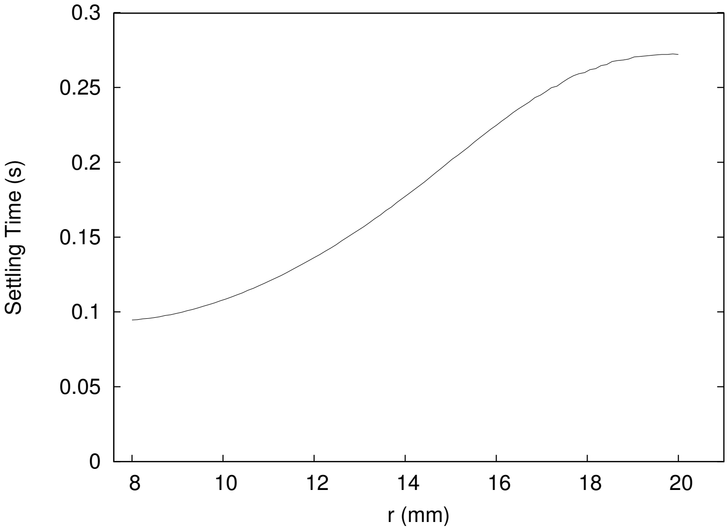

Figure 3.5: Effect of radius on the settling time.

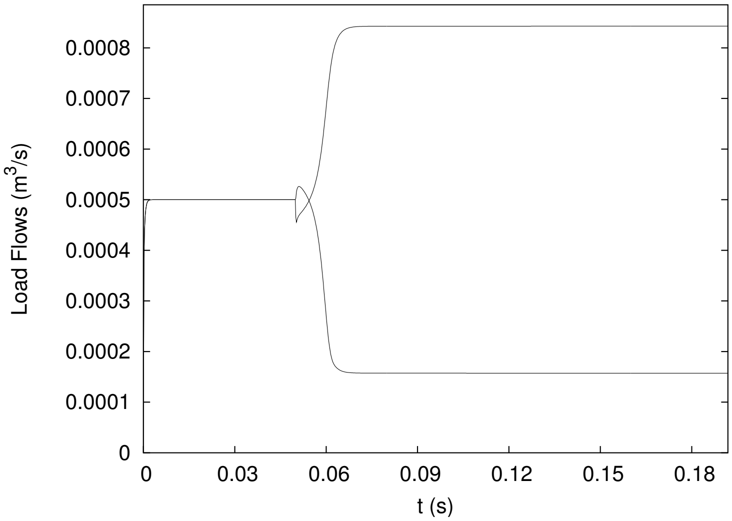

Figure 3.6: The valve appears to show instability with a radius of 3 mm.

The next variable to be examined is the circumferential groove width, b. As the pilot stage geometric constant, c, is given by

$$c = \frac{6b^4h}{185r^2\delta^3}, \tag{3.23}$$

and includes b to the fourth power, this can be expected to have an important effect on the valve (see equation 2.21). The simulation was run with values of b between 0.3 and 2.0 mm. The results are shown in Figures 3.7 through 3.9. These curves show a complex shape, as a number of factors come into play. For smaller widths, the steady state and dynamic errors are relatively small. For very large widths, the groove size becomes comparable to that on the main flow orifice, causing a large portion of flow to bypass the variable orifice, via the pilot stage. In this case, the steady state error becomes large, and there may be instability, as shown in the response before the step in Figure 3.7.

As the c constant also includes the clearance, δ, to the third power, one would expect that it too would have a significant effect. The clearance was varied between 0.001 and 0.02 mm. The results are shown in Figures 3.10 through 3.11. This effect is largely related to the steady state properties; the settling time and dynamic error are mostly unaffected. A tighter clearance allows less leakage, which translates into a lower steady state error. The cost of this increase in accuracy is that a valve with a small clearance is more expensive to manufacture and is more prone to failure due to particulate contamination and thermal expansion effects. The tighter clearance does increase the viscous damping force, but this force makes an insignificant contribution to the overall dynamics under most conditions and can be ignored.

Kwan (1978) and many others have stated that one can “buy” accuracy in a flow divider at the cost of pressure losses. This valve configuration is no different. Figures 3.12 to 3.14

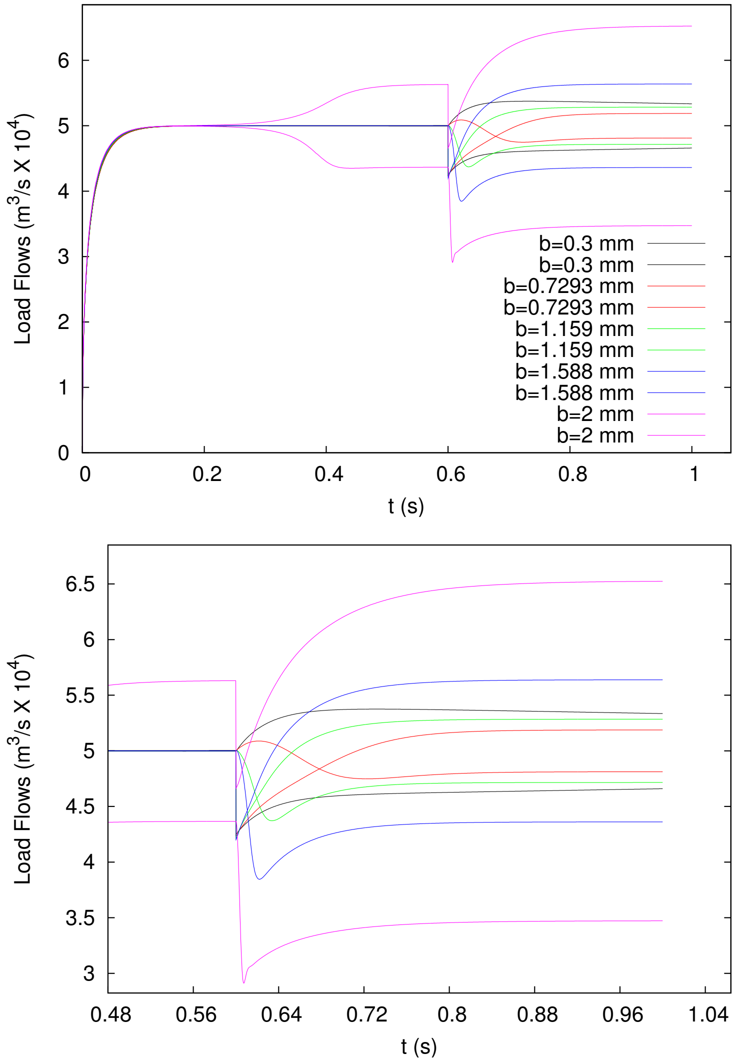

Figure 3.7: Load flow response to a step in load orifice area, showing effect of changing the circumferential groove thickness, *b*. Lower image is an enlarged view of the step response (with the same color key).

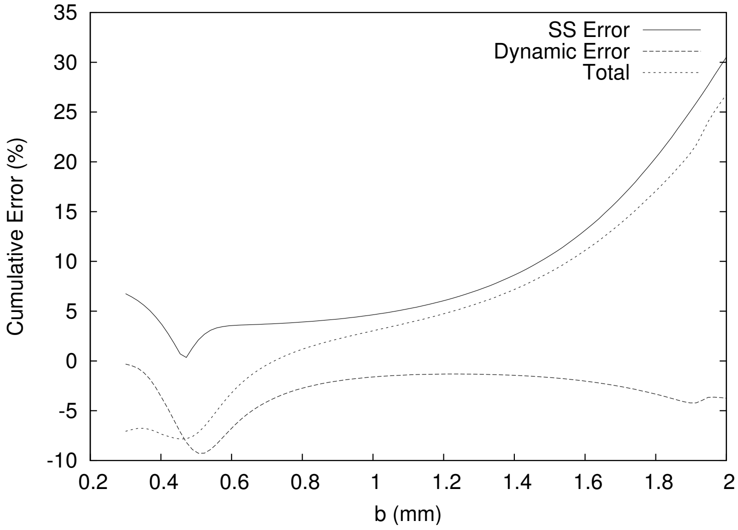

Figure 3.8: Effect of groove thickness on the accumulated error after 0.2 s

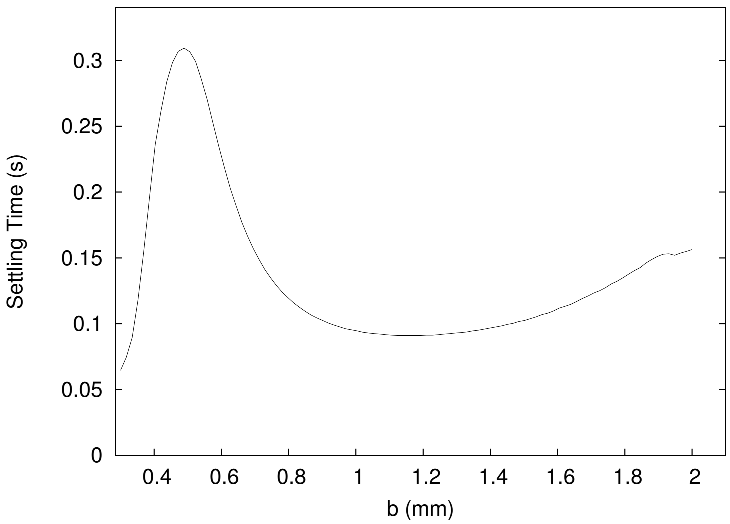

Figure 3.9: Effect of groove thickness on the settling time.

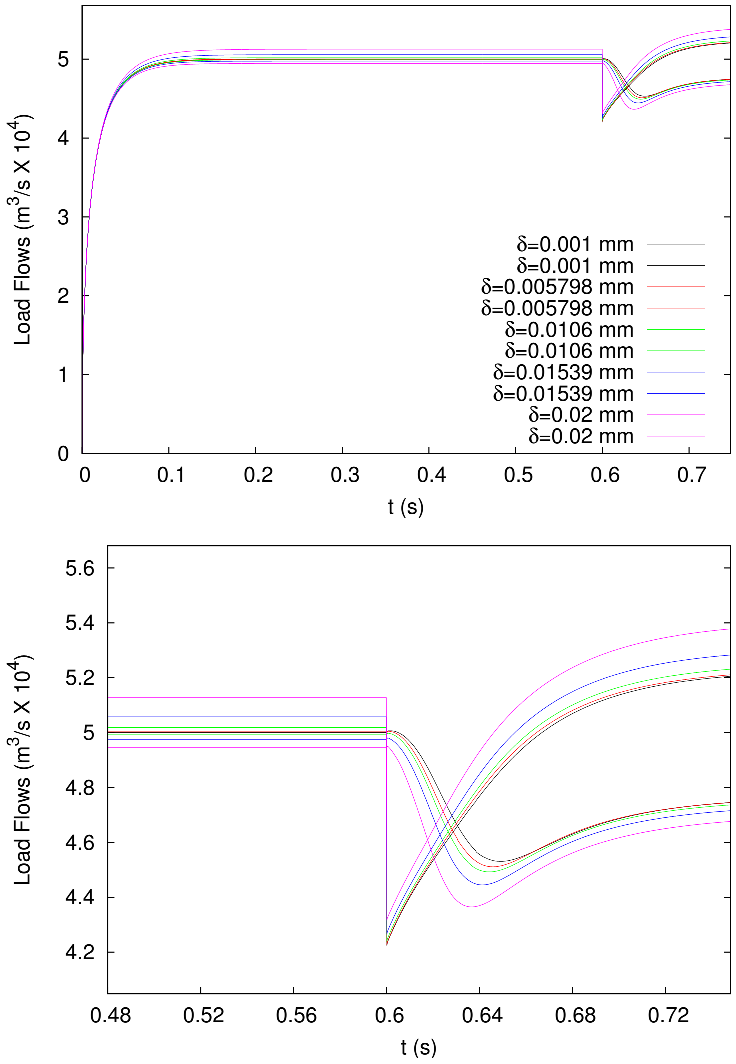

Figure 3.10: Load flow response to a step in load orifice area, showing effect of changing the spool's radial clearance, δ. Lower image is an enlarged view of the step response (with the same color key).

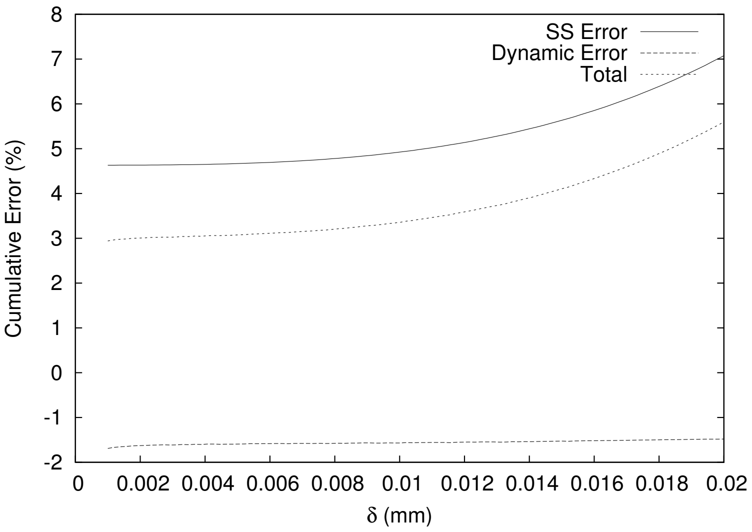

Figure 3.11: Effect of clearance on the accumulated error after 0.2 s

show the effect of varying the total pressure drop across the valve (by changing the orifice sizes). Notice that if the pressure drop is too small, the flows overshoot. As the pressure drop increases, both the dynamic and steady state error decrease, as does the settling time. It must be noted that the pressure drop described in this section is the pressure drop when the the load pressures are equal (as defined in equation 3.18), and can change when the load pressures are different.

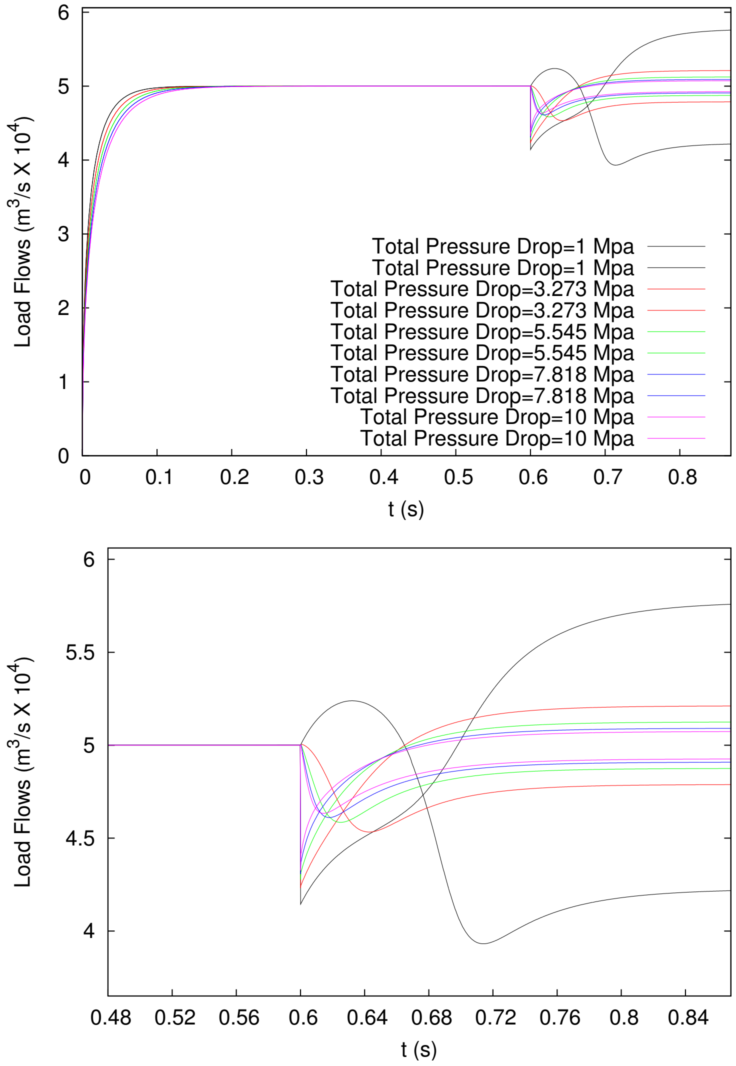

Figure 3.12: Load flow response to a step in load orifice area, showing the effect of changing the pressure drop, ΔP_t. Lower image is an enlarged view of the step response (with the same color key).

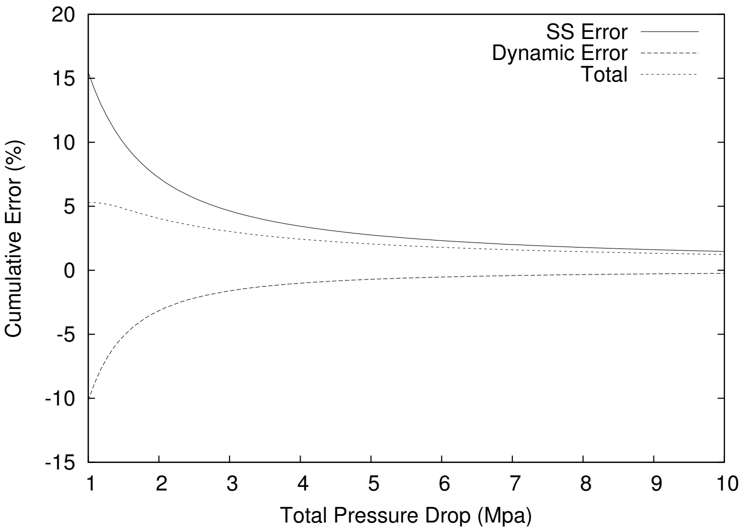

Figure 3.13: Effect of the total pressure drop on the accumulated error after 0.2 s

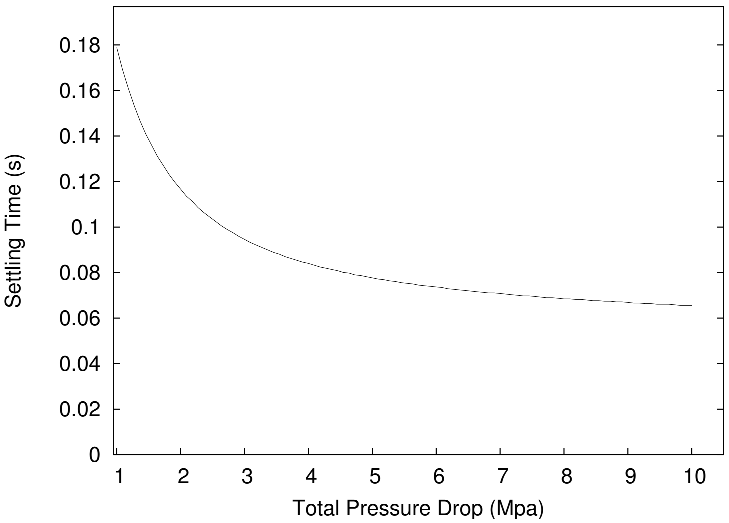

Figure 3.14: Effect of pressure drop on the settling time.

Related to the total pressure drop, the ratio of pressure drops across the fixed orifice to the total pressure drop also has an effect (as shown in Figures 3.15 through 3.17). This ratio has quite a strong effect on both the steady state error and the dynamic error. Both the dynamic and steady state error decrease as the portion of the pressure drop across the fixed orifice increases. Again, notice that the dynamic and steady state error act in opposite directions, and cancel each other out at a ratio of about 0.95.

Another related parameter is how open the variable orifices are when the spool is centred. This fractional opening (defined in equation 3.19) has strong effects on both types of accuracy, settling time and pressure drop. The settling time increases as the fractional

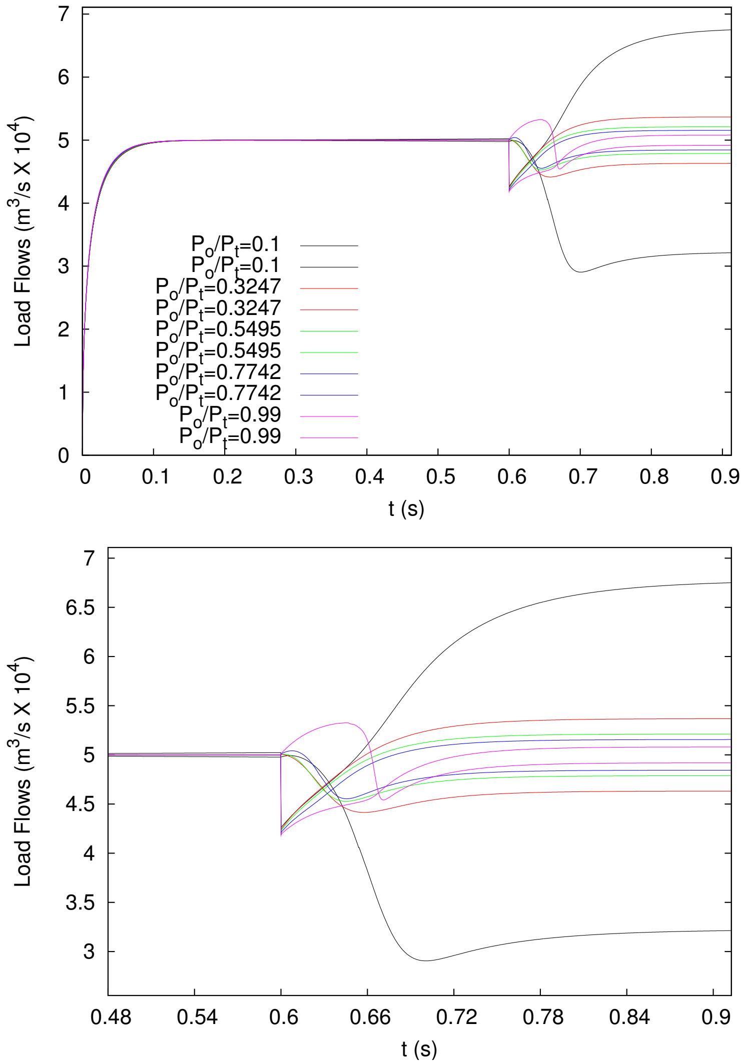

Figure 3.15: Load flow response to a step in load orifice area, showing the effect of changing the ratio of the pressure drop across the fixed orifice to the total drop. Lower image is an enlarged view of the step response (with the same color key).

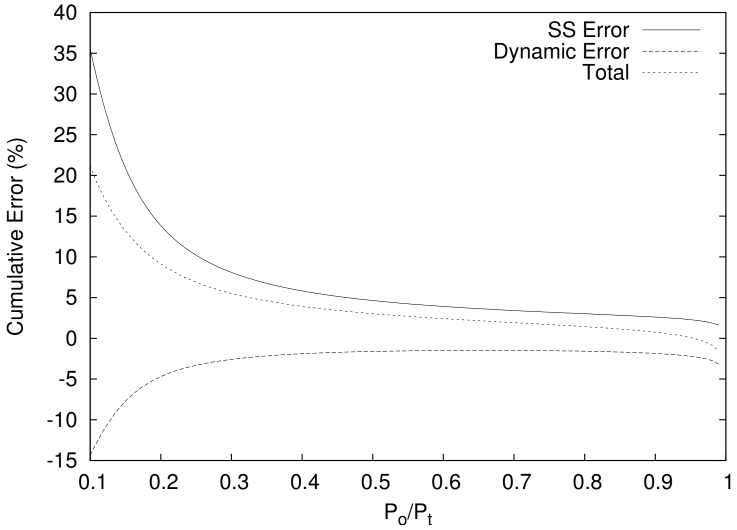

Figure 3.16: Effect of the pressure drop ratio on the accumulated error after 0.2 s

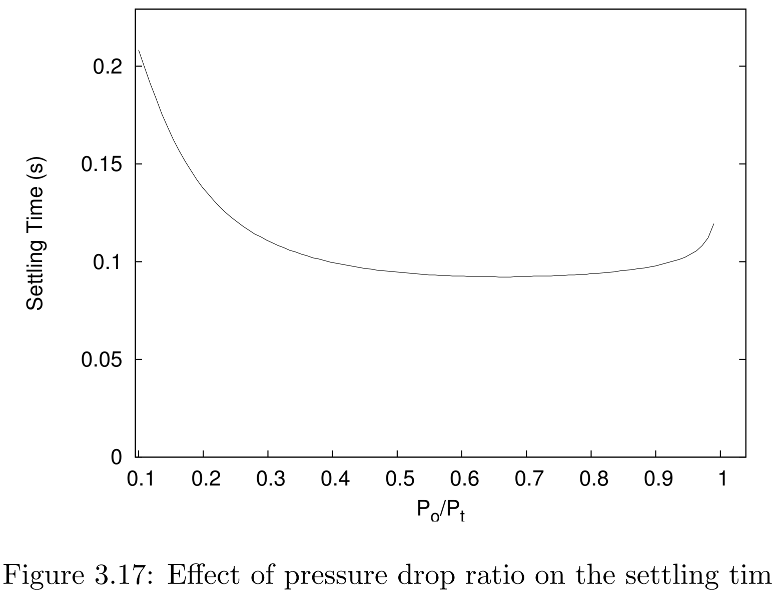

Figure 3.17: Effect of pressure drop ratio on the settling time.

opening increases, since the spool must move further to reach the equilibrium point and pressure builds up more slowly. This effect also shows up as an increase in dynamic error. The steady state error also increases with a larger fractional opening. Unfortunately, as the fraction open decreases, there is more restriction in the non-regulated branch so the source pressure must increase, as shown in Figure 3.20.

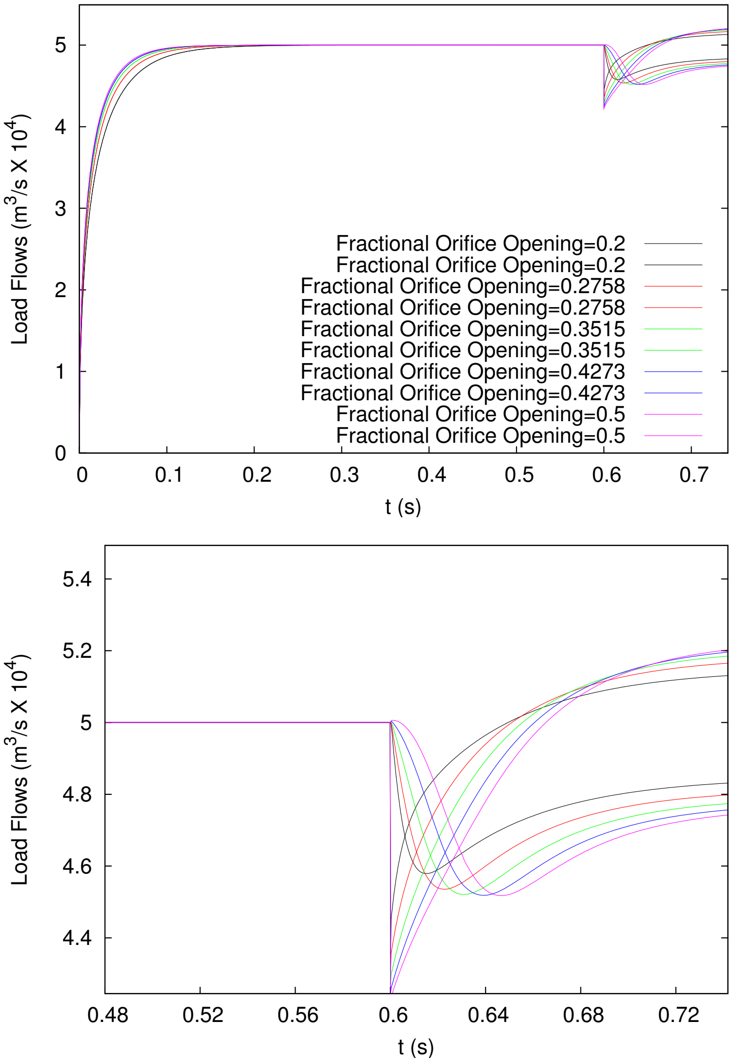

Figure 3.18: Load flow response to a step in load orifice area, showing the effect of changing the fraction that the variable orifices are open when the valve is centred.

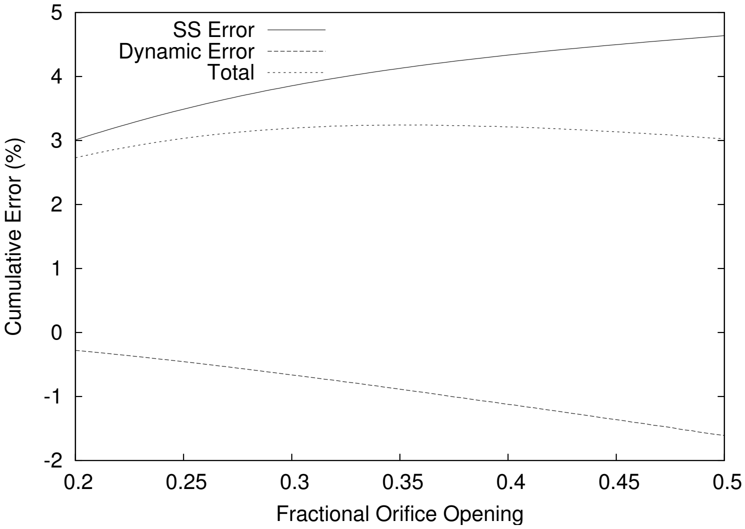

Figure 3.19: Effect of the opening fraction on the accumulated error after 0.2 s

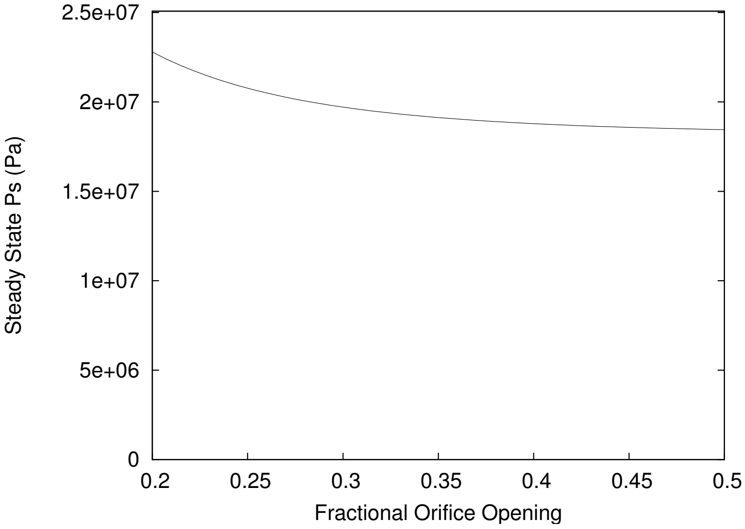

Figure 3.20: Effect of opening fraction on the steady state source pressure

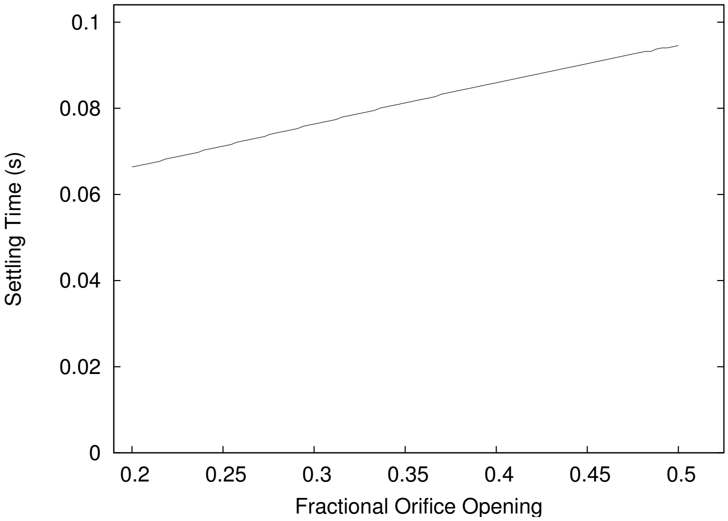

Figure 3.21: Effect of opening fraction on the settling time.

Referring to equation 2.17, the flow forces are proportional to the thickness of the rim, t_{rim}. As such, the errors due to this force should also depend on the rim thickness. This is largely the case (refer to Figures 3.22 to 3.23). While the effect is not especially noticeable in the the dynamic response, the steady state error shows a nearly linear relationship and could theoretically go to a value very near zero if the the rim could be made infinitely thin. This shows that the flow forces are the largest contributor to steady state error with this parameter set. The cost of *this* increase in accuracy is that as the rim becomes thinner, it becomes weaker, less durable, and more difficult to machine.

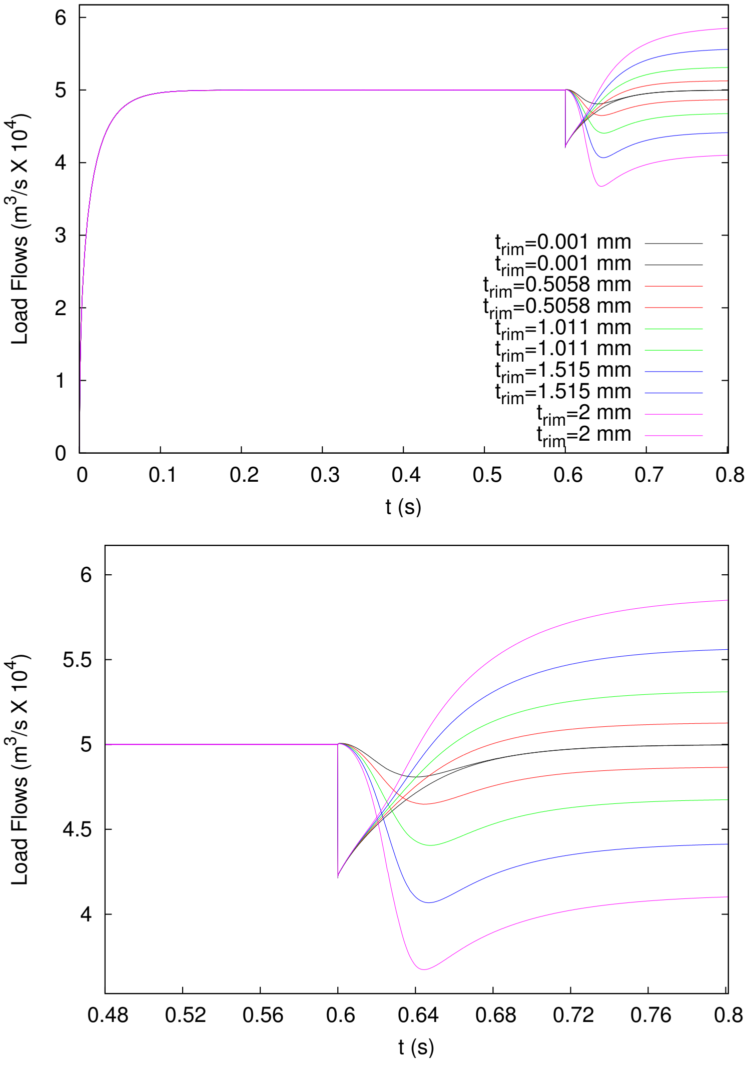

Figure 3.22: Load flow response to a step in load orifice area, showing the effect of changing the rim thickness, t_{rim}. Lower image is an enlarged view of the step response (with the same color key).

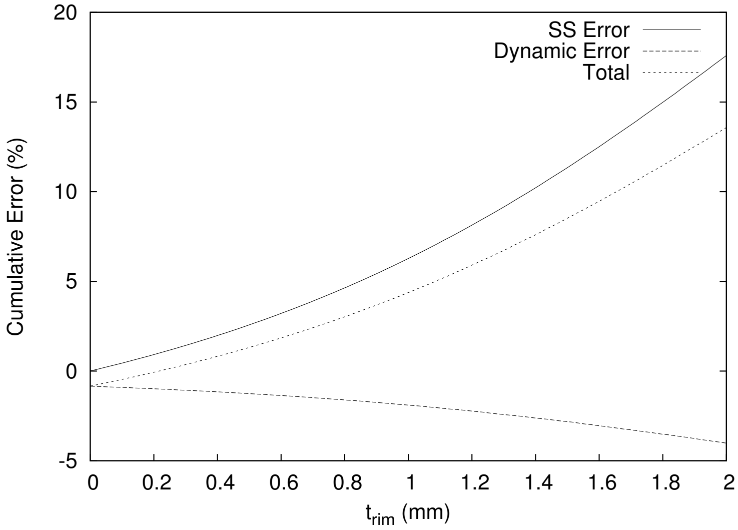

Figure 3.23: Effect of the rim thickness on the accumulated error after 0.2 *s*

Although Coulomb friction is not exactly a design parameter (in that it can not be directly controlled), its effect is important to examine because it is not easy to predict theoretically. Therefore, it is important to simulate the response of the valve over the range of possible values. In this case, the simulation was run with friction values, F_c, covering the expected range of of 0 to 10 N. The Coulomb friction does have quite a strong effect on the steady state error although it appears to act counter to the other sources, reducing the total steady state error (see Figure 3.25). From the results shown in Figures 3.24 and 3.25, Coulomb friction does not have a major effect on the dynamic response, so the uncertainty in its value is not likely to cause instability.

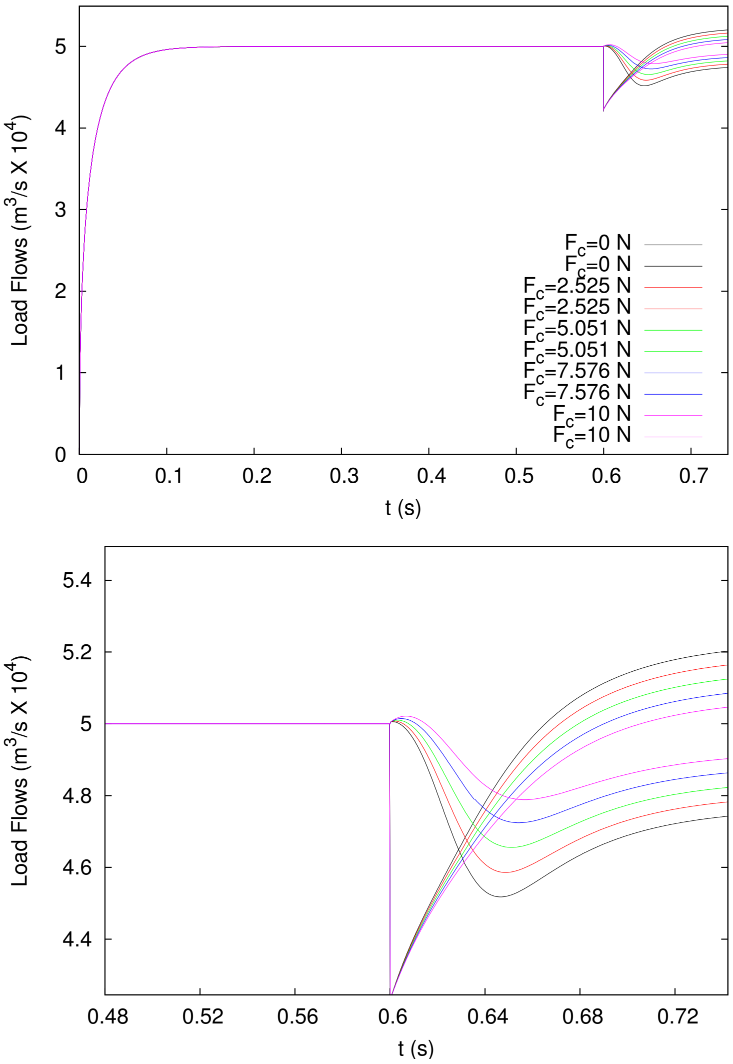

Figure 3.24: Load flow response to a step in load orifice area, showing the effect of changing the Coulomb friction, F_c. Lower image is an enlarged view of the step response (with the same colour key).

Another parameter that has an unknown value is the fluid's viscosity, which is temperature

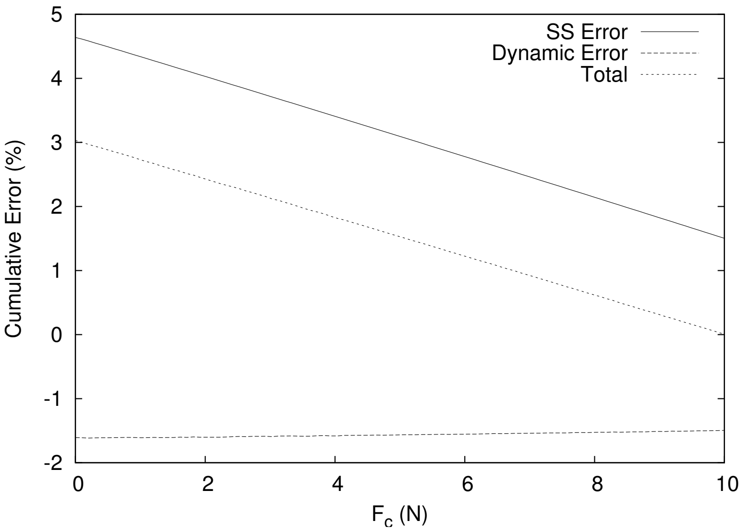

Figure 3.25: Effect of Coulomb friction on the accumulated error after 0.2 s

dependent. It is important that the valve work over a range of temperatures. The simulated test was run with kinematic viscosities ranging from 15 to 66 mm^2/s, corresponding to the viscosity of Nuto 30 hydraulic oil between temperatures of 60 and 25$°C$, respectively. The results are shown in Figures 3.26 to 3.28. While these results show that temperature will have a small effect on the proposed valve's performance, they do not show the valve to be unuseable under any expected conditions.

All the remaining parameters have relatively small effects on the valve's performance, so can be selected for ease of manufacturing or assembly.

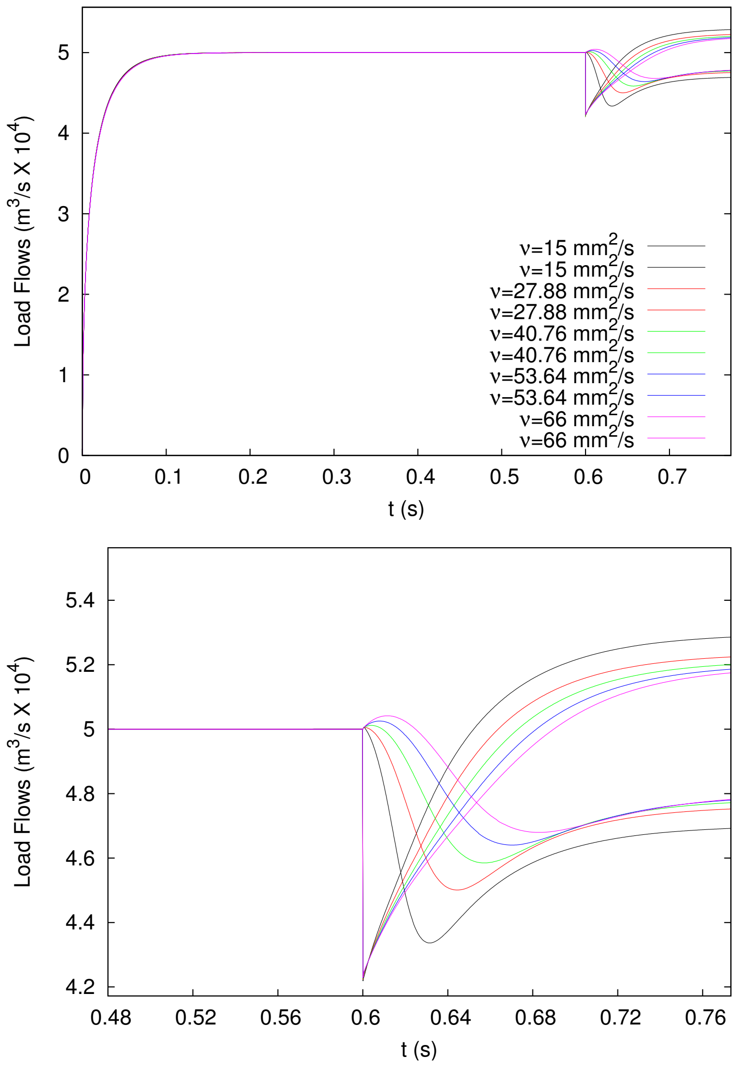

Figure 3.26: Load flow response to a step in load orifice area, showing the effect of changing the viscosity, ν. Lower image is an enlarged view of the step response (with the same color key).

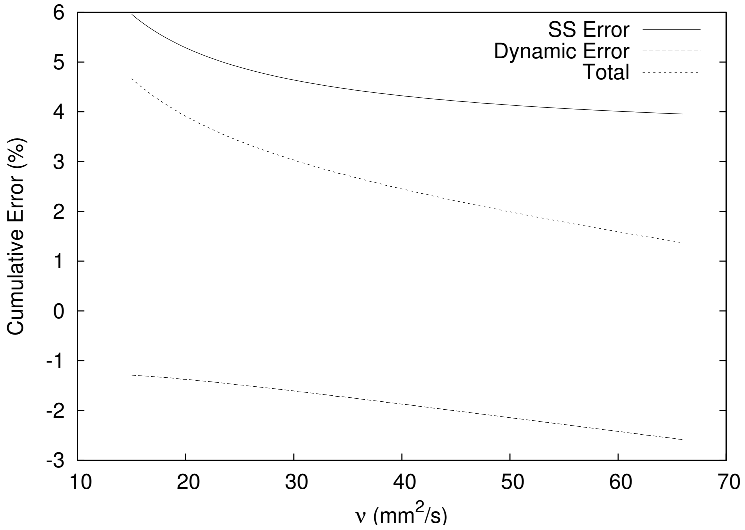

Figure 3.27: Effect of the viscosity on the accumulated error after 0.2 s

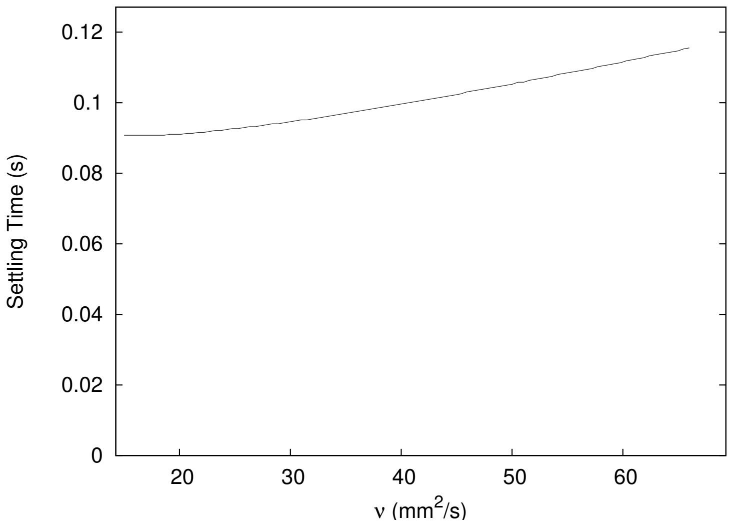

Figure 3.28: Effect of viscosity on the settling time.

3.5 Optimization of Parameters

In the previous section, the effects of the various physical parameters were examined. Most parameters show a trade-off of one objective for another. For example, by increasing the fixed orifice area, valve accuracy can be increased, but at the cost of reduced efficiency. This section presents the method used to determine the optimum parameters used for the first valve prototype. Much of the analysis contained in this section is based on the excellent work found in Andersson (2001) which is recommended reading before undertaking any similar optimization.

As detailed in Section 3.1, there are five main performance criteria desired of the valve prototype:

1. low steady state error,
2. low dynamic error,
3. low pressure losses,
4. stable, and
5. cheap and easy manufacture.

The qualitative effect of parameters on these qualities can be displayed in tabular form using the "House of Quality" (Andersson, 2001), shown in Table 3.1. In this table, a higher number indicates that the parameter has a strong effect on the objective, while a blank or low number shows a weak relationship. The table also includes a column ranking the importance of each objective (higher numbers mean more important and a "D" stands for a demand requirement; for example, the valve *must* be stable, but there is no advantage to being "more" stable). This table can be used to help determine which parameters should be included in the optimization.

Table 3.1: House of Quality

	weight	r	b	δ	ΔP_t	$\frac{P_o}{P_t}$	FO	t_{rim}
steady state error	3	4	3	4	4	2	1	4
dynamic error	3	3	3	1	4	2	3	1
pressure losses	1		1		4	2	3	
stability	D	4	2	1	3	1	1	1
cost	2	2	2	4				3

Since there are a number of objectives that work in opposition to each other, this problem is classified as a "multiobjective optimization problem". A number of researchers have examined this type of problem. One approach to this problem is to combine the objectives into one aggregate number, which is referred to by a number of terms such as the fitness or cost function. The major drawback of this approach is that it is often difficult to quantitatively compare the value of two different qualities, for example, accuracy and pressure drop. The goal attainment method was used to partially overcome this problem, and is explained in Section 3.5.3.

Once the aggregation function has been chosen, one must pick a method of minimizing (or maximizing) the function. As the problem being studied in this study is highly non-linear, many of the standard methods of optimization are not valid. Also, since the calculation of the objective values is based on numerical simulation, no analytical function for any derivatives is available. This eliminates many gradient or hill-climbing methods. Andersson (2001) suggests two methods of solving this type of problem: the Complex Method and a Genetic Algorithm, which are presented in the next two sections.

3.5.1 Complex Method

The complex method is a fast way to optimize functions when no derivatives are available. Its “quickness” exhibits itself in two ways; the algorithm itself is computationally efficient, and it is very easy to implement (there is little need to optimize the optimization routine for a specific problem).

In order to use the complex method, the objective functions must be aggregated into one fitness function (see Section 3.5.3). The first step is to randomly select a number of points in the parameter space, checking to make sure no constraints are violated. The number of points must be greater than the number of parameters and is typically double the number of parameters. The fitness of each point in the “population” is then calculated. The worst point is removed from the population and a new point is added, on a line through the centroid of the remaining points (as shown in Figure 3.29). A random component is added to this point to ensure all of the population’s values for a certain parameter don’t collapse to the same number. If the newly generated point is better than the worst point (which was removed) the new point enters the population and the process is repeated. If the new point is not an improvement, the point is moved toward the centroid until an improvement is achieved. The process is then repeated until the solution converges to the desired accuracy. Details on the implementation of this algorithm can be found in Appendix C.

3.5.2 Genetic Algorithm

A genetic algorithm is based on the theory of evolution in nature, in which fitter individuals are more likely to procreate, producing offspring which resemble their parents. Like the

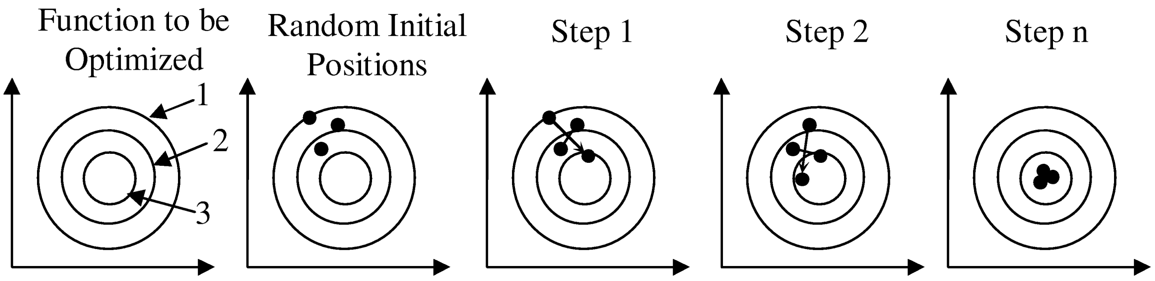

Figure 3.29: The complex method used to solve a two-dimensional optimization problem with the optimum located in the centre. The initial population is randomly distributed in the parameter space. For each step, the worst point it reflected through the centroid of the remaining points. (Figure based on Andersson (2001))

complex method, it requires no knowledge of the derivatives of the fitness function. The greatest advantage of genetic algorithms is their robustness; they can reliably find global optimum of a wide range of different types of functions with little prior knowledge of the function topography.

The implementation of a genetic algorithm is more involved than the complex method, although there are a number of readily available toolboxes to base the code on. In this case, the "GAOT" toolbox for Matlab was used. As with the complex method, a population of initial points is randomly selected in the parameter space, and their "fitness" is evaluated, typically based on the aggregation of the desired objectives. Two (or more) parents are then selected to "breed", based on one of a number of algorithms. These selection algothithms generally select the parents randomly with weighting applied to bias the selection toward fitter individuals. The parameters of the parents are then combined (using one of a number of "crossover" algorithms) to create the offspring individual, which then enters the population and the cycle continues. Mutations can be used to maintain genetic diversity. As in nature, mutations are random changes in parameter values, which are then passed on hereditarily. Refer to Appendix C for more details with respect to the actual implementation.

3.5.3 Aggregation of Objectives

If one can aggregate the multiple objectives into one value for the "goodness" of a solution, a search can be made for the best combination of parameters to achieve this. Following the goal attainment method (Matlab, 2002), a general aggregate objective function can be calculated by trying to minimize the maximum value of the matrix λ which is equal to

$$\lambda_i = \frac{F_i(X) - F_i^*}{F_i^*} w_i \tag{3.24}$$

where $F_i(X)$ is the i^{th} objective for the parameter vector X, F_i^* is the goal for that objective, and w_i is the weight assigned to that objective (from the House of Quality). Notice that the weight vector used in this formulation is the reciprocal of that suggested by the Matlab documentation, which presents the weight in a counter-intuitive form where a lower value means the objective is more important. In this formulation, a greater weight signifies greater importance. The F_i^* in the denominator scales the objectives so that the weights are directly comparable.

The House of Quality used for the optimization is shown in Table 3.2. In this case, the spool clearance and rim thickness do not appear as they are set at $\delta = 3\ \mu m$ and $t_{rim} = 0.8\ mm$, based on an estimate of the best values possible, supplied by the machinist who was to produce the prototype. The objectives ease and cost of manufacture also do not appear, as they are difficult to quantify (see Section 3.1). The weights are assigned to the criteria based on the application at hand and the values under the parameter columns are based on the sensitivity analysis, with "0" meaning no effect on that criteria and "4" signifying a strong effect.

The weights given to the parameters are qualitatively based on the sensitivity analysis of the previous section.

Table 3.2: House of Quality

criterion	weight	r	b	ΔP_t	$\frac{P_o}{P_t}$	FO
steady state error (see eqn. 3.6)	3	4	3	4	2	1
dynamic error (see eqn. 3.10)	3	3	3	4	2	3
pressure losses (see pg 23)	1	0	1	4	2	3
stability	D	4	2	3	1	1

Based on the House of Quality, the most important parameters were selected for optimization, namely, r, b, ΔP_t, $\Delta P_o/\Delta P_t$, and FO. A genetic algorithm and the complex method[1] were used in parellel to minimize the above function, and the resultant parameter set is shown in Table 3.3. This parameter set was then used to manufacture the first prototype (machining drawings can be found in Appendix D). An experimental evaluation of this prototype is presented in the next chapter.

Table 3.3: Optimized Parameters

r	13.3 mm
b	1.35 mm
ΔP_t	7.91 MPa
$\Delta P_o/\Delta P_t$	0.886
FO	0.421

---

[1] The code used can be found in Appendix C

Chapter 4

Experimental Verification

4.1 Introduction

In the previous chapter, a nonlinear multi-objective optimization strategy was used to determine the optimum physical parameters for a prototype valve. This valve was then manufactured by machine shops in Hangzhou, China and Saskatoon, Canada. The production process demanded very precise machining procedures including Electron Discharge Machining (EDM), cylindrical grinding, and surface hardening to achieve the intricate shapes, smooth finishes (0.2 μm) and small tolerances required (3 μ m).

As this valve was intended to be a research valve, it was designed to be modular, with external (adjustable) fixed orifices and external plumbing. This greatly increased the involved volumes (slowing performance) and introduced pressure losses (reducing the range of division ratios), but the extent of these effects could be estimated using the numerical simulation. Also, many ports were drilled in the casing to facilitate pressure measurements, which also increased the volumes.

The prototype is shown in Figure 4.1 and machining drawings can be found in Appendix D. Notice that the valve block only houses the spool, while the fixed orifices are connected externally.

The circuit used to verify the performance of the valve is shown in Figures 4.2 and 4.3. Counterbalance valves are used as the load and a three-way valve is used to bypass one of the counterbalance valves in an attempt to create a step in the load pressure. An approximately constant source flow was provided by a load sensing pump. This pump was fitted with a reservoir cooler to help control the fluid temperature. Flow measurements were made using drag-type flow meters and pressure measurements were made using a combination of absolute and differential pressure transducers. The output of the transducers was

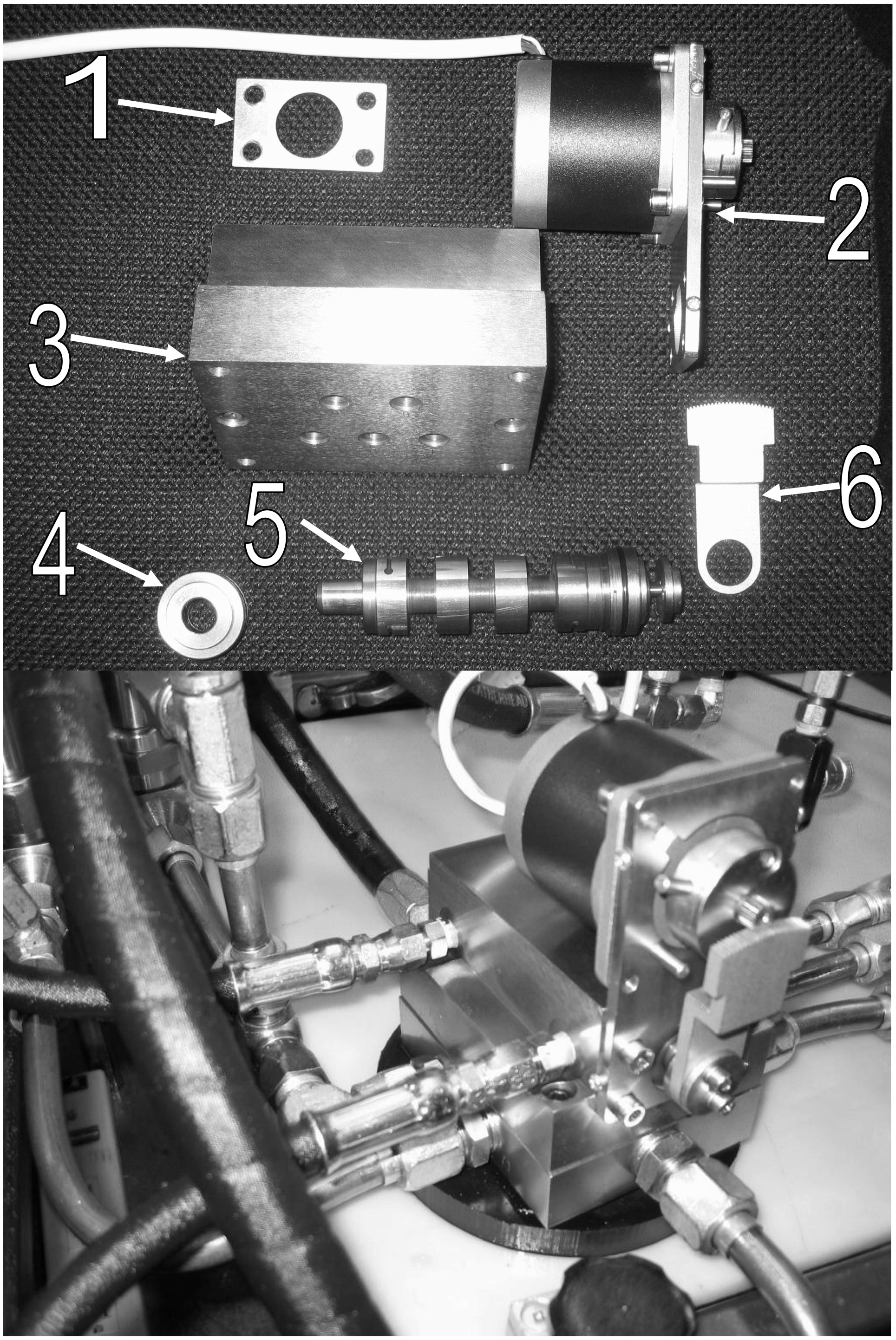

Figure 4.1: Photos of the valve prototype, showing holding plate (1), stepper motor and mounting plate (2), valve block (3), seal gland (4), spool (5), and gear (6).

recorded using a 12-bit data acquisition board and Matlab Simulink, generally sampling at 250 Hz. This board was also used to generate the digital signal for the stepper motor driver used to rotate the spool. Details on the equipment used and their calibration can be found in Appendix E.

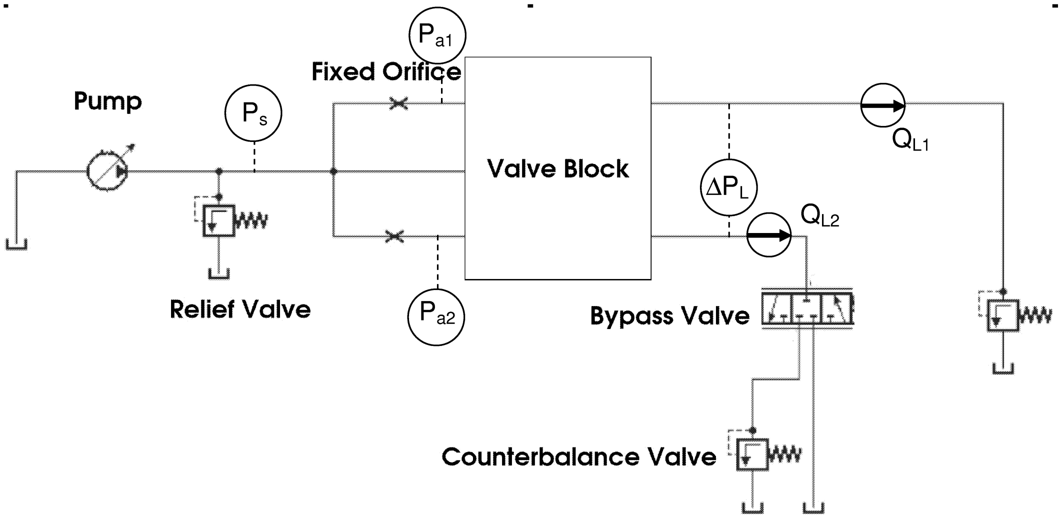

Figure 4.2: The circuit diagram of the system used to test the valve prototype. The valve body contains the pilot stages and the variable orifices.

4.2 Tests

Various experimental tests were performed to verify the analysis in Chapter 2. The simulated step responses will not be compared to the actual step responses, as this would require determining actual physical values for the many parameters used in the model. Rather, since the numerical simulation was only intended to be used as a design tool, the trends it predicts will be examined. For example, the experimental program can be used to verify the prediction that the steady state error increases when the pressure drop across the fixed orifices decreases.

4.3 Initial Tests

The objective of the first test performed was to verify that the valve could compensate for changes in load flow. The valve was connected as described above and the response of the flow to a step[1] change in load pressure was recorded. The two outlet flows are shown in

---

[1] Actually, the counterbalance valves do take some time to respond to changes in the load pressure, as can be seen in Figure 4.5

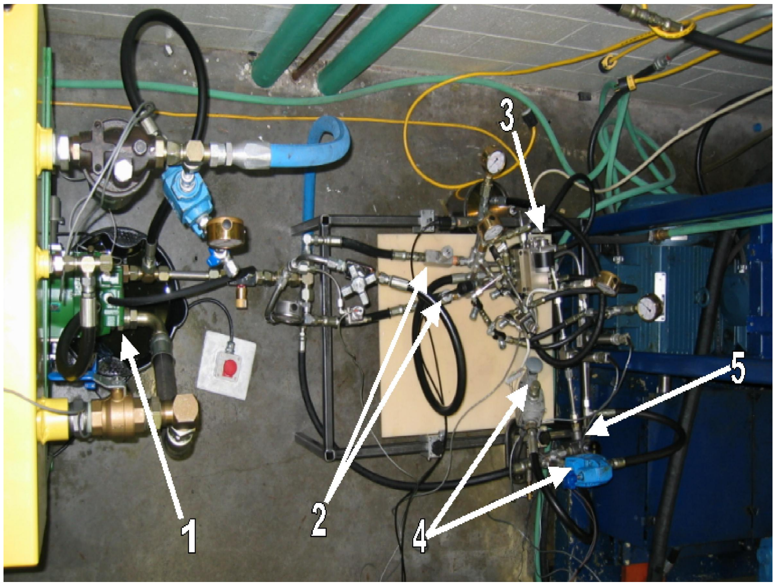

Figure 4.3: Photo of the test circuit, showing pump (1), fixed orifices (2), valve block (3), counterbalance valves (4), and three-way bypass valve (5).

Figure 4.4. This test was performed with a total flow of 4.89 m^3/s, a 427 kPa pressure drop across the fixed orifices and the spool's rotary position set for approximately equal flow division. The load pressures were initially set to be approximately equal and at the step the pressure in branch number 1 dropped so that the load pressure difference was 1640 kPa. The pressure measurements recorded are shown in Figure 4.5.

The valve behaved as expected; before the step, the flows were nearly equal, and the valve attempted to equalize them after the load disturbance. There was some steady state division error due to flow forces and static friction (see section 3.4), in this case 1.23%. There was also an accumulated flow error as the valve could not respond instantaneously. For the test shown below, the accumulated error was $-0.55\ L$.

4.4 Test for Repeatability

The next test performed was to verify that valve performance was repeatable at an arbitrary typical operating point. Three step responses were recorded at similar operating conditions. The responses are superimposed over each other in Figure 4.6. These tests were performed at the same operating conditions as above. The standard deviation of the multiple tests is plotted in Figure 4.7. Notice that the difference between tests was greatest in the time period just after the step, but decreased as time progressed. This suggests that the valve's steady state performance was quite stable, but its transient response varied from test to test (perhaps in response to variables such as operating temperature).

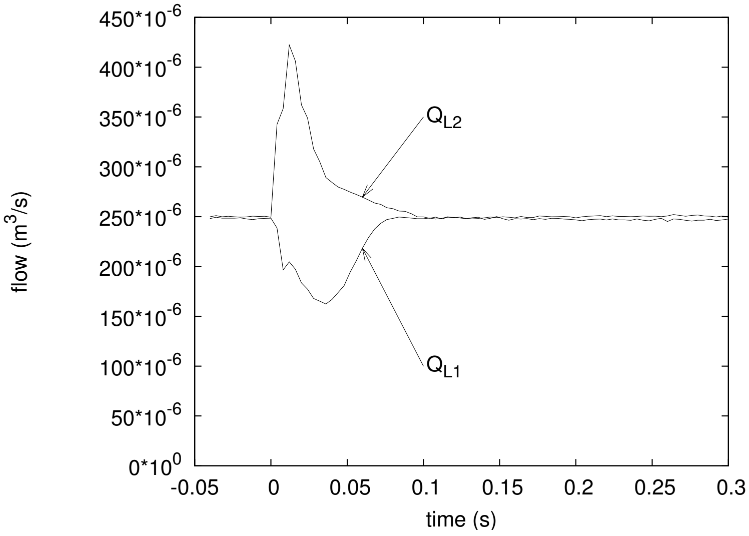

Figure 4.4: Load flow response to a step in load pressure difference. This Figure shows the two outlet flows responding to a 1.64 MPa step in load pressure difference at time zero. The flows converge after the initial disturbance, settling to a steady state error of 1.23%.

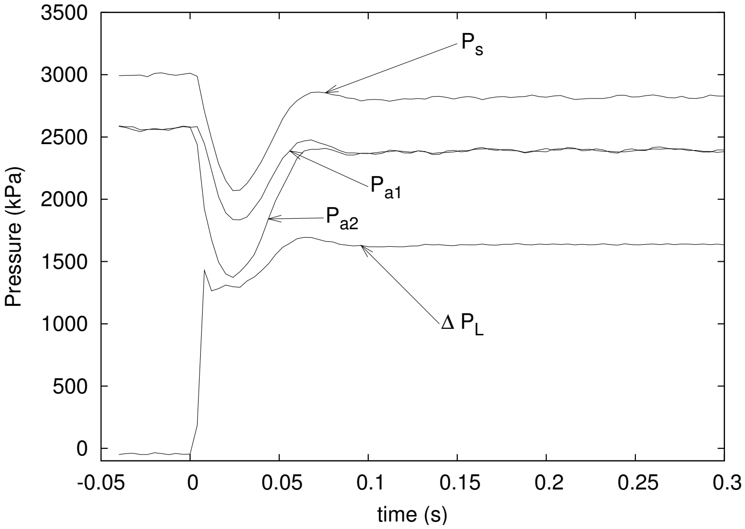

Figure 4.5: Valve pressures during the above test, including P_s, the source pressure; P_{a1} and P_{a2}, the pressures between the fixed orifices and spool in each branch; and ΔP_L, the difference in load pressures. Notice that the load pressure differential was not actually a step.

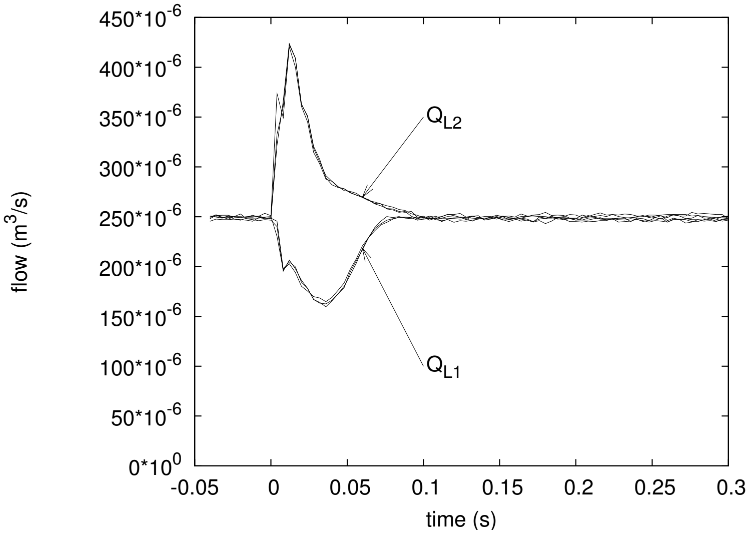

Figure 4.6: Three responses at the same operating conditions as Figure 4.5, showing the repeatability of the valve and measurement instruments.

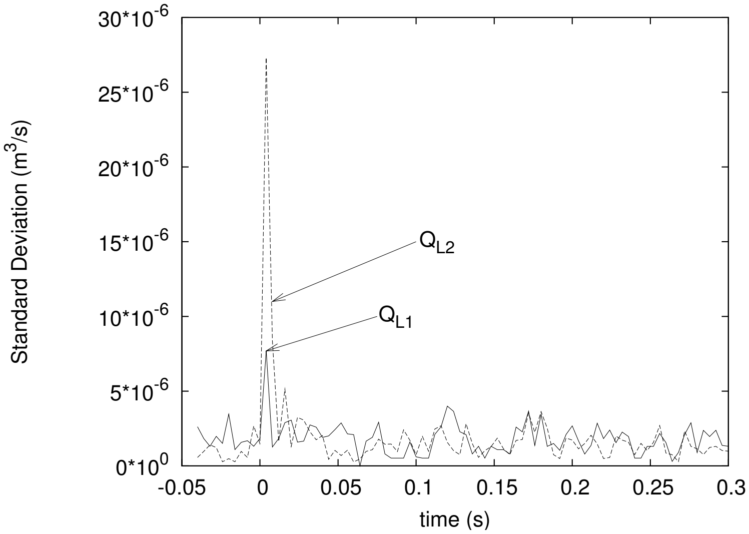

Figure 4.7: Standard deviation of the above three flows. The difference between flows is greatest during the transient portion of the response immediately after the step, but quickly decreases during the steady portion.

In addition to the repeatability of the valve itself, it is necessary to also consider the experimental error in the flow measurements. This error has two parts: bias and a random component. The bias error was estimated by re-calibrating the flow meters after the experimental program had been completed and examining the difference in calibration. Details of this procedure can be found in Appendix E. The random error was determined by recording a sample of data at a flow believed to be constant and calculating the standard deviation of the noise. These two errors can then be combined into the "total experimental error" for the flow measurements. The experimental error for the pressure measurements was calculated in the same manner. The error in the flow is large compared to the differences used to calculate the steady state error, but this is largely due to the bias error which does not effect the result as the magnitude of the flows are not important, only the changes, which are relately small. Similarly, the random error for one measurement is larger than the steady state error, but can be reduced by taking the average of multiple measurements.

4.5 Effect of Pressure Drop

As mentioned earlier, the purpose of the experimental program was to verify the trends as predicted by the pre-design analysis. The first trend to be examined was that the steady state and cumulative dynamic error increase as the pressure drop across the fixed orifice decreases. That is, accuracy can be obtained, but at the cost of efficiency. Numerous tests were performed at approximately the same operating conditions, while varying the size of the fixed orifices. These tests were performed with $Q_s \approx 4.99 \times 10^{-4}\ m^3/s$ and $\Delta P_L \approx 1630\ kPa$. The results are shown in Table 4.1, and behave as expected: the steady state error decreased from 1.23% to 0.73% as the pressure drop increased from 154 kPa to 1460 kPa and the accumulated dynamic error decreased from -0.71 to -0.39 L.

Table 4.1: The effect of the pressure drop across the fixed orifices on the steady state and cumulative dynamic error. These data are the average of a number of tests taken with a mean $Q_s = 4.96 \times 10^{-4}\ m^3/s$ and a mean $\Delta P_L = 1630\ kPa$.

$\Delta P_{fixed}\ (kPa)$	$ERR_{SS}\ (\%)$	$ERR_{CUDY}\ (L)$
154	1.23	-0.712
430	0.87	-0.549
1459	0.73	-0.386

4.6 Effect of Load Pressure Difference

The next test to be performed verified that the steady state error increased with load pressure difference. This would show the effect of flow forces on the valve. Again, a number of step responses were recorded at varying load pressure differences and the error was calculated. The steady state results, shown in Table 4.2, also agree with this theoretical prediction.

Table 4.2: The effect of the load pressure difference on the steady state error. These data are the average of a number of tests taken with a mean $Q_s = 4.96 \times 10^{-4}\ m^3/s$ and a mean $\Delta P_{fixed} = 534\ kPa$.

ΔP_L (kPa)	ERR_{SS} (%)	ERR_{CUDY} (L)
679	-0.070	-0.348
1649	0.734	-0.430
3350	1.257	-0.425

4.7 Effect of Spool Rotation

All of the above tests were performed with the spool rotary position centred (for equal flow division). The purpose of the final test was to verify the valve's ability to adjust the ratio of flows by changing the spool rotary position. Pursuant to this purpose, a number of step responses were recorded with the spool in two rotary positions: centred and fully counter-clockwise at the end of the gear travel (the spool could be rotated further if a gear was used with more teeth). The resultant flow responses are shown in Figure 4.8. Clearly, the ratio of outlet flows can be adjusted, as expected. The range of this valve is smaller than a production valve for two reasons; the gear used did not have a large enough rotary range and any pressure losses in the long pilot line connected to P_s caused the ratio to tend toward 50:50 (if similar fixed orifices are used).

4.8 Summary

In this chapter, the prototype valve's performance was experimentally determined. The valve behaved as expected and the trends predicted by the dynamic simulation were verified. The steady state error was well within the acceptable range for a flow divider; it was less than 1.5% for all tests and was measured to be as low as 0.07%. The dynamic error also appears to be acceptable (although no data for commercial valves is available for comparison). Finally, it was shown that it is possible to adjust the ratio of outlet flows by rotating the spool with the stepper motor.

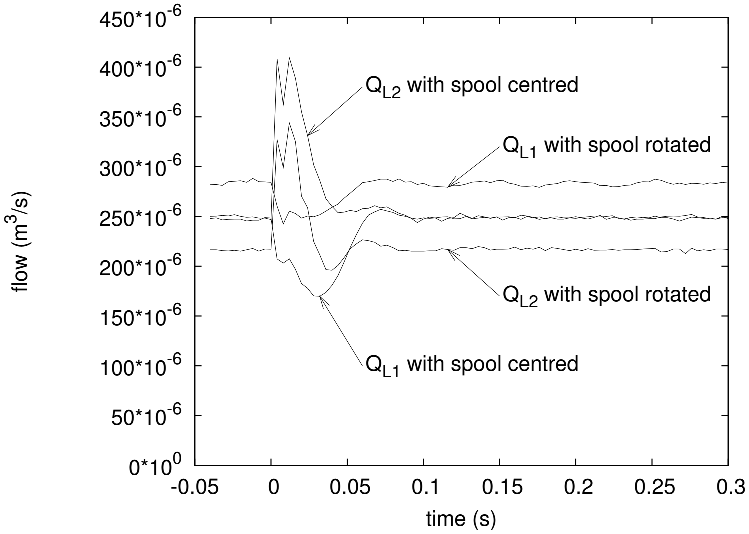

Figure 4.8: Flow responses, showing the effect of rotating the spool. These data are the average of a number of tests taken with a mean $Q_s = 4.96 \times 10^{-4}\ m^3/s$, a mean $\Delta P_{fixed} = 553\ kPa$, and a mean $\Delta P_L = 1649\ kPa$.

Chapter 5

Conclusions and Recommendations

5.1 Conclusions

As presented in Section 1.3, the main objective of this thesis was to determine the feasibility of an adjustable ratio flow divider valve. This objective was split into a number of sub-objectives or tasks:

1. develop a novel concept of valve operation,
2. development of steady state and dynamic simulations,
3. theoretical feasibility study using simulation,
4. optimization of parameters,
5. manufacture prototype, and
6. experimentally test prototype.

Each of these objectives was accomplished in turn. The conceptual schematic can be found in Section 2.1: a flow divider valve including a rotary pilot stage that modifies the spool end pressures so that the ratio of outlet flows is adjustable. Sections 2.2 and 2.3 present the steady state and dynamic simulation models. The dynamic model has more than 30 equations, many of which are non-linear, and results in a stiff system of ODEs. This model was then used to predict the valve's performance and the effect of the various physical parameters and it was found that the concept had sufficient feasibility to warrant production of a prototype. The same model was used in conjunction with two methods of optimization, the complex method and a genetic algorithm, to determine the geometrical parameters to be used for the prototype (Section 3.5). Finally, in Chapter 4, the prototype valve was experimentally evaluated and was found to show acceptable steady state and dynamic accuracy, speed of response and the ability to adjust the ratio of outlet flows. The experimental analysis also showed that the trends predicted by the dynamic simulation were accurate.

The valve described in this thesis is a novel type of valve, previously never presented to the world of fluid power. Although conventional flow divider valves exist, none permit the user to change the ratio of outlet flows without requiring remachining. Furthermore, the valve has only one moving part and is therefore more realiable and less expensive to produce than a valve with separate pilot and main stages. The prototype constructed exhibits low dynamic and steady state error with low pressure losses is experimental tests. This novel valve shows sufficient feasibility to warrent future study and development for commercialization.

5.2 Recommendations for Further Work

There are a number of areas where further research can be performed. First, while a dynamic model was constructed, it was only used in the design process *before* the construction of the prototype. Therefore, it includes many terms that the author believes to be insignificant but were included for completeness. The result is an overly complex model that can be greatly simplified. Further, due to time constraints, the model's accuracy was never experimentally verified, only the design trends it predicts. Before using the model for any further work, this verification should be performed and corrections made for any discrepancy.

Once the accuracy of the dynamic model is verified, the next step would be to expand the sensitivity study. This analysis was performed over a narrow range of points, varying parameters one at a time around a single operating point. It is believed that the effect of some parameters is very dependent on the operating point and the other parameters, so these interactions should be examined to better understand the effect of the various parameters on the valve's performance and stability and find their optimum values.

Once the valve's theoretical operation is better understood, a more realistic prototype can be produced. The prototype manufactured in the course of this research was designed so as to be modular and easily adjustable, rather than optimized for performance. As such, there are some very large volumes and pressure drops that could be avoided, and the physical size of the valve is much larger than it need be.

Another field of research that could be investigated is that of combiner and divider/combiner valves. The author believes that this valve configuration is easily adaptable to either configuration. For example, for combiner operation, only a change the orifice geometry is needed. A possible divider/combiner concept that needs the addition of only four check valves and a small amount of additional machining can be found in Appendix F.

Finally, many of the performance enhancements that have been developed for typical flow divider valves may be applied to this adjustable ratio divider valve. For example, in order to extend the valve's flow range, it may be possible to apply the autoregulator stage, developed by Zhang et al. (1988) and Fedoroff (1990). This, and the other performance improvement techniques found in the literature should be applied to the new valve.

References

Andersson J. *Multiobjective Optimization in Engineering Design.* PhD thesis, Linköping Universitet, Sweden, 2001.

Bevington P. R and Robinson D. K. *Data Reduction and Error Analysis for the Physical Sciences, 3rd Ed.* McGraw-Hill Higher Education, New York, 2003.

Chan R, Schoenau G, , and Burton R. A Simple Design Modification for Improved Accuracy of Piston Type Flow Divider Valves. *Proceedings of the 35th Conference on Fluid Power*, October 1981. Chicago.

Chan R. "Computer simulation and design of a new single-stage piston flow-divider valve". Master's thesis, University of Saskatchewan, 1980.

Cui P. "Development of a high-speed on/off valve". Master's thesis, University of Saskatchewan, 1991.

Fedoroff M, Burton R, Schoenau G, , and Zhang H. Dynamic and Steady-State Analysis of an Auto-Regulator in Flow Divider and/or Combiner Valve. *Journal of Dynamic Systems, Measurement and Control, Transactions of the ASME*, vol 114:pages 306–314, June 1992.

Fedoroff M. "Analysis of steady state and dynamic characteristics of an auto-regulator valve". Master's thesis, University of Saskatchewan, 1990.

Guo Q, Burton R, , and Schoenau G. Dynamic Response of Flow Divider Valves. *Journal of Fluid Control*, vol 19(no 1):pages 20–42, July 1988.

Guo Q. Dynamic response characteristics of flow divider valves. Master's thesis, University of Saskatchewan, 1987.

Hogan P and Burrows C. R. "Synchronising unevenly-loaded hydraulic cylinders". *Fluid Power Systems and Technology: Collected Papers*, pages 75–80, 1994.

Kwan D. "Development of a high precision flow-divider valve for synchronization control". Master's thesis, University of Saskatchewan, 1978.

Kwan D, Schoenau G, Burton R, and Wilson J. A new high precision flow divider valve. *Proceedings of the 35th National Conference on Fluid Power*, November 1979. Chicago.

Matlab . *Matlab Help.* The Mathworks, Natick, MA, 2002.

Merritt H. E. *Hydraulic Control Systems.* John Wiley and Sons, New York, 1967.

Phillips C and Harbor R. *Feedback Control Systems*. Prentice Hall, New Jersey, 2000.

Ruan J, Burton R, Ukrainetz P, and Xu Y. "2-D pressure control valve". *Proceedings of the Institution of Mechanical Engineers, Part C: Journal of Mechanical Engineering Science*, 215(9):1031–1038, 2001.

Stroempl P. "Flow divider and flow divider/combiner valves for closed loop hydrostatic transmissions". *SAE 1990 Transactions: Journal of Commercial Vehicles*, pages 276–286, 1990.

Zhang Y, Burton R, and Schoenau G. "An autoregulated flow divider/combiner valve". *Proceedings of 43rd National Conference on Fluid Power*, pages 409–417, 1988.

Zhang Y, Xin S, Burton R, and Schoenau G. An Autoregulated, High Precision Flow Divider/Combiner Valve. *Off-Highway and Powerplant Congress and Exposition*, September 1993. Milwaukee.

Appendix A

Derivation of Equations Governing Pilot Stage Flow

In this Appendix, the equations governing the flow in the pilot stage are developed, first for the left hand side of the valve (branch 1), then the corresponding equations are presented for the other side. This development follows the analysis contained in Ruan et al. (2001).

In this analysis it is assumed that the leakage flow in the clearance between the spool and casing follows a path in the axial direction and that the spool is concentric with the casing. The gooves are assumed to cover a large portion of the spool's circumference, so that the leakage in the space between grooves is neglected. The flow in the left hand end is then shown in Figure A.1.

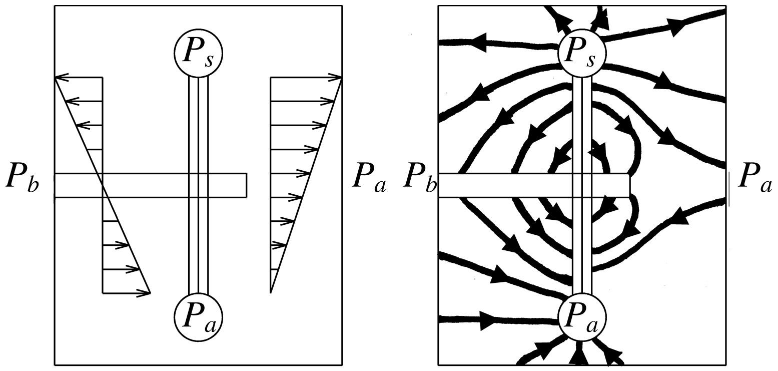

Figure A.1: This figure shows the difference between the simplified leakage paths used for the analysis (left) and flow lines for a more realistic leakage path (right). All the leakage is assumed to flow in the axial direction between the spool's pilot groove and either edge of the land. Since the pressure changes approximately linearly between ends of the groove, the flow also varies linearly. In reality there is likely some leakage between the pilot groove and the sensing groove, and also in the circumferential direction between the ends of the two grooves.

Consider a small control volume of length dl cut from a section of the circumferential groove, shown in Figure A.2. If the volume of the groove is assumed to be neglible, the continuity equation is

$$\left(Q(l) + \frac{dQ}{dl}dl\right) - Q(l) = dQ_{la1}(l) - dQ_{lb1}(l) \tag{A.1}$$

where the flows are as shown in the diagram. This can be simplified to

$$\frac{dQ}{dl}dl = dQ_{la1} - dQ_{lb1}. \tag{A.2}$$

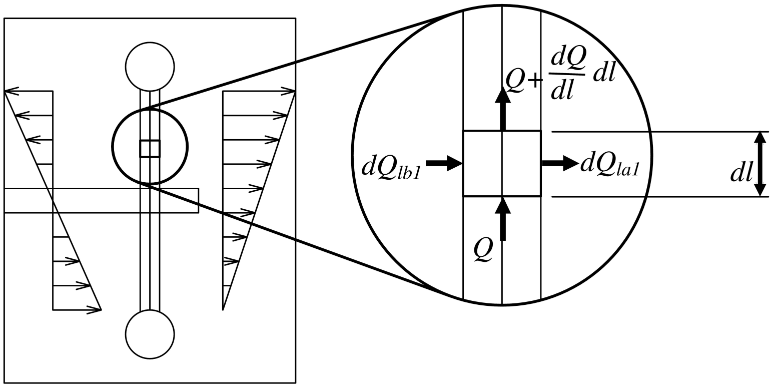

Figure A.2: Differential control volume for the pilot stage, used in equation A.1

The equation for laminar flow through a equilateral triangular passage is given by Merritt (1967) as

$$Q = \frac{-b^4}{185\mu}\frac{dP}{dl} \tag{A.3}$$

or

$$\frac{dQ}{dl} = \frac{-b^4}{185\mu}\frac{d^2P}{dl^2} \tag{A.4}$$

where b is the length of each side of the triangle and μ is the fluid viscosity.

Now consider the leakage from P_{b1} to the groove. Merritt (1967) gives the equation for annular flow for a complete circle as

$$Q = \frac{\pi r \delta^3}{6\mu h}\Delta P \tag{A.5}$$

where r is the radius, δ is the radial clearance, and h is the path length. For the particular case of this analysis, the equation can be scaled for use on a portion of the circle's circumference:

$$dQ_{lb1} = \frac{\pi r \delta^3}{6\mu h}\frac{dl}{2\pi r}\left(P_{b1} - P(l)\right) \tag{A.6}$$

which simplifies to

$$dQ_{lb1} = \frac{\delta^3}{12\mu h}dl\left(P_{b1} - P(l)\right). \tag{A.7}$$

The same can be written for the leakage to $Pa1$

$$dQ_{la1} = \frac{\delta^3}{12\mu h}dl\left(P(l) - P_{a1}\right). \tag{A.8}$$

If one substitutes equations A.8, A.7, and A.4 into A.2, the result is

$$\frac{-b^4}{185\mu}\frac{d^2P}{dl^2}dl = \frac{\delta^3}{12\mu h}dl\left(2P(l) - P_{a1} - P_{b1}\right). \tag{A.9}$$

This may be converted into angular coordinates by the transform $dl = rd\phi$ as follows:

$$\frac{-b^4}{185\mu r}\frac{d^2P}{d\phi^2}d\phi = \frac{\delta^3}{12\mu h}rd\phi\left(2P(l) - P_{a1} - P_{b1}\right) \tag{A.10}$$

which simplifies to

$$\frac{6b^4h}{185r^2\delta^3}\frac{d^2P}{d\phi^2} = -P(l) + \frac{P_{a1} + P_{b1}}{2}. \tag{A.11}$$

This is now an ordinary differential equation in the form

$$c\frac{d^2P}{d\phi^2} = -P(l) + \frac{P_{a1} + P_{b1}}{2} \tag{A.12}$$

where

$$c = \frac{6b^4h}{185r^2\delta^3}. \tag{A.13}$$

The solution for the pressure distribution along the length of the groove is then

$$P(\phi) = C_1\cos\left(\frac{\phi}{\sqrt{c}}\right) + C_2\sin\left(\frac{\phi}{\sqrt{c}}\right) \tag{A.14}$$

where C_1 and C_2 are integration constants. In order to apply boundary conditions, the problem must be split into two parts: the section above the horizontal groove ($\phi > \phi_1$) and the part below ($\phi < \phi_1$). There will now be two equations with four constants:

$$P(\phi > \phi_1) = C'_{a1}\cos\left(\frac{\phi}{\sqrt{c}}\right) + C'_{b1}\sin\left(\frac{\phi}{\sqrt{c}}\right) \tag{A.15}$$

$$P(\phi < \phi_1) = C_{c1}\cos\left(\frac{\phi}{\sqrt{c}}\right) + C_{d1}\sin\left(\frac{\phi}{\sqrt{c}}\right) \tag{A.16}$$

where ϕ_1 is the angular position of the groove. For the sake of ease of calculations (which will become visable later), equation A.15 may be rewritten in a slightly different form:

$$P(\phi > \phi_1) = C_{a1}\cos\left(\frac{\phi_0 - \phi}{\sqrt{c}}\right) + C_{b1}\sin\left(\frac{\phi_0 - \phi}{\sqrt{c}}\right) \tag{A.17}$$

where ϕ_0 is the angle of the spool covered by the circumferential groove.

Boundary conditions may now be applied:

$$P(\phi_0) = P_{a1} = C_{a1}\cos\left(\frac{\phi_0 - \phi_0}{\sqrt{c}}\right) + C_{b1}\sin\left(\frac{\phi_0 - \phi_0}{\sqrt{c}}\right) \tag{A.18}$$

$$P(\phi_1^+) = P_{b1} = C_{a1}\cos\left(\frac{\phi_0 - \phi_1}{\sqrt{c}}\right) + C_{b1}\sin\left(\frac{\phi_0 - \phi_1}{\sqrt{c}}\right) \tag{A.19}$$

$$P(\phi_1^-) = P_{b1} = C_{c1}\cos\left(\frac{\phi_1}{\sqrt{c}}\right) + C_{d1}\sin\left(\frac{\phi_1}{\sqrt{c}}\right) \tag{A.20}$$

$$P(0) = P_s = C_{c1}\cos(0) + C_{d1}\sin(0) \tag{A.21}$$

This system of equations can be solved simultaneously to find the constants:

$$C_{a1} = P_{a1} \tag{A.22}$$

$$C_{b1} = \frac{P_{b1} - P_{a1}\cos\left(\frac{\phi_0-\phi_1}{\sqrt{c}}\right)}{\sin\left(\frac{\phi_0-\phi_1}{\sqrt{c}}\right)} \tag{A.23}$$

$$C_{c1} = P_s \tag{A.24}$$

$$C_{d1} = \frac{P_{b1} - P_s\cos\frac{\phi_1}{\sqrt{c}}}{\sin\frac{\phi_1}{\sqrt{c}}} \tag{A.25}$$

The pressure distribution along the length of the circumferential groove has now been determined. This information can then be used to find the flows, both the flow along the circumferential groove and the leakage flows. Equation A.3 can be used to find the flow through the triangular groove at any position. First the equation must be converted to angular coordinates, again using $dl = rd\phi$:

$$Q(\phi) = \frac{-b^4}{185r\mu}\frac{dP}{d\phi} \tag{A.26}$$

This equation can be applied to the top end of the groove ($\phi = \phi_0$) to find the flow out of the pilot stage. The derivative of equation A.17 is

$$\frac{dP(\phi > \phi_1)}{d\phi} = \frac{C_{a1}}{\sqrt{c}}\sin\left(\frac{\phi_0 - \phi}{\sqrt{c}}\right) - \frac{C_{b1}}{\sqrt{c}}\cos\left(\frac{\phi_0 - \phi}{\sqrt{c}}\right) \tag{A.27}$$

which may be evaluated at $\phi = \phi_0$ to give

$$Q_{a1o} = \frac{-b^4}{185r\mu}\frac{dP(\phi_0)}{d\phi} = \frac{-b^4}{185r\mu}\left(\frac{C_{a1}}{\sqrt{c}}\sin(0) - \frac{C_{b1}}{\sqrt{c}}\cos(0)\right) \tag{A.28}$$

which expands and simplifies to

$$Q_{a1o} = \frac{b^4}{185\mu r\sqrt{c}}C_{b1}. \tag{A.29}$$

A similar process can be used to find the other flows in the groove, as shown in Figure A.3.

$$Q_{c1i} = \frac{-b^4}{185\mu r\sqrt{c}}C_{d1} \tag{A.30}$$

$$Q_{a1i} = \frac{b^4}{185\mu r\sqrt{c}}\left[-C_{a1}\sin\frac{\phi_0 - \phi_1}{\sqrt{c}} + C_{b1}\cos\frac{\phi_0 - \phi_1}{\sqrt{c}}\right] \tag{A.31}$$

$$Q_{c1o} = \frac{b^4}{185\mu r\sqrt{c}}\left[C_{c1}\sin\frac{\phi_1}{\sqrt{c}} - C_{d1}\cos\frac{\phi_1}{\sqrt{c}}\right] \tag{A.32}$$

Continuity may be applied to three flows at the junction of the grooves to find the flow through one axial groove to the end chamber:

$$Q_{b1} = Q_{c1o} - Q_{a1i} \tag{A.33}$$

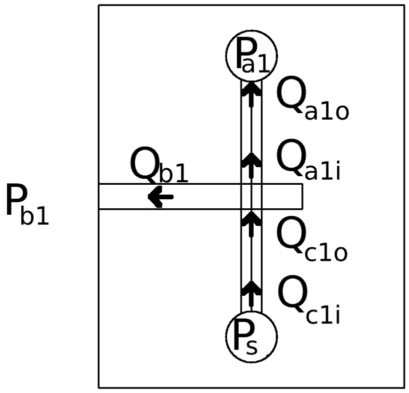

Figure A.3: Nomenclature used for pilot flows. The flow entering the pilot groove (e.g. Q_{c1i} Pilot flow entering sensing groove) is different than that leaving (Q_{c1o}) because of leakage.

In order to determine the leakage flows, equations A.7 and A.8 were applied to the pressure profile found in equations A.16 and A.17. The flow to the end chamber from one circumferential groove is given by

$$Q_{lb1} = \int_0^{\phi_0} \frac{\delta^3}{12\mu h} \left(P_{b1} - P(\phi)\right) r d\phi \tag{A.34}$$

but there are two symmetrical grooves so the total leakage is given by

$$Q_{lb1} = \int_0^{\phi_0} \frac{2r\delta^3}{12\mu h} \left(P_{b1} - P(\phi)\right) d\phi \tag{A.35}$$

which appears in the following form when the pressure distribution is introduced

$$\begin{aligned} Q_{lb1} &= \frac{r\delta^3}{6\mu h} \left[\int_0^{\phi_0} P_{b1} d\phi - \int_0^{\phi_1} \left(C_{c1} \cos\left(\frac{\phi}{\sqrt{c}}\right) + C_{d1} \sin\left(\frac{\phi}{\sqrt{c}}\right)\right) d\phi \ldots \right. \\ & \left. - \int_{\phi_1}^{\phi_0} \left(C_{a1} \cos\left(\frac{\phi_0 - \phi}{\sqrt{c}}\right) + C_{b1} \sin\left(\frac{\phi_0 - \phi}{\sqrt{c}}\right)\right) d\phi \right] \end{aligned} \tag{A.36}$$

$$\begin{aligned} Q_{lb1} &= \frac{r\delta^3}{6\mu h} \left(\frac{P_{b1} - P_{a1}}{2} \phi_0 + \sqrt{c} \left[-C_{c1} \sin\frac{\phi_1}{\sqrt{c}} + C_{d1} \left(\cos\frac{\phi_1}{\sqrt{c}} - 1 \right) \ldots \right.\right. \\ & \left.\left. -Ca1 \sin\frac{\phi_0 - \phi_1}{\sqrt{c}} - C_{b1} \left(1 - \cos\frac{\phi_0 - \phi_1}{\sqrt{c}} \right) \right] \right) \end{aligned} \tag{A.37}$$

The same procedure can be performed to the other side of the groove to get Q_{la1}, the leakage from the groove to the main flow chamber:

$$Q_{la1} = \frac{r\delta^3}{6\mu h} \left(\frac{P_{b1} - P_{a1}}{2} \phi_0 - \sqrt{c} \left[-C_{c1} \sin\frac{\phi_1}{\sqrt{c}} + C_{d1} \left(\cos\frac{\phi_1}{\sqrt{c}} - 1 \right) \ldots \right.\right.$$

$$-Ca1\sin\frac{\phi_0-\phi_1}{\sqrt{c}} - C_{b1}\left(1-\cos\frac{\phi_0-\phi_1}{\sqrt{c}}\right)\Bigg]\Bigg) \tag{A.38}$$

Notice that the only difference is one sign change.

Thus far in this appendix, equations have been developed to determine all of the flows involved with the left hand side pilot stage operation. The right hand side may be developed following the same procedure to get the following.

$$C_{a2} = P_s \tag{A.39}$$

$$C_{b2} = \frac{P_{b2} - P_s\cos\left(\frac{\phi_0-\phi_1}{\sqrt{c}}\right)}{\sin\left(\frac{\phi_0-\phi_1}{\sqrt{c}}\right)} \tag{A.40}$$

$$C_{c2} = P_{a2} \tag{A.41}$$

$$C_{d2} = \frac{P_{b2} - P_{a2}\cos\frac{\phi_1}{\sqrt{c}}}{\sin\frac{\phi_1}{\sqrt{c}}} \tag{A.42}$$

$$Q_{a2i} = \frac{b^4}{185\mu r\sqrt{c}}\left[-C_{c2}\sin\frac{\phi_1}{\sqrt{c}} + C_{d2}\cos\frac{\phi_1}{\sqrt{c}}\right] \tag{A.43}$$

$$Q_{c2o} = \frac{b^4}{185\mu r\sqrt{c}}\left[C_{a2}\sin\frac{\phi_0-\phi_1}{\sqrt{c}} - C_{b2}\cos\frac{\phi_0-\phi_1}{\sqrt{c}}\right] \tag{A.44}$$

$$Q_{a2o} = \frac{b^4}{185\mu r\sqrt{c}}C_{d2} \tag{A.45}$$

$$Q_{c2i} = \frac{-b^4}{185\mu r\sqrt{c}}C_{b2} \tag{A.46}$$

$$Q_{b2} = Q_{c2o} - Q_{a2i} \tag{A.47}$$

$$\begin{aligned} Q_{lb2} = \frac{r\delta^3}{6\mu h}\Bigg(&\frac{P_{b2}-P_{a2}}{2}\phi_0 + \sqrt{c}\Bigg[-C_{c2}\sin\frac{\phi_1}{\sqrt{c}} + C_{d2}\left(\cos\frac{\phi_1}{\sqrt{c}} - 1\right)\ldots \\ &-Ca2\sin\frac{\phi_0-\phi_1}{\sqrt{c}} - C_{b2}\left(1-\cos\frac{\phi_0-\phi_1}{\sqrt{c}}\right)\Bigg]\Bigg) \end{aligned} \tag{A.48}$$

$$\begin{aligned} Q_{la2} = \frac{r\delta^3}{6\mu h}\Bigg(&\frac{P_{b2}-P_{a2}}{2}\phi_0 - \sqrt{c}\Bigg[-C_{c2}\sin\frac{\phi_1}{\sqrt{c}} + C_{d2}\left(\cos\frac{\phi_1}{\sqrt{c}} - 1\right)\ldots \\ &-Ca2\sin\frac{\phi_0-\phi_1}{\sqrt{c}} - C_{b2}\left(1-\cos\frac{\phi_0-\phi_1}{\sqrt{c}}\right)\Bigg]\Bigg) \end{aligned} \tag{A.49}$$

Note that in the main body of the text, for simplicity the angular position of the groove is referred to as ϕ, rather than ϕ_1, as in this appendix.

Appendix B

Physical Parameters

This appendix includes copies of the Matlab m-files used to set the base parameters for the model. Section B.1 presents the unoptimized parameters that were arbitrarily selected as the starting point for the sensitivity analysis and optimization. Section B.2 presents the optimized parameters. Some values from both files come from other research, especially Ruan et al. (2001)

B.1 dividerparams.m

```
%This sets the base parameters for ALL simulations

global beta rho nu r b phi0 Cdo1 Cdo2 Cdv1 Cdv2 Vs delta h Fc t_rim Ld SL;
global mu m A Ao1 Ao2 rv d0 xmax Vs V1o V2o c Vc1 Vc2 LL Bf Arim;

beta=1e9;            %(Pa) bulk modulus
rho=900;             %(kg/m^3) density
nu=30e-6;              %(m^2/s)kinematic viscosity
r=8e-3 ;         %(m) spool land radius  (Jian 8e-3)
rs_r=0.3;          %ratio of stem radius to spool radius
b=1e-3 ;    %(m)groove width (Jian 0.3mm)
phi0=pi/2;  %rad max phi (another form of theta)
Cdo1=.61;    %Cd for left fixed orifice
Cdo2=Cdo1 ;  %Cd for right fixed orifice
Cdv1=.61 ;  %Cd for left variable orifice
Cdv2=.61 ;  %Cd for right variable orifice
Qs1o=5e-4  ; %flow through one leg at set point
deltaPt=3e6 ;%pressure drop across both orifices at above flow with
% one totally open
Po_Pt=0.5 ;  %ratio of pressure drop across fixed orifice to total
xo_w=3;  %ratio of xo to w (rectangular orifices)
frac_open=0.5 ; %fractional linear opening of ports at x=0 (circular opening)
Vs=1000e-6;%pi/4*(10e-3)^2*100e-3 ;    %source volume
Lv1=2.5e-3;  %(m) clearance at left end of spool stroke (Jian 1.2e-3)
Lv2=2.5e-3 ; %(m) clearance at right end of spool stroke
delta=0.0029e-3   ;     %(m) spool clerance (Jian 0.0029e-3)
```

```
h=5e-3   ;          %m distance from groove to edge of land
Fc=0    ;  %(N) spool coulomb friction
t_rim=0.8e-3 ; %m rim thickness
LL_h=8 ; %total land length wrt h (for viscous damping)
LL_LT=0.4 ;%total land length length wrt spool total length
mr=0.5   ;%ratio of mass to a mass of spool with no cutouts
La=20e-3           ;%length between lands
Ld=10e-3;          %(m) damping length
Ls=5e-3;           %(m) seal length
%Load orifice
global VL1 VL2 CdL1 CdL2
VL1=pi/4*(6e-3)^2*0.10; %Volume between valve and load #1
VL2=VL1;                %Volume between valve and load #2
CdL1=0.61;         %CD for Load Orifice #1
CdL2=0.61;         %CD for Load Orifice #2
```

B.2 optimizedparams.m

```
%These are the "drawing" parameters

global beta rho nu r b phi0 Cdo1 Cdo2 Cdv1 Cdv2 Vs delta h Fc t_rim Ld SL;
global mu m A Ao1 Ao2 rv d0 xmax Vs V1o V2o c Vc1 Vc2 LL Bf Arim;

beta=1e9;          %(Pa) bulk modulus
rho=900;           %(kg/m^3) density
nu=30e-6;            %(m^2/s)kinematic viscosity
r=13.3e-3;        %(m) spool land radius  (Jian 8e-3)
rs_r=0.44361;     %ratio of stem radius to spool radius
b=1.35e-3 ;    %(m)groove width (Jian 0.3mm)
phi0=pi/2;  %rad max phi (another form of theta)
Cdo1=.61;   %Cd for left fixed orifice
Cdo2=Cdo1 ;  %Cd for right fixed orifice
Cdv1=.61 ;  %Cd for left variable orifice
Cdv2=.61 ;  %Cd for right variable orifice
Qs1o=5e-4  ; %flow through one leg at set point
deltaPt=7.91e6 ;%pressure drop across both orifices at above flow with one
%totally open
Po_Pt=0.886 ;  %ratio of pressure drop across fixed orifice to total
xo_w=3;  %ratio of xo to w (rectangular orifices)
frac_open=0.421 ; %fractional linear opening of ports at x=0 (circular opening)
Vs=1000e-6;%pi/4*(10e-3)^2*100e-3 ;   %source volume
Lv1=2.5e-3;  %(m) clearance at left end of spool stroke (Jian 1.2e-3)
Lv2=2.5e-3 ; %(m) clearance at right end of spool stroke
delta=0.0029e-3  ;    %(m) spool clerance (Jian 0.0029e-3)
h=5e-3   ;          %m distance from groove to edge of land
Fc=0    ;  %(N) spool coulomb friction?
t_rim=0.8e-3 ; %m rim thickness
LL_h=8 ; %total land length wrt h (for viscous damping)
LL_LT=0.4 ;%total land length length wrt spool total length
mr=0.5   ;%ratio of mass to a mass of spool with no cutouts
La=20e-3           ;%length between lands
Ld=10e-3;          %m damping length
Ls=5e-3;           %m seal length
```

```
%Load orifice
global VL1 VL2 CdL1 CdL2
VL1=pi/4*(6e-3)^2*0.10; %Volume between valve and load #1
VL2=VL1;                %Volume between valve and load #2
CdL1=0.61;        %CD for Load Orifice #1
CdL2=0.61;        %CD for Load Orifice #2
```

Appendix C

Matlab/Octave and C Code

This appendix includes code used to simulate and optimize the valve. The code in Section C.1 is used to calculate the parameters that the simulation needs to run, but need not be calculated at each time step. This, as with all of the other m-files, was written for Octave version 2.1.50, but should run on Matlab with some modifications. Section C.3 contains the code for the system of differential equations used to simulate the valve. This ".cc" file is written in a pseudo-C language specific to Octave. This code is compiled into an ".oct" file function that can be run in Octave at a much greater speed than a regular uncompiled function. Since the ODE solver will call this function thousands of times in the course of calculating a response curve, and hundreds of thousands of times when optimizing the valve, this speed increase is worth the effort of learning a new coding language. The `gadiv.m` file in Section C.4 is a script that initiates a Genetic Algorthim to optimize the `divfitag.m` function, found in Section C.5. The Genetic Algorithm requires the `GAOT` Genetic Algorithm Optimization Toolbox. Section C.6 includes a script that sets up an alternate optimization strategy, the complex method, which runs on the function found in Section C.7. Refer to Section 3.5 for details.

C.1 calcparams.m

```
%This script calculates all of the divider model parameters, based
%on dividerparam.m or optimizedparam parameters

global mu m A Ao1 Ao2 rv d0 xmax Vs V1o V2o c Vc1 Vc2 Va1 Va2 LL Bf Arim Cb3 Cb4 xo
%%%%%%
%Calculated values
%%%%%%%%
mu=nu*rho;

LL=LL_h*h ; %(m) total land length
Bf=2*LL*r*pi*mu/delta ;    %(N/(m/s)) viscous friction
LT=LL/LL_LT;     %(m) spool length

rs=r*rs_r;                 %spool rod radius
A=pi*(r^2-(rs)^2);         %(m^2) spool end area
```

```
m=mr*r^2*pi*LT*7870;     %(kg) spool mass

deltaPo=Po_Pt*deltaPt;
Ao1=Qs1o/(Cdo1*sqrt(2/rho*deltaPo)); %Area of left fixed orifice
Ao2= Ao1;   %Area of right fixed orifice

%rectangular orifice
w=sqrt(Qs1o/(Cdv1*2*xo_w*sqrt(2/rho*(deltaPt-deltaPo))));
xo=xo_w*w;   %orifice height at x=0

%for circular ports
rv=sqrt(Qs1o/(Cdv1*pi*sqrt(2/rho*(deltaPt-deltaPo))));
d0=rv*(1-2*frac_open);  %opening at x=0 is rv-d0
xmax=1.3*(d0+rv);

V1o=(Lv1+xmax)*A   ;      %left chamber vol at x=0
V2o=(Lv2+xmax)*A   ;      %right chamber vol at x=0

c=6*b^4*h/(185*r^2*delta^3);
Va1=pi*(r^2-(r/2)^2)*La ;   %left flow chamber vol
Vc1=Va1;
Va2=Va1;     %right flow chamber vol
Vc2=Va2;

Cb3=rs*pi*delta^3/(6*mu*Ls)      ;%leakage coefficient
Cb4=Cb3;

%Arim=w*t_rim; %rectangular
```

C.2 changeall.m

```
%this is useful. This is for my thesis. The program plots sensitivity
%Sgraphs for all the parameters in varname_m

tic
varname_m=["r";"b";"delta";"deltaPt";"Po_Pt";"frac_open";"t_rim";"Fc";\
"nu";"phi0"]; %variables to plot
plotvarname_m=["r";"b";"{/Symbol d}";"Total Pressure Drop";"P_o/P_t";\
"fractional orifice opening";"t_{rim}";"F_c";"{/Symbol n}";"{/Symbol f}_0"];\
%name that will appear on graphs. See gnuplot docs for /Symbol s.
units_m=["mm";"mm";"mm";"Mpa";" ";" ";"mm";"N";"mm/s";"degrees"];%units duh
unitmult_m=[1e3;1e3;1e3;1e-6;1;1;1e3;1;1e6;180/pi];%factor to scale\
values by, eg m->mm 1e3
range_m=[8e-3 20e-3;0.3e-3 2e-3;1e-6 0.02e-3;1e6 10e6;0.1 0.99;0.2 0.5;\
0.001e-3 2e-3;0 10;15e-6 66e-6;pi/3 pi];%range of values to plot
lin_m=ones(1,15);%1=linspace 0=logspace

nparam=100;%number of trials to run for each variable

t_test=1;%total test time (s)
steptime=0.6;%time of step (s) allows for initial transients to settle out
npoints=2000;%number of time points
```

```
tout=[linspace(0,0.99*steptime,round(npoints/3)) logspace(log10(0.99001*steptime),lo
%concentrates time points just after the step

x0 =zeros(9,1);%initial conditions
lsode_options("relative tolerance", 1e-3);
%lsode_options("integration method", "stiff")
lsode_options("step limit", 10000);

%Aggregate values
%Note weights are inverse of Matlab help, i.e. here higher weight means\
 more important
  W1=3;%ss error
  W2=1;%pressure drop
  W3=3;%dyn err

%Goals
   ss_err0=0.5;
   ssPs0=18e6;
   dynerr0=0.5e-6;
   t_cum=0.2;
   Pslimit=30e6;

   t_cum=0.2;

for j=1:rows(varname_m);%big loop, most of what is in this loop is taken \
from a program to plot the sensitivity for one variable, hence the reassignment\
 of some variables from a matrix. This isn't a computer science thesis, \
 so don't complain.

clear param ut QL1 QL2 ssPs ssPs maxP Fitness valFit dynerr dynerr_pc ss_err\
 cum_ss_err  t_set E_CUM %clears previous variables

dividerparam
%optimizedparam %loads base parameters

varname=deblank(varname_m(j,:));         %variable to be varied
plotvarname=deblank(plotvarname_m(j,:));%name for plots
units=deblank(units_m(j,:));%units for plots
unitmult=unitmult_m(j,:);%multiply result by this for plotted value

if lin_m(j)==1
param=linspace(range_m(j,1),range_m(j,2),nparam);%logrithmicly spaced \
range of parameters
else
param=logspace(-20,-7,nparam);%linear spacing
end



%test parameters
phi_phi0=0.5;
Qs=10e-4;
PL1=10e6;    %desired SS
AL1=(Qs/2)/(CdL1*sqrt(2/rho*PL1));
```

```
stepPL1=15e6;   %desired SS
stepAL1=(Qs/2)/(CdL1*sqrt(2/rho*stepPL1));
PL2=10e6;   %desired SS
AL2=(Qs/2)/(CdL2*sqrt(2/rho*PL2));

global uto
uto=[[0 phi_phi0 Qs AL1 AL2];[steptime phi_phi0 Qs stepAL1 AL2];\
[1000 phi_phi0 Qs stepAL1 AL2]];



for i=1:length(param)%this loops through the values for the parameters
%%%%%%%%%Insert parameter name into model

eval([varname '=' num2str(param(i)) ';']);
 calcparams
stepAL1=(Qs/2)/(CdL1*sqrt(2/rho*stepPL1));
uto=[[0 phi_phi0 Qs AL1 AL2];[steptime phi_phi0 Qs stepAL1 AL2];\
[1000 phi_phi0 Qs stepAL1 AL2]];
%%%%%%%%%%%%%%%%%%%%%%%%%%

  clear yout
  yout= lsode("divloadcc",x0,tout);
  x1=yout(end,7);
  PL1=yout(:,8);
  PL2=yout(:,9);

  AL1m=AL1.*(tout<steptime)+stepAL1.*(tout>steptime);
  QL1(:,i)=CdL1.*AL1m'.*sqrt(2/rho*PL1);%assume QL1=QLo1
  QL2(:,i)=CdL2*AL2*sqrt(2/rho*PL2);
  ssPs(i)=yout(length(yout),1);
  ssPa1(i)=yout(length(yout),2);
  ssPa2(i)=yout(length(yout),3);
  ssPL1(i)=yout(length(yout),8);
  ssPL2(i)=yout(length(yout),9);

  k_step=min(find(tout>=steptime)); %find which time step the step occurs at
  maxP(i)=max(max(yout(:,1:5)));%find maximum pressure

  ssQ1=QL1(end,i);
  ssQ2=QL2(end,i);
  k_set=max(k_step+1,max(find(abs((QL1(:,i)-ssQ1)/ssQ1)>0.02))); %settling\
   step number
  t_set(i)=tout(k_set)-steptime;%settling time
  dynerr(i)=(trapz(tout(k_step:k_set),(QL1(k_step:k_set,i)-ssQ1-(QL2(k_step:k_set,i
-ssQ2))));%dynamic error
  ss_err(i)=abs(ssQ1-ssQ2)/Qs*100;%steady state error at centre position(%)
  cum_ss_err(i)=(ssQ1-ssQ2)*t_cum;%cummulative steady state error (not %)
  E_CUM(i)=((cum_ss_err(i)+dynerr(i))/(Qs*t_cum)*100);%total accumulated error
  dynerr_pc(i)=dynerr(i)/(Qs*t_cum)*100;%dynamic error in %
  DeltaP(i)=ssPs(i)-max(PL2(end),stepPL1);%pressure drop

  Arim1=t_rim*2*sqrt(rv*rv-(d0-x1)*(d0-x1));
  Arim2=t_rim*2*sqrt(rv*rv-(d0+x1)*(d0+x1));
  ss_err_th(i)=(Arim1/2*(ssPL1(i)-ssPa1(i))-Arim2/2*(ssPL2(i)-ssPa2(i)))/(2*(ssPs(i)
  (ssPa1(i)+ssPa2(i))/2)*A); %some kind of theoretical steady state error
  % (don't remember exactly what theory)(fu ck)

%Calculate fitness
 Fitness(1,i)=(abs(ss_err(i))-ss_err0)/ss_err0*W1;

 Fitness(2,i)=(ssPs(i)-ssPs0)/ssPs0*W2;

 Fitness(3,i)=(abs(dynerr(i))-dynerr0)/dynerr0*W3;

 valFit=-max(Fitness);%goal attainment (negative to maximize valFit)

 if ssPs>Pslimit
  valFit=-1e4;
 endif

end

%%%%%%%%%%%%%%%%%%
%Plot Stuff
%%%%%%%
%if the x-label runs off the bottom of the figure change
%"50 50 translate" in the .eps file to about "50 55 translate".
%This moves the whole figure a little up. See psodc/ps_file.doc in
%the gnuplot documentation fo more.

if (deblank(units)=="");
 gvar=['"' plotvarname '"'];
else
 gvar=['"' plotvarname " ("  units ')"'];
end

figure(1);
gset terminal x11 %x11=screen
gset xtics nomirror %tic-marks only along bottom axis (not mirrored to top axis)
xti=round(100*(steptime+max(t_set))/10)/100;%calculate spacing between x-ticks
gset('xtics',num2str(xti));
hold off
gset xlabel 't␣(s)'
gset ylabel 'Load␣Flows␣(m^3/s␣X␣10^4)'
yscale=1e4;
gset key right bottom %legend
axis([0 steptime+1.5*max(t_set) 0 1.05*max(max([QL1 QL2]))*yscale]);

numberoflines=5 ;%number of lines to plot (approx)
spacing=ceil((nparam-1)/(numberoflines-1)); %spacing between parameter indices
i_m=[1:spacing:nparam-1 nparam]; %matrix of spaced indices plus last one
colour_m=[7 1 2 3 4 6 8 5 9 10:20];%matrix of line colour order
for ii=1:numberoflines;%loop through lines to plot
 i=i_m(ii);%sorry about this Kludge
 plot(tout,[QL1(:,i) QL2(:,i)]*yscale,[num2str(colour_m(ii)) ';' plotvarname '=' nu
 hold on;
end
```

```
hold off;
gset('output','"/dev/null"')
gset terminal postscript eps enhanced color  solid 20;%save as enhanced colour \
.eps with solid lines and size 20 font
fname=['"plots1/flows_' varname '.eps"'];%filename to save as. inserts variable nam
gset('output',fname);
gset('output','"/dev/null"')

%zoom in on step response and remove key
gset term x11
xti=round(50*(.2*steptime+1.5*max(t_set))/8)/50;
gset('xtics',num2str(xti));
axis([.8*steptime steptime+1.5*max(t_set) (Qs-1.1*max(max([QL1 QL2])))*yscale \
1.05*max(max([QL1 QL2]))*yscale]);
gset nokey;
replot;
gset terminal postscript eps enhanced color  solid 20;
fname=['"plots1/flows_' varname '_z.eps"'];
gset('output',fname);
gset('output','"/dev/null"')

figure(2);
gset term x11
axis([unitmult*min(param) unitmult*max(param) 0 1.1*max(ssPs)]);
gset xtics autofreq
gset ('xlabel', gvar)
gset nokey
gset ylabel 'Steady␣State␣Ps␣(Pa)'
plot(param*unitmult,ssPs)

gset terminal postscript eps enhanced monochrome 20;
fname=['"plots1/ssPs_' varname '.eps"'];
gset('output',fname)
gset('output','"/dev/null"')

figure(3);
gset term x11
axis;
gset ('xlabel', gvar);
gset nokey
gset ylabel 'Steady␣State␣Error␣(%)'
plot(param*unitmult, ss_err)
gset terminal postscript eps enhanced monochrome 20;
fname=['"plots1/ss_err_' varname '.eps"'];
gset('output',fname)
gset('output','"/dev/null"')

figure(4);
gset term x11
axis;
gset ('xlabel', gvar);
gset key
gset ylabel 'Cumulative␣Error␣(%)'
plot(param*unitmult, ss_err,";SS Error;", param*unitmult, dynerr_pc,\
";Dynamic Error;", param*unitmult, E_CUM,";Total;")

gset terminal postscript eps enhanced monochrome dashed 20;
fname=['"plots1/cum_err_' varname '.eps"'];
gset('output',fname)
%replot
gset('output','"/dev/null"')

figure(5);
gset term x11
axis([0.95*unitmult*min(param) 1.05*unitmult*max(param) 0 1.1*max(t_set)]);
gset ('xlabel', gvar);
gset nokey
gset ylabel 'Settling␣Time␣(s)'
plot(param*unitmult, t_set)

gset terminal postscript eps enhanced monochrome 20;
fname=['"plots1/t_set_' varname '.eps"'];
gset('output',fname)
%replot
gset('output','"/dev/null"')

axis;
gset term x11
gset ('xlabel', gvar);
gset key
gset ylabel 'Fitness'
plot(param*unitmult, Fitness,param*unitmult, valFit,";Total;")

gset terminal postscript eps enhanced color 20;
fname=['"plots1/fitness_' varname '.eps"'];
gset('output',fname)
gset('output','"/dev/null"')

end
toc
break
```

C.3 divloadcc.cc

```
#include <octave/oct.h>
#include <octave/variables.h>
#include "oct-obj.h"
// compile with mkoctfile divcc.cc
// added external leakage
// This is the working version. Seems to work at least.

DEFUN_DLD (divloadcc, args, ,"Divider␣Simulation␣with␣Orifice␣Load␣\n
␣␣␣␣␣␣␣␣[dPs␣dPa1␣dPa2␣dPb1␣dPb2␣dxdot␣dx␣dPL1␣dPL2]=divloadcc([Ps␣Pa1␣Pa2
␣␣␣␣␣␣␣␣Pb1␣Pb2␣xdot␣x␣PL1␣PL2],t)␣\n␣Requires␣global␣values␣for
␣␣␣␣␣␣␣␣parameters␣(run␣dividerparam.m␣and␣calcparam.m)␣and␣input
␣␣␣␣␣␣␣␣uto=[t␣fractional_phi␣Qs␣AL1␣AL2]␣\n␣this␣model␣uses␣a␣laminar
␣␣␣␣␣␣␣␣pilot␣stage␣with␣no␣entrance␣losses.␣␣There␣is␣now␣external␣leakage.")
```

```
{
octave_value_list retval;

ColumnVector dy (9);
ColumnVector y (args(0).vector_value ());

int no=2; //number of orifice holes in parallel
double t=args(1).double_value ();//time. duh.

//See dividerparam/calcparams for parameter documentation
const double beta = get_global_value("beta").double_value ();
const double rho = get_global_value("rho").double_value ();
const double nu = get_global_value("nu").double_value ();
const double r = get_global_value("r").double_value ();
const double b = get_global_value("b").double_value ();
const double phi0 = get_global_value("phi0").double_value ();
const double Cdo1 = get_global_value("Cdo1").double_value ();
const double Cdo2 = get_global_value("Cdo2").double_value ();
const double Cdv1 = get_global_value("Cdv1").double_value ();
const double Cdv2 = get_global_value("Cdv2").double_value ();
const double Vs = get_global_value("Vs").double_value ();
const double delta = get_global_value("delta").double_value ();
const double h = get_global_value("h").double_value ();
const double Fc = get_global_value("Fc").double_value ();
const double t_rim = get_global_value("t_rim").double_value ();
const double mu = get_global_value("mu").double_value ();
const double m = get_global_value("m").double_value ();
const double A = get_global_value("A").double_value ();
const double Ao1 = get_global_value("Ao1").double_value ();
const double Ao2 = get_global_value("Ao2").double_value ();
const double rv = get_global_value("rv").double_value ();
const double d0 = get_global_value("d0").double_value ();
const double xmax = get_global_value("xmax").double_value ();
const double V1o = get_global_value("V1o").double_value ();
const double V2o = get_global_value("V2o").double_value ();
const double c = get_global_value("c").double_value ();
const double Va1 = get_global_value("Va1").double_value ();
const double Va2 = get_global_value("Va2").double_value ();
const double LL = get_global_value("LL").double_value ();
const double Bf = get_global_value("Bf").double_value ();
const double CdL1 = get_global_value("CdL1").double_value ();
const double CdL2 = get_global_value("CdL2").double_value ();
const double VL1 = get_global_value("VL1").double_value ();
const double VL2 = get_global_value("VL2").double_value ();
const double Ld = get_global_value("Ld").double_value ();
const double Cb3 = get_global_value("Cb3").double_value ();
const double Cb4 = get_global_value("Cb4").double_value ();

//get dynamic values from y
double Ps=y(0);
double Pa1=y(1);
double Pa2=y(2);
double Pb1=y(3);
double Pb2=y(4);
double xdot=y(5);
double x=y(6);
double PL1=y(7);
double PL2=y(8);

//ensure Pressures are possitive
if (Ps<0) Ps=0;
if (Pa1<0) Pa1=0;
if (Pa2<0) Pa2=0;
if (Pb1<0) Pb1=0;
if (Pb2<0) Pb2=0;
if (PL1<0) PL1=0;
if (PL2<0) PL2=0;

//get input from global ut
Matrix uto (get_global_value("uto").matrix_value ());

int i;
for (i=0;i<15;i++){
if (uto(i,0) >= t)
break;
}
int k=i-1;
if (k<0) k=0;
double phi=uto(k,1) *phi0;
double Qs=uto(k,2) ;
double AL1=uto(k,3);
double AL2=uto(k,4) ;

//Model calculations
double Qs1;
if ((Ps-Pa1)>0)
 Qs1=Cdo1*Ao1*sqrt(2/rho*(Ps-Pa1));
else
 Qs1=-Cdo1*Ao1*sqrt(2/rho*(Pa1-Ps));

double Qs2;
if ((Ps-Pa2)>0)
Qs2=Cdo2*Ao2*sqrt(2/rho*(Ps-Pa2));
else
Qs2=-Cdo2*Ao2*sqrt(2/rho*(Pa2-Ps));

//limit x
if (x>xmax) {
    x=xmax;
    xdot=0;
}

if (x<-xmax) {
    x=-xmax;
    xdot=0;
    }
```

```
double x1=x;    // %limit area (no negative, or greater than pi rv^2)
if (x1>(d0+rv))
     x1=d0+rv;

if (x1<(d0-rv))
     x1=d0-rv;

//orifice areas
double Av1=no*rv*rv*acos((d0-x1)/rv)-(d0-x1)*sqrt(rv*rv-(d0-x1)*(d0-x1));
double Av2=no*rv*rv*acos((d0+x1)/rv)-(d0+x1)*sqrt(rv*rv-(d0+x1)*(d0+x1));

//rim area for flow force
double Arim1=no*t_rim*2*sqrt(rv*rv-(d0-x1)*(d0-x1));
double Arim2=no*t_rim*2*sqrt(rv*rv-(d0+x1)*(d0+x1));
if (x>d0+rv|x<d0-rv){
     Arim1=0;
     Arim2=0;
     }

double QL1;
double fftr1; //I *did* include transient flow forces.
if ((Pa1-PL1)>0)
 {QL1=Cdv1*Av1*sqrt(2/rho*(Pa1-PL1));
 fftr1=Ld*Cdv1*Arim1/t_rim*sqrt(2*rho*(Pa1-PL1))*xdot;}
else
 {QL1=-Cdv1*Av1*sqrt(2/rho*(-Pa1+PL1));
 fftr1=-Ld*Cdv1*Arim1/t_rim*sqrt(2*rho*(-Pa1+PL1))*xdot;}

double QL2;
double fftr2;
if ((Pa2-PL2)>0)
{QL2=Cdv2*Av2*sqrt(2/rho*(Pa2-PL2));
fftr2=Ld*Cdv2*Arim2/t_rim*sqrt(2*rho*(Pa2-PL2))*xdot;}
else
{QL2=-Cdv2*Av2*sqrt(2/rho*(-Pa2+PL2));
fftr2=-Ld*Cdv2*Arim2/t_rim*sqrt(2*rho*(-Pa2+PL2))*xdot;}

double Ca1=Pa1;
double Cb1=(Pb1-Pa1*cos((phi0-phi)/sqrt(c)))/sin((phi0-phi)/sqrt(c));
double Cc1=Ps;
double Cd1=(Pb1-Ps*cos((phi)/sqrt(c)))/sin((phi)/sqrt(c));


double Qa1i=pow(b,double( 4))/(185*mu*r*sqrt(c))*(-Ca1*sin((phi0-phi)/sqrt(c))+
         Cb1*cos((phi0-phi)/sqrt(c)));
double Qc1o=pow(b,double( 4))/(185*mu*r*sqrt(c))*(Cc1*sin(phi/sqrt(c))-Cd1*
         cos(phi/sqrt(c)));

double Qb1=Qc1o-Qa1i;

double Ca2=Ps;
double Cb2=(Pb2-Ps*cos((phi0-phi)/sqrt(c)))/sin((phi0-phi)/sqrt(c));
double Cc2=Pa2;
double Cd2=(Pb2-Pa2*cos((phi)/sqrt(c)))/sin((phi)/sqrt(c));
double Qa2i=pow(b,double( 4))/(185*mu*r*sqrt(c))*(-Cc2*sin(phi/sqrt(c))+
        Cd2*cos(phi/sqrt(c)));
double Qc2o=pow(b,double( 4))/(185*mu*r*sqrt(c))*(Ca2*sin((phi0-phi)/sqrt(c))-
        Cb2*cos((phi0-phi)/sqrt(c)));
double Qb2=Qc2o-Qa2i;
double Qa1o=b*b/mu*sqrt(pow(delta,double(3))/(6*185*h))*Cb1;
double Qa2o=b*b/mu*sqrt(pow(delta,double(3))/(6*185*h))*Cd2;
double Qc2i=-b*b/mu*sqrt(pow(delta,double(3))/(6*185*h))*Cb2;

double Vb1=V1o+A*x;
if (Vb1<0)//make sure no negative volume
    Vb1=1e-15;//arbitrary small number

double Vb2=V2o-x*A;
if (Vb2<0)
    Vb2=1e-15;

//%leakage%
double Qlbl1=0;
double Qlbg1=r*pow(delta,double(3))/(12*mu*h)*((Pb1-Pa1)/2*phi0+sqrt(c)*
        (-Cc1*sin(phi/sqrt(c))+Cd1*(cos(phi/sqrt(c))-1)-Ca1*
        sin((phi0-phi)/sqrt(c))-Cb1*(1-cos((phi0-phi)/sqrt(c)))));
double Qlb1=2*(Qlbl1+Qlbg1);
double Qlbl2=0;
double Qlbg2=r*pow(delta,double(3))/(12*mu*h)*((Pb2-Pa2)/2*phi0-sqrt(c)*
        (-Cc2*sin(phi/sqrt(c))+Cd2*(cos(phi/sqrt(c))-1)-Ca2*
        sin((phi0-phi)/sqrt(c))-Cb2*(1-cos((phi0-phi)/sqrt(c)))));
double Qlb2=2*(Qlbl2+Qlbg2);
double Qlal1=0;
double Qlag1=r*pow(delta,double(3))/(12*mu*h)*((Pb1-Pa1)/2*phi0-sqrt(c)*
        (-Cc1*sin(phi/sqrt(c))+ Cd1*(cos(phi/sqrt(c))-1)-Ca1*
        sin((phi0-phi)/sqrt(c))-Cb1*(1-cos((phi0-phi)/sqrt(c)))));
double Qla1=2*(Qlal1+Qlag1);
double Qlal2=0;
double Qlag2=r*pow(delta,double(3))/(12*mu*h)*((Pb2-Pa2)/2*phi0-sqrt(c)*
        (-Cc2*sin(phi/sqrt(c))+ Cd2*(cos(phi/sqrt(c))-1)-Ca2*
        sin((phi0-phi)/sqrt(c))-Cb2*(1-cos((phi0-phi)/sqrt(c)))));
double Qla2=2*(Qlal2+Qlag2);
double Qla3=0;
double Qla4=0;
double Qlb3=Cb3*Pb1;
double Qlb4=Cb4*Pb2;

//%Load
double QLo1=CdL1*AL1*sqrt(2/rho*PL1);
double QLo2=CdL2*AL2*sqrt(2/rho*PL2);


//%diff equations
double dPs=beta/Vs*(Qs-Qs1-Qs2-2*Qc1i-2*Qc2i);
double dPa1=beta/Va1*(Qs1-QL1+2*Qa1o+Qla1+Qla3);
double dPa2=beta/Va2*(Qs2-QL2+2*Qa2o+Qla2+Qla4);
double dPb1=beta/Vb1*(2*Qb1-xdot*A-Qlb1-Qlb3);
double dPb2=beta/Vb2*(2*Qb2+xdot*A-Qlb2-Qlb4);
double dxdot;
double xdotfric=1e-6;

dxdot=1/m*((Pb1-Pb2)*A+Arim1/2*(PL1-Pa1)-Arim2/2*(PL2-Pa2)-Bf*xdot-
        Fc*tanh(xdot/xdotfric)-fftr1-fftr2);
double dx=xdot;
double dPL1=beta/VL1*(QL1-QLo1);
double dPL2=beta/VL2*(QL2-QLo2);

//send output into dy
dy(0)=dPs;
dy(1)=dPa1;
dy(2)=dPa2;
dy(3)=dPb1;
dy(4)=dPb2;
dy(5)=dxdot;
dy(6)=dx;
dy(7)=dPL1;
dy(8)=dPL2;

retval=octave_value (dy);

return retval;
}
```

C.4 gadiv.m

```
%this works. Runs a GA on the aggregated fitness function
%requires the GAOT package
tic

population=50
gennum=250;%number of generations
clear global poptrace
global poptrace

%set bounds for params
bounds=[[0.006 0.016];[0.6e-3 2e-3];[2e6 10e6];[0.3 0.9];[0.2 0.7]];\
   %r b delta deltaPt Po_Pt frac_open

%initialize population
initPop=initializega(population,bounds,'divfitag');

%be fuitful and multiply!!!
[x endPop bPop TraceInfo] = ga(bounds,'divfitag',[],initPop,[1e-6 1 0],'maxGenTerm'

timtoc=toc

%%%%%%%%%%
%find best
%%%%%%%%%%
dividerparam;
r=x(1);
```

```
b=x(2);
deltaPt=x(3);
Po_Pt=x(4);
frac_open=x(5);
calcparams
runsimloadcc

bestx=min(find(poptrace(:,1)==x(:,1)&poptrace(:,2)==x(:,2)\
&poptrace(:,3)==x(:,3)&poptrace(:,4)==x(:,4)&poptrace(:,5)==x(:,5)))

beep %moo
```

C.5 divfitag.m

The genetic algorithm in this section is run with default GAOT parameters with a population of 50 and 250 generations.

```
function [sol,valFit] = divfitag(sol,options)
% this function aggregates the objectives for the divider
% sol=[r b deltaPt Po_Pt frac_open initialFitness]
% other parameters come from dividerparam
% options = blah (could use to pick method)
%
% this requires the trapz function


if nargin<2
 options=[0 0]; %default to goal attainment
end

if length(options)<2
 options(2)=0;
end

global poptrace Fitness Pslimit

clear param ut QL1 QL2 ssPs ssPs maxP Fitness valFit dynerr ss_err cum_ss_err t_set

dividerparam;
%optimizedparam;
r=sol(1);
b=sol(2);
deltaPt=sol(3);
Po_Pt=sol(4);
frac_open=sol(5);
calcparams;

%%%%%%%%%%%%%%%%%%%%%%%%%%
% Setup Test Parameters %
%%%%%%%%%%%%%%%%%%%%%%%%%%
phi=phi0/2;
Qs=10e-4;
PL1=10e6;     %desired SS
```

```
AL1=(Qs/2)/(CdL1*sqrt(2/rho*PL1));
stepPL1=15e6;    %desired SS
stepAL1=(Qs/2)/(CdL1*sqrt(2/rho*stepPL1));
PL2=10e6;    %desired SS
AL2=(Qs/2)/(CdL2*sqrt(2/rho*PL2));
steptime=0.05;
global uto
uto=[[0 phi/phi0 Qs AL1 AL2];[steptime phi/phi0 Qs stepAL1 AL2];[1000 phi/phi0 Qs st

%%%%%%%%%%%%%%%%%%%%%%%%%%%%%%%%
% Setup Aggregation Parameters %
%%%%%%%%%%%%%%%%%%%%%%%%%%%%%%%%

%Note weights are inverse of Matlab help, i.e. here higher weight means more import
  W1=3;%ss error
  W2=1;%pressure drop
  W3=3;%dyn err

%Goals
  ss_err0=0.5;
  ssPs0=18e6;
  dynerr0=0.5e-6;
  t_cum=0.2;

Pslimit=30e6; %limit source pressure


%%%%%%%%%%%%%%%%%%%%%%%%%%%
% Setup Solver Parameters %
%%%%%%%%%%%%%%%%%%%%%%%%%%%

npoints=1000;%approx number of time points

t_test=1; %(s) test total time

x0=zeros(9,1); %ititial conditions
lsode_options("relative tolerance", 1e-3)
%lsode_options("integration method", "stiff")
lsode_options("step limit", 10000)

tout=[linspace(0,0.99*steptime,round(npoints/3)) logspace(log10(0.99001*steptime),lo
clear yout

%%%%%%%%%%%%
% Solve DE %
%%%%%%%%%%%%

try; %check for error
  yout= lsode("divloadcc",x0,tout); %run solver
catch; %if error set fitness to bad value and exit function
  valFit=-100
  break
end;
```

```
%%%%%%%%%%%%%%%%%%%%%%%%%
% Calculate Performance %
%%%%%%%%%%%%%%%%%%%%%%%%%

  PL1=yout(:,8);
  PL2=yout(:,9);

  AL1m=AL1.*(tout<steptime)+stepAL1.*(tout>steptime);
  QL1=CdL1.*AL1m'.*sqrt(2/rho*PL1);%assume QL1=QLo1
  QL2=CdL2*AL2*sqrt(2/rho*PL2);
  ssPs=yout(length(yout),1);

  k_step=min(find(tout>=steptime));
  maxP=max(max(yout(:,1:5)));

  ssQ1=QL1(end);
  ssQ2=QL2(end);
  k_set=max(find(abs((QL1-ssQ1)/ssQ1)>0.02)); %settling step number
  t_set=tout(k_set)-steptime;
  dynerr=(trapz(tout(k_step:k_set),(QL1(k_step:k_set)-ssQ1-\
  (QL2(k_step:k_set)-ssQ2))));
  ss_err=(ssQ1-ssQ2)/Qs*100;
  cum_ss_err=(ssQ1-ssQ2)*t_cum;
  E_CUM=abs((cum_ss_err+dynerr)/(Qs*t_cum)*100);
  DeltaP=ssPs-max(PL2(end),stepPL1);
  dynerr_pc=dynerr/(Qs*t_cum)*100;

%%%%%%%%%%%%%%%%%%%%%%%%
% Aggregate Objectives %
%%%%%%%%%%%%%%%%%%%%%%%%

if (options(2)==0); %Goal attainment
 Fitness(1)=(abs(ss_err)-ss_err0)/ss_err0*W1;

 Fitness(2)=(ssPs-ssPs0)/ssPs0*W2;

 Fitness(3)=(abs(dynerr)-dynerr0)/dynerr0*W3;

 valFit=-max(Fitness);%goal attainment \
 (negative to maximize valFit)

 if ssPs>Pslimit
  valFit=-1e4;
 endif

else
  if (options(2)==1);
  Fitness(1)=abs(ss_err/ss_err0)^(1+(1+W1)/2);
  Fitness(2)=(ssPs/ssPs0)^(1+(1+W2)/2);
  Fitness(3)=abs(dynerr/dynerr0)^(1+(1+W3)/2);

  valFit=-sum(Fitness);

  if ssPs>Pslimit
```

```
    valFit=-1e4;
   endif
  else
   break
  endif
 endif

sol(end)=valFit;

%end

%%%%%%%%%%%%%%%%%%%%%%%%%
% Write to Population Trace %
%%%%%%%%%%%%%%%%%%%%%%%%%

  try
   poptrace=[poptrace; [sol ss_err ssPs dynerr_pc]];
  catch
   poptrace=[sol ss_err ssPs dynerr_pc];
  end_try_catch
end
```

C.6 complexdiv.m

```
%this uses the complex method to optimize divfitag.
%Make sure the path is set to find it.
%Requires the genetic algorithm files for setup

tic
population=7 %population size, must be larger than number\
of dimensions
gennum=200 %number of generations
clear global poptrace
global poptrace



bounds=[[0.006 0.016];[0.6e-3 2e-3];[2e6 10e6];[0.3 0.99];[0.1 0.9]];\
   %r b delta deltaPt Po_Pt frac_open
initPop=initializega(population,bounds,'divfitag');
disp('initialized');
[x endPop] = complex(bounds,'divfitag',gennum,initPop);

timtoc=toc

%%%%%%%%%%
%find best
%%%%%%%%%%
r=x(1);
b=x(2);
deltaPt=x(3);
Po_Pt=x(4);
```

```
frac_open=x(5);
calcparams
runsimloadcc
bestx=min(find(poptrace(:,1)==x(:,1)&poptrace(:,2)==x(:,2)\
&poptrace(:,3)==x(:,3)&poptrace(:,4)==x(:,4)&poptrace(:,5)==x(:,5)))
```

C.7 complex.m

```
function [x,endPop] = complex(bounds,evalFN,evalOps,startPop)
%this solves a MOO by using the complex method.
%evalOps=number of generations

n=nargin;
if n<2
  disp('Insufficient␣arguements')
end
if n<3 %Default evalation opts.
  evalOps=[100];
end
if n<4
  %randomly populate
  initPop=initializega(4,bounds,evalFN); %use initializer from ga, population 4
end

evstr=['[c1␣c1(xZomeLength)]=' evalFN '(c1,[]);␣gen=gen+1;'];

xZomeLength  = size(startPop,2);          %Length of the xzome=numVars+fittness
numVar       = xZomeLength-1;
popul=rows(startPop);   %number of points
xpop=zeros(popul,xZomeLength);
maxgen=evalOps;
xpop=startPop;
gen=1

for i=1:popul
 c1=xpop(i,:);
 eval(evstr); %get fitness
 xpop(i,:)=c1;
end

do; %start main loop

[bestfit bestdx]=max(xpop(:,xZomeLength));
bestx=xpop(bestdx,:);

[worstfit worstdx]=min(xpop(:,xZomeLength));
worstx=xpop(worstdx,:);

centroidx=(sum(xpop)-worstx)/(popul-1);

alpha=1.3;
nr=4;
newx=centroidx+alpha*(centroidx-worstx);
```

```
if (any(newx(1:numVar)<bounds(:,1)'|newx(1:numVar)>bounds(:,2)')); %check bounds
 for i=1:numVar;
  if (newx(i)<bounds(i,1));
   newx(i)=bounds(i,1);
  end
  if (newx(i)>bounds(i,2));
   newx(i)=bounds(i,2);
  end
 end
end


c1=newx;
eval(evstr);
newx=c1;

if (newx(xZomeLength)<worstx(xZomeLength)); %make sure we have an improvement
 kr=1;
 do;
  epsil=(nr/(nr+kr+1))^((nr+kr-1)/nr);
  R=rand;
  oldnewx=newx;
  newx=(oldnewx+epsil*centroidx+(1-epsil)*bestx)/2+(centroidx-bestx)*(1-epsil)*(2*R
  if (any(newx(1:numVar)<bounds(:,1)'|newx(1:numVar)>bounds(:,2)')); %check bounds
   for i=1:numVar;
    if (newx(i)<bounds(i,1));
     newx(i)=bounds(i,1);
    end
    if (newx(i)>bounds(i,2));
     newx(i)=bounds(i,2);
    end
   end
  end

  c1=newx;
  eval(evstr);
  newx=c1;
  kr=kr+1;

 until(newx(xZomeLength)>worstx(xZomeLength));
end;
xpop(worstdx,:)=newx;


until(gen>maxgen);

endPop=xpop

[bestfit bestdx]=max(xpop(:,xZomeLength));
bestx=xpop(bestdx,:);

x=bestx;
```

Appendix D

Prototype Machining Drawings

This appendix includes drawings used to produce the prototype valve used to experimentally verify the theory. These are the orginal drawings and a number of changes were made, for example, drilling holes for pressure measurements. As such, they are provided for information purposes only and no guarantees are made as to their accuracy. These drawings should not be scaled.

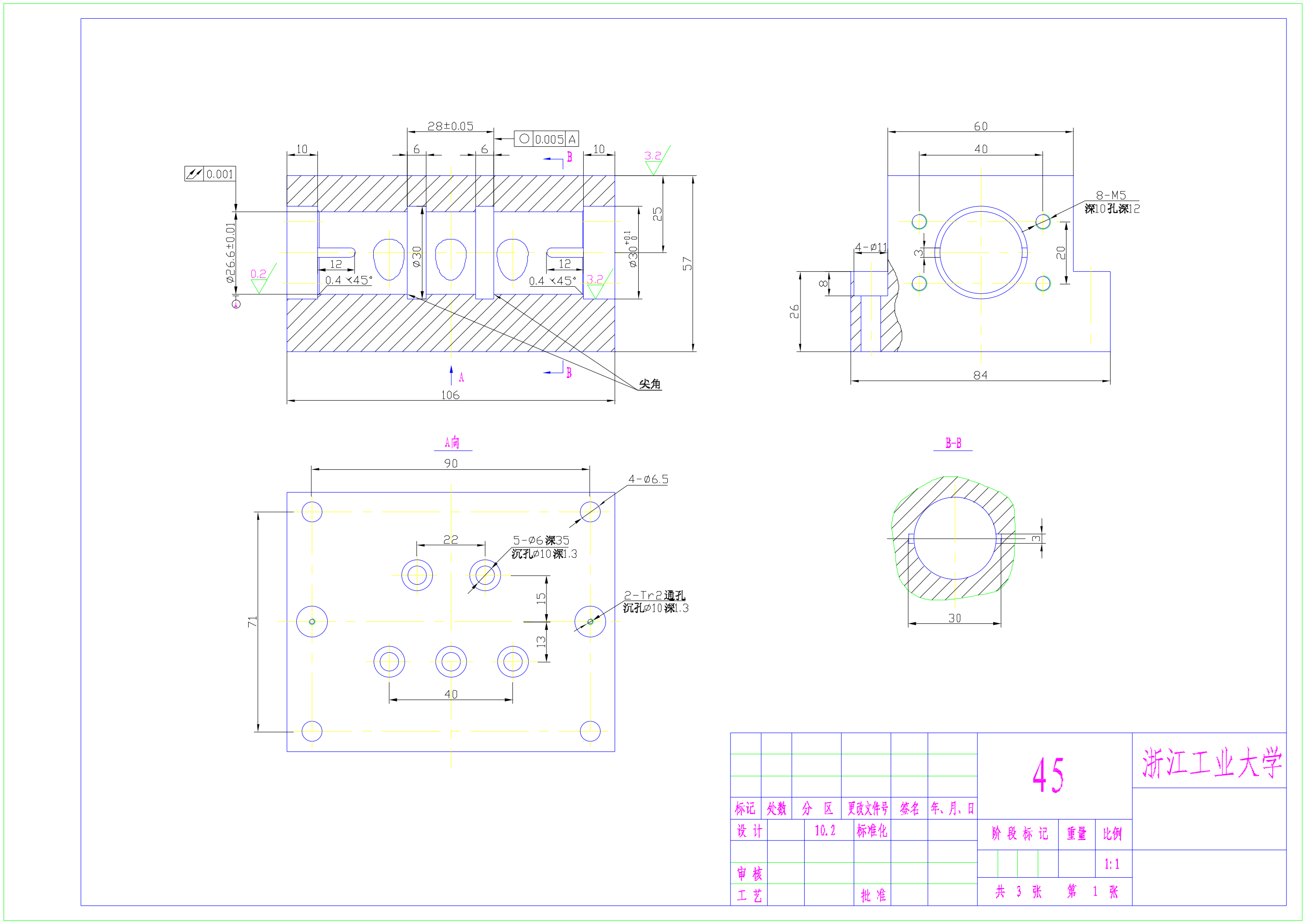
0.001
0.005 A
28±0.05
10
6
6
10
3.2
B
ø26.6±0.01
0.2
12
0.4 ×45°
ø30
12
0.4 ×45°
3.2
ø30 +0.1 0
25
57
A
B
106
尖角
60
40
8-M5
深10孔深12
4-ø11
3
8
20
26
84
A向
90
4-ø6.5
22
5-ø6深35
沉孔ø10深1.3
15
2-Tr2通孔
沉孔ø10深1.3
71
13
40
B-B
3
30
标记
处数
分 区
更改文件号
签名
年、月、日
设 计
10.2
标准化
审 核
工 艺
批 准
45
阶 段 标 记
重量
比例
1:1
共 3 张
第 1 张
浙江工业大学

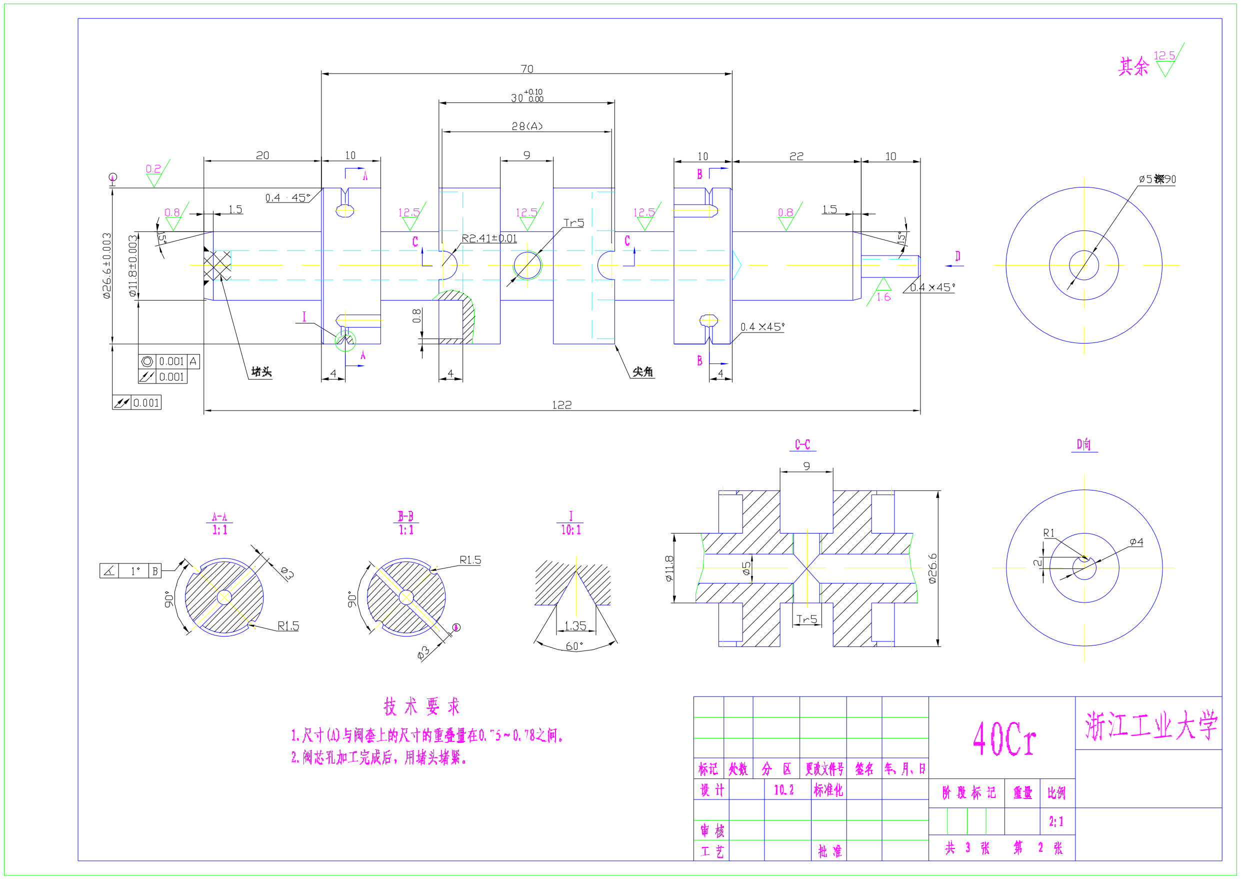
其余 12.5
70
30 +0.10 0.00
28(A)
20
10
9
10
22
10
1.5
1.5
0.4 45°
0.4×45°
0.4×45°
0.2
0.8
0.8
12.5
12.5
12.5
1.6
R2.41±0.01
Tr5
A
A
B
B
C
C
D
I
0.8
4
4
4
15°
15°
φ26.6±0.003
φ11.8±0.003
0.001 A
0.001
0.001
堵头
尖角
122
ø5 深90
C-C
9
φ11.8
φ5
φ26.6
Tr5
D向
R1
2
φ4
A-A 1:1
1° B
90°
φ2
R1.5
B-B 1:1
90°
R1.5
φ3
I 10:1
1.35
60°
标记
处数
分 区
更改文件号
签名
年、月、日
设 计
10.2
标准化
审 核
工 艺
批 准
40Cr
浙江工业大学
阶 段 标 记
重量
比例
2:1
共 3 张
第 2 张

技 术 要 求

1. 尺寸(A)与阀套上的尺寸的重叠量在0.75～0.78之间。
2. 阀芯孔加工完成后，用堵头堵紧。

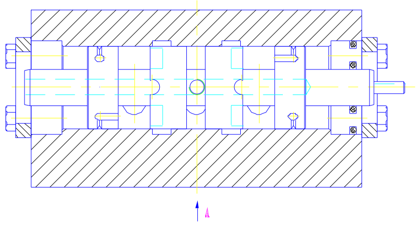

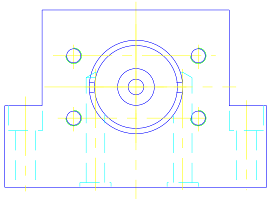

A向

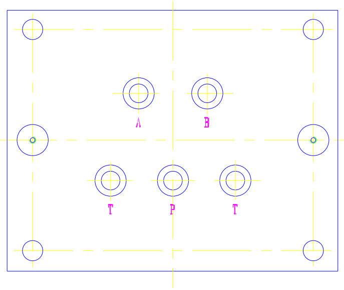

技 术 要 求

1. 在Φ26.6和Φ11.8处阀芯与孔之间的配合半径间隙在0.003～0.005。
2. 装配前去毛刺，先用煤油清洗，然后用机油。
3. 按要求在图示位置打上各相应字母的标记。

标记	处数	分 区	更改文件号	签名	年、月、日
设 计		10.2	标准化		
审 核					
工 艺			批 准		

阶 段 标 记	重量	比例
		1:1
共 3 张	第 3 张	

浙江工业大学

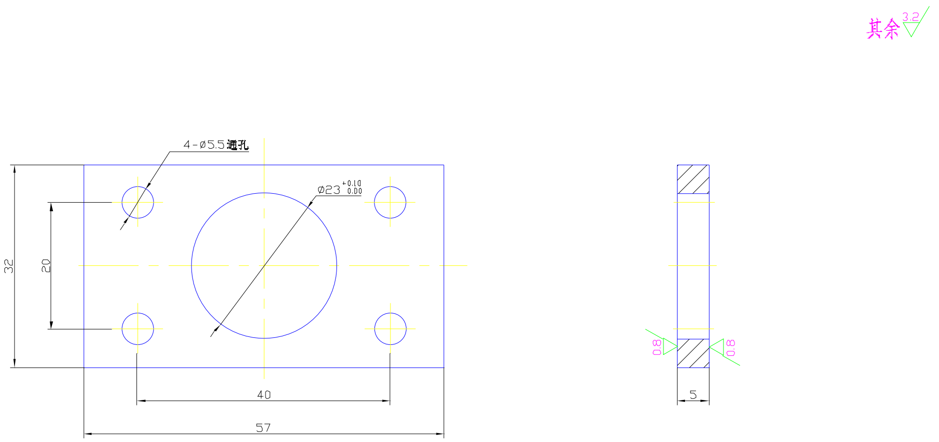
其余 3.2
4-ø5.5通孔
ø23 +0.10 0.00
32
20
40
57
0.8
0.8
5

技 术 要 求

1.去毛刺，边角倒钝。

标记	处数	分 区	更改文件号	签名	年、月、日				浙江工业大学
设 计		10.2	标准化			阶 段 标 记	重量	比例	
								2:1	
审 核									
工 艺			批 准			共 3 张	第 1 张		

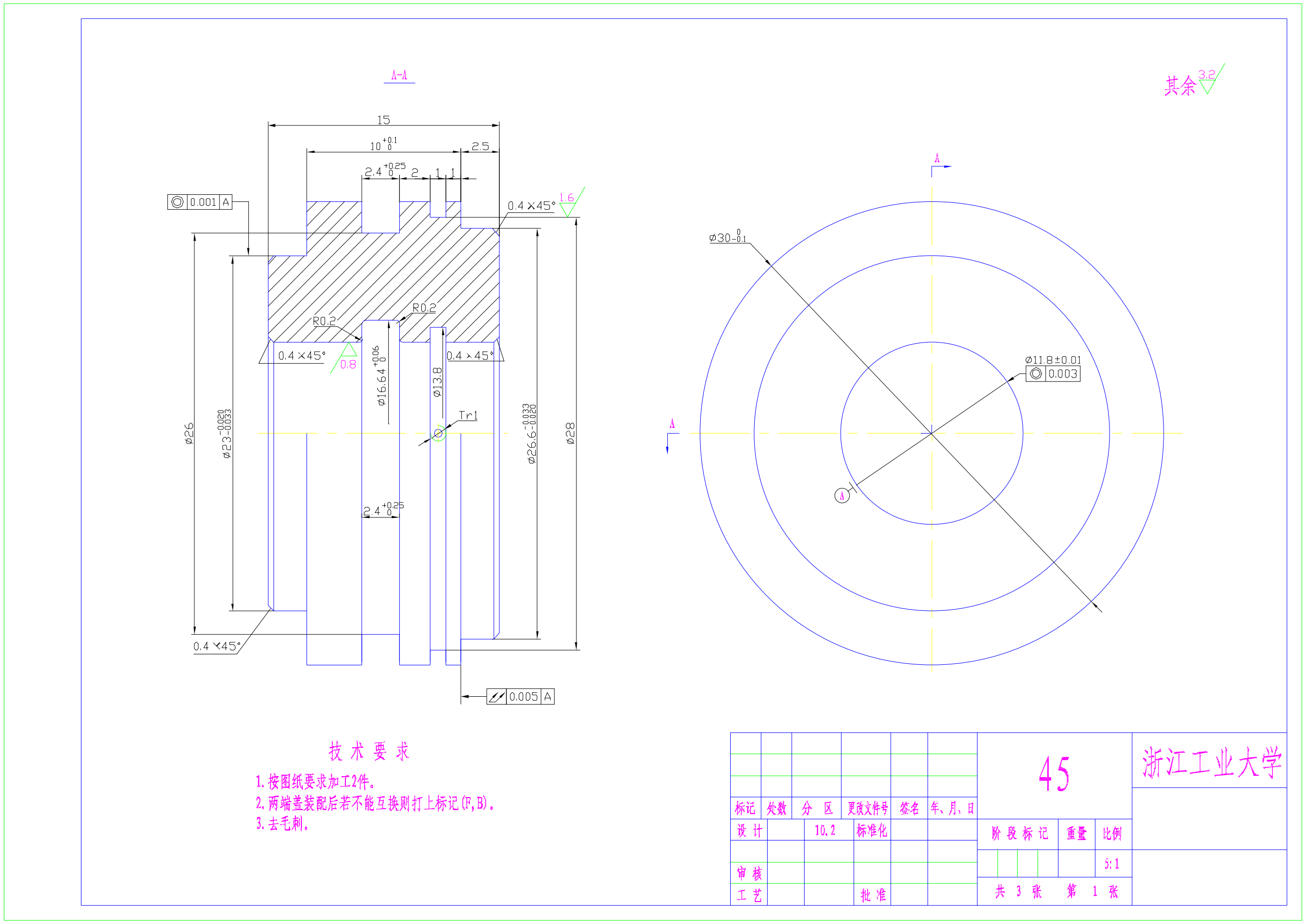
A-A
15
10 +0.1 0
2.5
2.4 +0.25 0
2
1
1
0.001 A
0.4×45°
1.6
R0.2
R0.2
0.4×45°
0.8
0.4×45°
ø16.64 +0.06 0
ø13.8
Tr1
ø26
ø23 -0.020 -0.033
ø26.6 -0.020 -0.033
ø28
2.4 +0.25 0
0.4×45°
0.005 A
其余 3.2
A
A
ø30 0 -0.1
ø11.8±0.01
0.003
A
45
浙江工业大学
标记
处数
分 区
更改文件号
签名
年、月、日
设 计
10.2
标准化
审 核
工 艺
批 准
阶 段 标 记
重量
比例
5:1
共 3 张
第 1 张

技 术 要 求

1. 按图纸要求加工2件。
2. 两端盖装配后若不能互换则打上标记(F,B)。
3. 去毛刺。

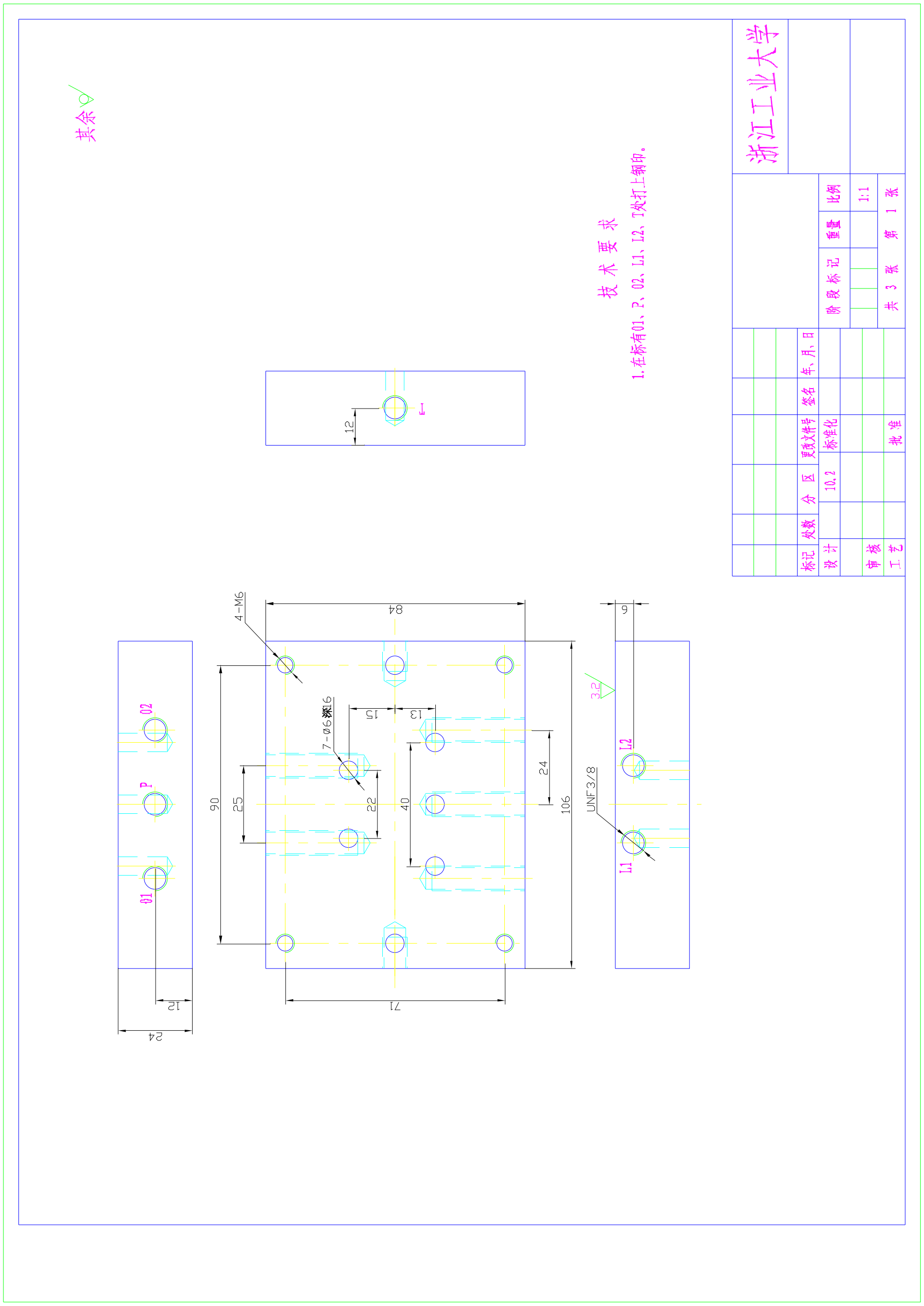
其余
技术要求
1.在标有O1、P、O2、L1、L2、T处打上钢印。
浙江工业大学
标记
处数
分区
更改文件号
签名
年、月、日
设计
10.2
标准化
审核
工艺
批准
阶段标记
重量
比例
1:1
共 3 张
第 1 张
4-M6
84
90
106
71
25
22
40
24
15
13
12
24
6
7-ø6深16
UNF3/8
3.2
O1
P
O2
L1
L2
T

Appendix E

Experimental Procedures

This appendix describes the various procedures and equipment used to experimentally evaluate the valve. This includes both calibration of the transducers and the procedures used to collect the data. Additionally, an analysis of the measurement uncertainties involved is presented.

E.1 Instrumentation

A number of different instruments were used in the course of the experimental program contained in this thesis. These include flow meters, and absolute and differential pressure transducers. The flow meters were drag-type meters, one of which was labeled Ramapo Model V-.5-AOS5K6-E and the other was U of S serial number 01746. The amplifiers used were “2310 Signal Conditioning Amplifiers” serial number 0047293 and 0013760. The absolute pressure transducers were Durham Industries type P1021-0005, serial numbers 113128 and 113127 with amplifiers made by Engineering Shops, serial numbers 00120 and 00121. The differential pressure transducers used were made by Valdyne, serial number 47974 and 83055 with amplifiers made by Engineering Shops (serial number 0077062) and Valdyne (model CD15, serial number 83055).

E.2 Calibration of Instruments

Before measuring any physical quantity, the transducer must be calibrated. This typically involves comparing the instrument output to some standard. In this experimental program, two important transducer types must be calibrated: pressure and flow measurement instruments.

The calibration of pressure transducers was performed using a deadweight tester. A known weight was applied to a piston of known area to create a pressure. The piston was specially designed to have low friction and was rotated to eliminate any static friction. At each applied pressure, the data acquisition software (Simulink) used to record the actual data was used to measure the calibration output of the amplifier. This allows the calibration of not only the transducer, but also the amplifier, data acquisition system, and software. The first data point to be recorded was at zero pressure; for all subsequent measurements, before any data was recorded, the amplifier's "zero" setting was adjusted so that the output voltage was as near to zero as possible at zero pressure. Next, a number of different weights were applied over the transducer's expected operating range and the output voltage was recorded. This data was then fit to the curve $P = AV + B$ where P is pressure, V is voltage, and A and B are calibration constants. The data and curve fits are shown in Figures E.1 and E.2. From this data, the calibration coefficients can be found in Table E.1.

Table E.1: Pressure calibration coefficients

	P_{a1}	P_{a2}	P_s	ΔP_L
A	1.75×10^6	1.73×10^6	1.73×10^6	1.72×10^6
B	2.33×10^3	2.44×10^3	-6.40×10^4	6.90×10^3

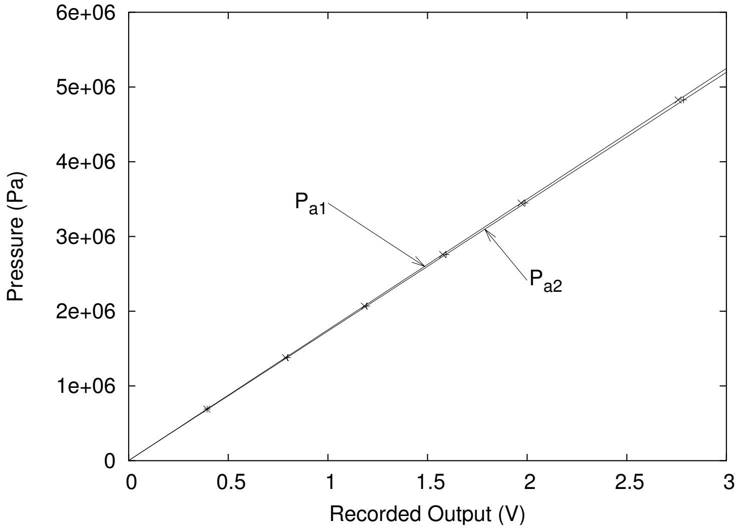

Figure E.1: Calibration curves for the absolute pressure transducers.

The flow meters used in this experimental program were calibrated using the "bucket and stopwatch" method. This means that the standard flow was determined by collecting the flow in a container. Knowing the volume, one can then determine the average flow rate, which was then compared to the output voltage (again, measured via the data acquisition software). This data was fit to the curve $Q = AV^B$ where Q is the flow, as presented in Figure E.3. The calibration constants were found to be $A = 0.000317$ and $B = 0.553$ for Q_1, and $A = 0.000306$ and $B = 0.552$ for Q_2.

E.3 Experimental Procedure

The following procedure was used for each test. The circuit used is shown in Figures E.4 and E.5.

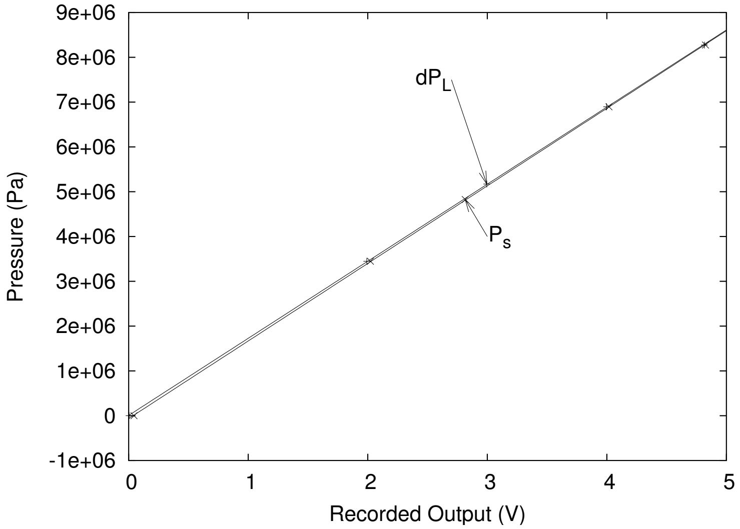

Figure E.2: Calibration curves for the differential pressure transducers.

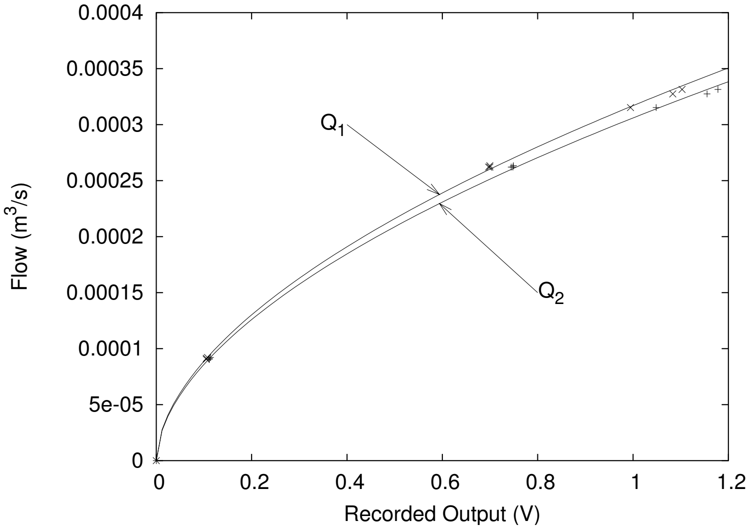

Figure E.3: Calibration curves for the flow transducers.

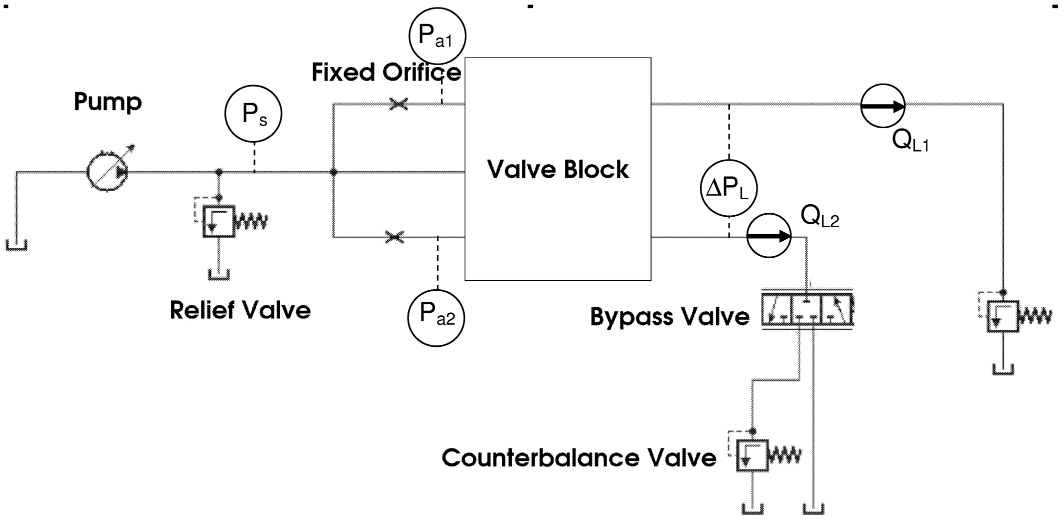
Pump
Relief Valve
P_s
Fixed Orifice
P_{a1}
P_{a2}
Valve Block
ΔP_L
Q_{L1}
Q_{L2}
Bypass Valve
Counterbalance Valve

Figure E.4: The circuit diagram of the system used to test the valve prototype. The valve body contains the pilot stages and the variable orifices.

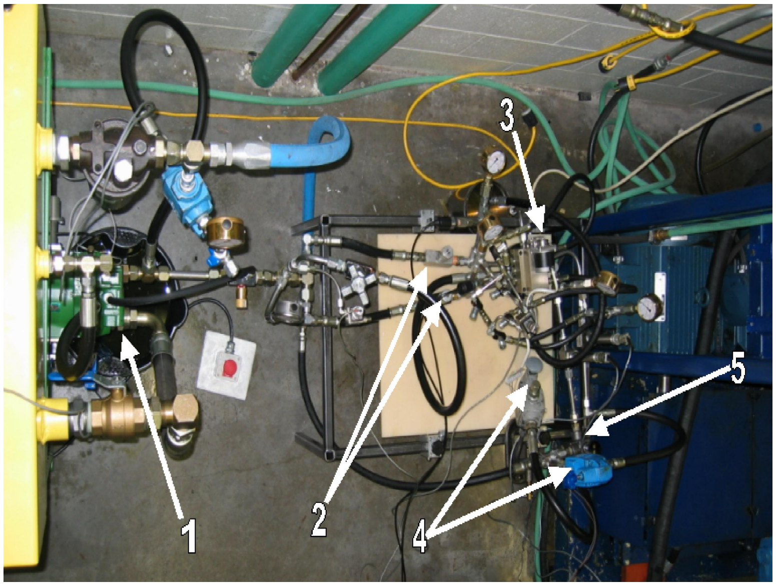

Figure E.5: Photo of the test circuit, showing pump (1), fixed orifices (2), valve block (3), counterbalance valves (4), and three-way bypass valve (5).

1. Allow the fluid to warm up by running the apparatus until the temperature reaches the operating temperature.
2. Rotate the spool to the desired angular position. Close the valve connecting the divider to the source pressure.
3. Adjust the pump's output flow to the desired total flow and adjust the relief valve so that it is just above the highest expected pressure
4. With the fixed orifices set for approximately the desired flow ratio and one flow branch bypassing one load counterbalance valve, adjust the other counterbalance valve for the desired load pressure difference.
5. With the bypass valve set so that the flow is now not bypassing, adjust the counterbalance valve so that the load pressures are equal.
6. Adjust the fixed orifices so that the flows are in the desired ratio and the pressure drop across them is as desired.
7. Readjust the counterbalance valves and fixed orifices so that the flows and pressures are all at the desired values.
8. Open the valve connecting the divider to the source pressure to re-enable the pilot stage.
9. Record data while creating steps in load pressure by shifting the bypass valve in the load circuit.

E.4 Experimental Error

One important question to be asked whenever data is presented is "how much confidence do you have in this data?" This section will attempt to answer this question through an analysis of the errors involved the experimental program.

There are three sources of error in any experimental program:

1. blunders and mistakes,
2. systematic errors, and
3. random errors.

Blunders and mistakes include such errors as incorrectly writing down a number or performing a calculation incorrectly. These errors can generally be identified by noticing obvious outliers and can be avoided by having an idea of what reasonable values should be and by repeating experiments. Therefore, this analysis will not discuss mistakes or blunders further.

Systematic errors are repeatable errors in measurement, such as a bias in calibration. These errors can be evaluated by comparing the measured value to a known "true" value or standard.

Thirdly, random errors are a measurement uncertainty due to “fluctuations in observations that yield different results each time the experiment is repeated, and thus require repeated experimentation to yield precise results” (Bevington and Robinson, 2003). The magnitude of these uncertainties can be evaluated statistically; the most common expression is the standard deviation, although other measures are sometimes used.

E.4.1 Flow Measurement Uncertainty

One of the most important experimental measurements gathered in the course of this thesis work was the valve’s outlet flow, as this was used to determine the valve’s accuracy. As noted in Section E.2, the flow transducers and data acquisition equipment were calibrated using a computer controlled bucket and stopwatch method. Before one can evaluate the accuracy of the transducers, one must determine the accuracy of the standard used in the calibration. In this case, the average flow was calculated using

$$Q = \frac{\Delta V}{\Delta t} \tag{E.1}$$

which includes two sources of systematic error: volume measurement and time measurement. The error in Q, δQ, due to errors in ΔV and Δt is given by

$$\delta Q = \left|\delta \Delta V \frac{\partial Q}{\partial \Delta V}\right| + \left|\delta \Delta t \frac{\partial Q}{\partial \Delta t}\right| \tag{E.2}$$

$$\delta Q = \frac{\delta \Delta V}{\Delta t} + \frac{\delta \Delta t \Delta V}{\Delta t^2} \tag{E.3}$$

The uncertainty in ΔV was estimated by pouring a measured amount of fluid into the container and recording the computer’s output. When 0.920 L of fluid (measured with a graduated cylinder) was added, the computer measured a 0.780 L change. Therefore, the uncertainty in the volume measurements was estimated to be approximately 0.14 L. The uncertainty in Δt is dominated by the computer’s reaction time, which is believed to be negligible. As the test time for the calibration was 60 s, the error in the flow standard was estimated to be $2.3 \times 10^{-6}\ m^3/s$.

The “bucket and stopwatch” flow was then compared to the average transducer output. The output was recorded for approximately 600 data points, which had a standard deviation of $s < 0.02\ V$. An estimation of the standard deviation of the mean of N measurements can be determined using

$$\sigma_\mu = \frac{s}{\sqrt{N}} \tag{E.4}$$

from Bevington and Robinson (2003). Due to the large number of data points used, this error is well under 0.1%, less than the error in the flow standard. This permits a much simpler method of determining the error due to the curve fit. If we assume that the voltages are exact, the uncertainty due to the curve fit can be determined from the standard deviation of the data from the curve. That is

$$s^2 = \frac{1}{N-1} \frac{\Sigma\left[(1/\sigma_i^2)[Q_i - Q(V_i)]^2\right]}{(1/N)\Sigma(1/\sigma_i^2)} \tag{E.5}$$

where σ_i^2 is the variance in each flow measurement. The calculated standard deviation, s, can be converted into an error with 90% confidence by multiplying by 1.64. These errors were calculated to be 3.9×10^{-6} for Q_1 and 3.7×10^{-6} for Q_2.

The next step after determining the error in the calibration method was to determine the error in each transducer reading. This includes both systematic and random error components. In order to evaluate the systematic uncertainty, the calibration procedure was repeated after the experimental program had been completed. This calibration was then compared to the original calibration to get a measure of how much the transducers drift in time with respect to the standard. The resultant calibration curves are shown in Figure E.6. The root mean square difference between each pair of curves was calculated at 100 evenly spaced points to determine an estimate of the change in calibration over time. This standard deviation was used to calculate an error (at a 90 % confidence interval) of 1.7×10^{-6} for Q_1 and 7.7×10^{-6} for Q_2. The fact that the error in Q_2 is much larger than than of Q_1 suggests that something has happened to change the calibration, other than just drift; perhaps the gain adjustment knob was accidentally moved between calibrations, or there was some faulty wiring in the circuit.

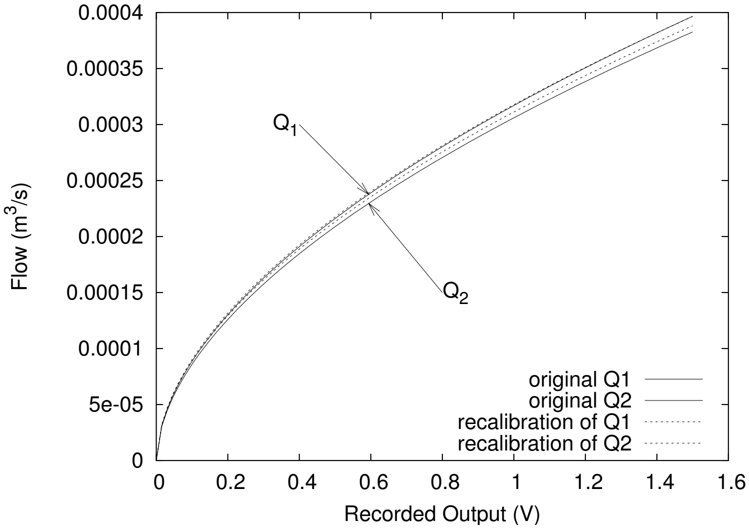

Figure E.6: Comparison of how the flow calibration curves have drifted over time. The solid curves show the calibration used to collect the data, while the dashed curves show the result of a recalibration after the data was collected.

The final source of error in the flow measurements to be considered was the random fluctuations in readings. This was estimated by recording a sample of data believed to be at a constant flow and calculating the standard deviation. The standard deviation for Q_1 at 2.60×10^{-4} m^3/s was 1.1×10^{-5} m^3/s, translating into an error of 1.7×10^{-5} m^3/s with 90% confidence, or 6.5%. The corresponding error values for Q_2 at the same flow were 2.4×10^{-5} m^3/s and 10.8%, respectively.

In order to determine the total uncertainty of the flow measurements, the above four sources must be combined: errors in the calibration standard, errors due to the curve fit, errors estimated by changes in the calibration curve, and random errors. These four errors were added (using a root sum of squares) and were found to be 1.8×10^{-5} m^3/s for Q_1 and

$2.6 \times 10^{-5}\ m^3/s$ for Q_2. Notice that the random error component dominates the total error for a single measurement, but this can be reduced by averaging multiple measurements. It is also important to note that while this is an estimate of the uncertainty at one flow rate, it can be used to give an idea of the errors at other flow rates.

E.4.2 Pressure Measurement Uncertainty

The other important quantity recorded was pressure. The uncertainty in these measurements was determined using a procedure identical to that found in Section E.4.1 with one exception: the standard pressure used for calibration was produced directly by a deadweight tester with a stated accuracy of 0.1%, eliminating the need to calculate the uncertainty (as in equation E.3). Table E.2 includes the calculated results. Notice that the calibration curves have changed considerably for P_{a1} and P_s. In the future, it may be worthwhile to check the pressure calibrations on a more regular basis in order to eliminate this source of error.

Table E.2: Estimated Pressure Uncertainty (90%)

	P_{a1}	P_{a2}	ΔP_L	P_s
Calibration Standard @4830 kPa (kPa)	4.8	4.8	4.8	4.8
Curve fit (kPa)	2.7	5.8	2.9	2.7
Calibration Changes (kPa)	120	14	22	114
Random Fluctuations @ 4830 kPa (kPa)	7.6	13.9	8.5	8.0
Total (kPa)	120	21	24	114

Appendix F

Combiner and Divider/Combiner Valve Concept

In this thesis attention was paid to the divider configuration, because that is the most common synchonizing valve in hydraulic power. However, there is also a need for both flow combiner valves, and flow divider/combiner valves. A combiner valve is one that combines two flows in a contant ratio independent of the supply pressure. This is used in meter-out hydraulic circuits and chemical mixing operations. A divider/combiner valve is one that works in both directions: as a divider if the flow is in one direction and as a combiner if the flow reverses. This appendix presents concepts for both types of valve.

A combiner valve could be contructed by using an identical valve with a different orifice geometry. The operational difference between divider and combiner valves is that when the pressure between the fixed and moving orifices of a divider increases, that orifice opens, while in a combiner, it closes. Therefore, a combiner can be achieved by using the configuration shown in Figure F.1.

A divider/combiner valve is then simply a combination of the two configurations shown in Figure F.1, which includes both orifice types and check valves used to direct the flow to the appropriate orifice, as shown in Figure F.2.

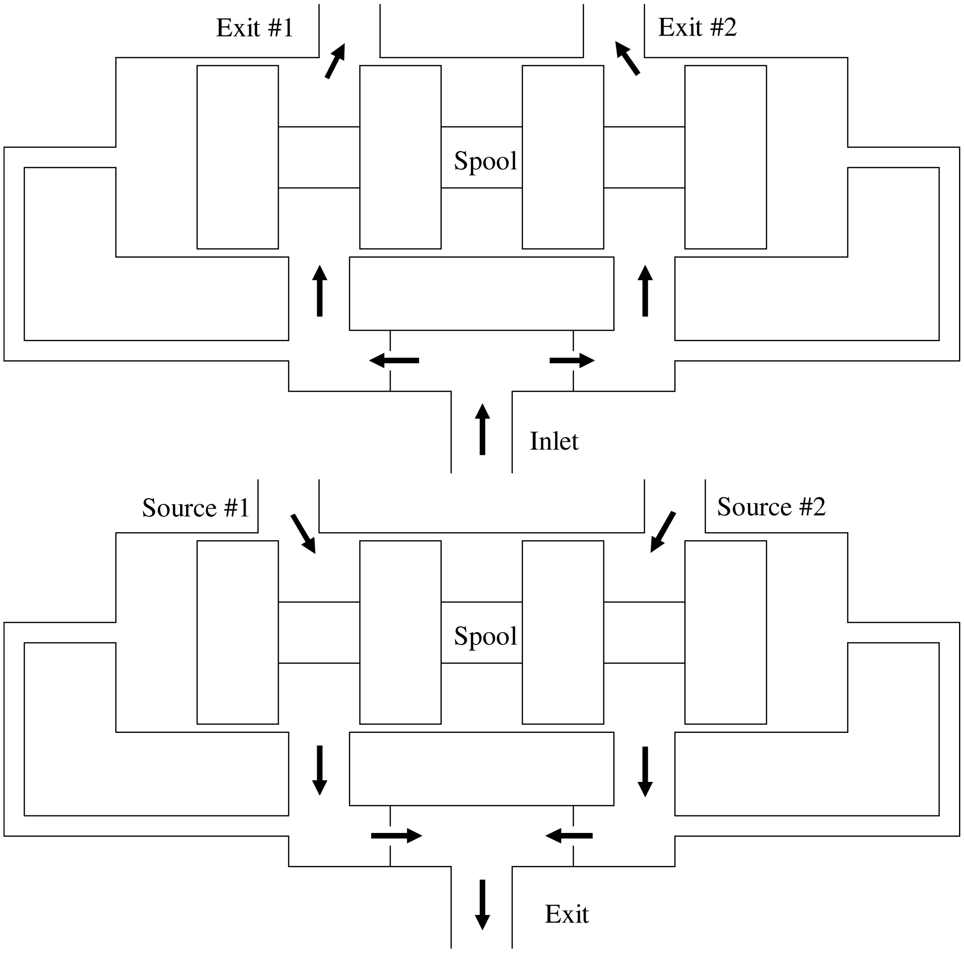
Exit #1
Exit #2
Spool
Inlet
Source #1
Source #2
Spool
Exit

Figure F.1: The difference between a divider (top) and combiner valve (bottom) is that when a divider orifice opens, the combiner orifice closes, and vice versa.

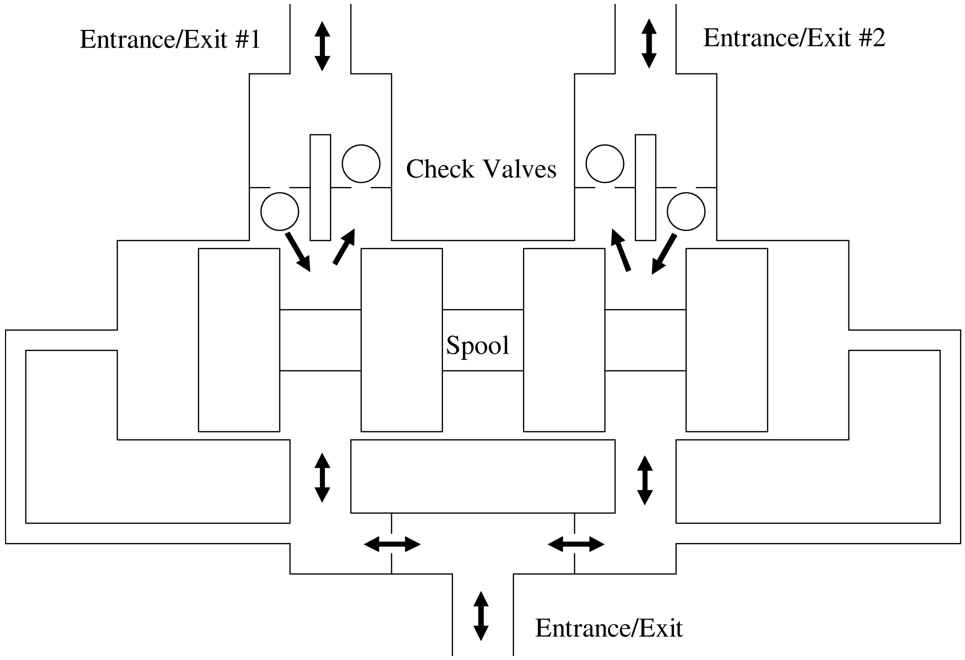
Entrance/Exit #1
Entrance/Exit #2
Check Valves
Spool
Entrance/Exit

Figure F.2: The proposed divider/combiner valve has two pairs of variable orifices and uses check valves to direct flow to the appropriate pair.